Dragline-Assisted Pitch Angle Righting

Dynamic analysis and robot design inspired by pitch anglerighting mechanism of the jumping spider

Prepared by:

Stacey Shield

SHLSTA001

Department of Electrical Engineering

University of Cape Town

Prepared for:

Amir Patel

Department of Electrical Engineering

University of Cape Town

October 2011

Submitted to the Department of Electrical Engineering at the University of Cape Town in partial fulfilment of the academic requirements for a Bachelor of Science degree in Mechatronics

Key Words: BIOINSPIRATION, MOBILE ROBOTICS, AERIAL RIGHTING, CONTROL, ARACHNOLGY

Declaration

1. **I know that plagiarism is wrong. Plagiarism is to use another's work and pretend that it is one's own.**
2. **I have used the IEEE convention for citation and referencing. Each contribution to, and quotation in, this final year project report from the work(s) of other people, has been attributed and has been cited and referenced.**
3. **This final year project report is my own work.**
4. **I have not allowed, and will not allow, anyone to copy my work with the intention of passing it off as their own work or part thereof**

Name: Stacey Shield

Signature: _____ Date: 18 October 2014

Acknowledgments

There are a number of people I would like to thank, as I would never have made it through this thesis without your support and assistance:

My supervisor, Amir Patel, for you guidance, patience and unrelenting interest and optimism about the success of this project. Thank you for giving me the opportunity to take on this fascinating topic, and for always been there to help.

Prof. Edward Boje and Robyn Verrinder for your advice and direction.

Callen Fisher, for providing the iNEMO development board, the code libraries and, most valuably, your time to help me troubleshoot.

My parents, for your love, support, and encouragement, which made it possible for me to persevere with this challenging course of study.

My friends and fellow mechatronics students. We got through this odyssey of stress, unexplained malfunctions and late night vending machine visits together, and you helped me keep a sense of humour even when things were at their most pressured.

Abstract

In response to a recent study by Chen, et al [1], this paper investigates the use of a mechanism imitating the silk dragline of a jumping spider to achieve pitch angle control in a mobile robot. A dynamic analysis of the dragline system was conducted using two different mathematical representations. An explanation of the observed behaviour of the spider and a discussion of the system as a control problem was undertaken based on this analysis. A possible design for a line-equipped autonomous platform (or LEAP) was then presented, although this could only be tested in a simplified form.

It was demonstrated that the dragline can indeed reverse the initial pitch rotation of a mobile robot, but that it would likely be complicated to implement. Compared to other methods of aerial righting, it was found to have potential advantages in applications where minimizing the size and weight of the device is desirable. Additional research, especially into the design of a controller using the dragline, would be necessary to conclusively determine whether this approach to pitch righting is practical and feasible. The findings of this study are, however, sufficient to show that the dragline mechanism warrants further investigation.

Table of Contents

List of Figures

List of Tables

1 Introduction

"If anyone wanted ter find out some stuff, all they'd have ter do would be ter follow the spiders. That'd lead 'em right! That's all I'm sayin'."

- Rubeus Hagrid in *Harry Potter and the Chamber of Secrets,* J.K. Rowling

1.1 Background

From capturing prey to attracting mates, the more than 40 000 known species of spider utilize their silk in an incredible variety of applications. A recent study [1] has drawn attention to another potential function of this versatile material: aerial righting.

Before jumping spiders take a leap, they attach a silk dragline to the substrate. Besides acting as a safety line in the event of a failed jump, by pulling on this thread, the spider is able to alter its pitch and slow itself down in mid-air, allowing it to execute a safe and controlled landing. [1]

The spider's need for a method of aerial stabilization is shared by mobile robots. Navigating rough terrain may involve ballistic motion, and it is vital that they are able to land in a favourable way to prevent damage [2].

The purpose of this study is to investigate the application of a mechanism inspired by the jumping spider's dragline to implement aerial righting on a mobile robot.

1.2 Objectives of the study

1.2.1 Problems to be investigated

Before the dragline mechanism can be adapted to a robot, it must first be thoroughly understood in its natural context. The first aim of this project is therefore to analyse and explain the motion of the spider. To accomplish this, a mathematical model of the spider must be derived and used to simulate its dynamics under different conditions.

While digital simulations can provide valuable insight, physical experiments will also be required to determine the feasibility of the dragline as a method of aerial righting. The second aim of this project is therefore to design a simple line-enabled autonomous platform (or LEAP) which can be used to investigate the effects of the dragline.

1.2.2 Research Questions

The objectives of this study can be summarized by the following research questions, which this report will attempt to answer:

1. What are the possible applications of a dragline-inspired mechanism in the field of mobile robotics?

2. How does the spider achieve pitch control utilizing the dragline?

3. What are the effects of the initial velocity, launch angle, initial body rotation and magnitude of the silk force on jump performance?
4. How can the spider's observed pitch angle response be explained?
5. What other methods of aerial righting are available, and how do they compare to the dragline solution?
6. Is it possible to bring about pitch rotation in a mobile robot using only the dragline?
7. What are the advantages and disadvantages associated with the dragline as a method of aerial righting?

The last three form the basis for the main question this study aims to answer: is the adaption of the dragline mechanism for pitch righting in a mobile robot feasible?

1.2.3 Purpose of the study

Ultimately, the purpose of this study is to gain an understanding of how the dragline is implemented to achieve aerial control, both in the context of the spider and possible robotic applications. The design of a platform equipped with a dragline also contributes to this goal by facilitating physical investigation into this mechanism.

From the perspective of robotics engineering, this research is valuable as it could improve the ability of robots to navigate rough terrain autonomously. It is also beneficial to the field of biology, as research into the jumping mechanism of spiders has been limited, and an attempt to imitate their behaviour in a robot could give significant insights into the spiders themselves.

1.3 Scope and Limitations

This project will investigate the use of a dragline for aerial righting through simulation and the design of a simple line-equipped robotic platform. The experiments will consider a sub-horizontal jump with parameters derived from the study by Chen et al [1]. While the problem of overpitch on landing will be discussed, the simulations will only represent the jump up until the point of first touch-down. The effects of body articulation during the jump will be ignored, and the system will be assumed to be in planar motion.

While this study aims to identify the key aspects of implementing pitch control using a dragline, and explain the motion of the spider using some concepts of control theory, it will not cover the actual design of a controller. The testing platform will, however be designed to facilitate the future implementation of feedback control.

Due to the time constraints of the project, there will be limited opportunity to test the platform designed. Rather than pursuing an ideal landing, the objective of the tests will simply be to provide a proof-of-concept demonstrating the capacity of the dragline to bring about rotation in the context of a mobile robot.

1.4 Plan of Development

The structure of this report is divided into three distinct parts: the first four chapters provide the background to the study, by presenting the relevant theory and literature on this topic and establishing the purpose of this research. They also describe how the study will be approached

over the subsequent sections. The next two sections document the research itself: the first covers the dynamic analysis which was conducted, from the modelling and simulation of the system to a discussion of the results of this investigation. The final section details the design and testing of the LEAP. The report will then conclude with a summary of the answers to the stated research questions, and recommendations for future research into this topic. Appendices containing additional information can be found at the end of the report.

2 Literature Review

Spiders, cockroaches and other crawling creatures are some of the most feared and reviled members of the animal kingdom, but rather than putting them under a heavy boot as many others might, robotics engineers have instead been putting them under scientific scrutiny. From hexapedal locomotion [3] to silk spinning [4], there has been great interest in adapting the features of these animals to improve the ability of mobile robots to move through challenging environments. A recent study by Chen, et al [1] has drawn attention to another mechanism used in spiders with potential engineering applications: the use of a dragline for pitch righting.

The purpose of this review is to establish the current scientific understanding of this mechanism and its possible uses in the context of bioinspired robotics. It will focus on the following research questions:

- What are the possible applications of a dragline-inspired mechanism in the field of mobile robotics?
- How does the spider achieve pitch control utilizing the dragline?
- What other methods of aerial righting are available, and how do they compare to the dragline solution?

In order to provide answers, the review will proceed as follows: first, a brief introduction to the field of mobile robotics will be given, focussing on the problem of pitch righting and the influence of biology in their design. An explanation of how the dragline is applied by the spider will then be presented, specifically detailing the manner of jumping, the braking mechanism used to apply force to the line and the properties of the silk dragline itself. Finally, alternative methods of pitch righting –both in nature and other robots – will be discussed and compared to the dragline method.

2.1 Mobile robotics

With their ability to perform repetitive tasks faster, more precisely and for longer hours than human workers, robots have become indispensible to many industries, however most commercially applied robots still work from a stationary base, rather than being able to move about freely. [2] With the increasing availability of small, powerful digital processing devices, there has been growing interest in developing autonomous mobile robots: robotic devices which are able to move unassisted through their environment.

2.1.1 Aerial stability in mobile robots

The applications for mobile robots centre around two types of tasks: menial jobs requiring mobility, such as vacuuming a room or military transport, and jobs performed under conditions which are unsafe for humans, such as space exploration or search and rescue operations [2] [3] [4] [5]. Because these actions require the robot to operate outside the controlled conditions of a laboratory, one of the key aspects in their development is ensuring that they are adapted to navigate unknown environments and obstacles.

Particularly if the robot must move over rough terrain, there is a good chance that traversing these obstacles could involve ballistic motion [6]. This could be intentional, where the robot jumps or ramps itself into the air, or unintentional, as in the case of a fall.

In either situation, it is important that the robot lands in a way which allows it to continue operating. If it lands with a large velocity, or at an unfavourable angle, it may be damaged or unable to right itself [5].

To achieve a safe landing, the robot needs some mechanism which it can use to control its angle in the air and slow itself down sufficiently. Because this need is shared by a variety of animals, it may be possible to find a solution by adapting one already applied in nature [6].

2.1.2 The influence of biology in the design of mobile robots

Aerial righting is just one example of a problem faced by mobile robots that could be solved by imitating the natural world. Throughout history, many technological breakthroughs have been inspired by mechanisms developed over millions of years by the process of evolution [3] [5]. With supporting technologies becoming advanced enough to make imitation of often complex natural processes feasible, bio-inspired robotics is now one of the fastest-growing technological fields [4].

Bioinspiration vs. Biomimetics

As would be expected within such a large field, there are several different philosophies governing how robots are designed around biology. Depending on how the question "how closely should we copy nature?" is answered, these can be split into two main approaches:

The first option is to imitate the organism as closely as technology allows, even if the function of a particular feature is not completely understood [5]. This field is called Biomimetics, and is supported by the argument that these features could be useful for reasons which are not immediately apparent, and that reproducing them could give insight into their role [5].

The alternative is called Bioinspiration, and can be summarized by martial artist Bruce Lee's famous quote: *"Adapt what is useful, reject what is useless and add what is specifically your own."* This approach aims to understand the natural mechanisms considered as completely as possible, and then adapt the essential principals to the design [3]. Aeroplanes are examples of the benefits of this approach: while the first flying contraptions were based on the Wright brothers' observations of bird flight [4], they did not attempt to copy birds directly, and the addition of increasingly powerful engines allowed these craft to far exceed the capabilities of the animals they were inspired by [5]. This is the approach which will be kept in mind for the duration of this paper.

The relationship between robotics and biology

Another factor driving the growth of mobile robotics is the increasing body of knowledge about how different organisms function [4]. Research in areas such as biomechanics is vitally important to robotics engineers, as it allows features with potential technological applications to be identified and understood [5].

The gains from research do not just go one way, though: the fields of biology and robotics exist in a symbiotic relationship where both benefit from advances in the other. Studying robots can increase the understanding of the organisms they are based on, as the process of reverse-engineering and adapting a biological feature often gives important insight into how that feature works [3] [5] [4].

There are still many biological discoveries with potential engineering applications that have not been realized. The finding by Chen, et al. that jumping spiders use their silk draglines to control their motion in the air [1] is an example, as this idea could be adapted to solve the problem of aerial righting in a mobile robot. Before it can be imitated technologically, however, it must be understood as it applies to the spider.

2.2 The use of draglines for aerial righting in jumping spiders

Jumping spiders – spiders belonging to the Salticid family – are the stealth assassins of the arachnid world. Much like cats, they use their acute vision to stalk their prey, until they are close enough for a final, deadly pounce. They are capable of jumping many times their own body length, and besides prey capture, they use this ability to navigate through vegetation and escape predators. [3]

Because jumping is a crucial part of their hunting behaviour, it is vitally important that they are able to jump accurately and land in a controlled way. Aside from the loss of prey, an uncontrolled landing or fall wastes valuable energy, and could result in injury. To imitate their method of satisfying these requirements in a mobile robot, it is necessary to understand the spider's jumping motion, internal braking mechanism and silk properties.

2.2.1 Jumping motion

There has been very little research into the mechanism of jumping in spiders, and of the available studies, the majority are concerned with take-off mechanisms or overall jumping performance, rather than pitch control and stability in the air. [1]

The first study into the way salticids execute their jumps was performed by Parry and Brown [5] and focussed specifically on determining the hydraulic pressure in the legs necessary to achieve lift-off. A more recent study, conducted by Hill [10] addressed the ability of salticids to jump accurately at suspended lures from surfaces at different angles, elevations and distances relative to the target.

Although both these papers suggested that the dragline is involved in correcting the spider's pitch, the recent study by Chen, et al. [1] is the first to research this mechanism specifically and attempt to quantify the forces involved. Their findings that the spider begins to reverse its initial pitch relatively early in the jump contradict the two previous studies, however this can be explained by the technologies used. Parry and Brown and Hill utilized multi-image photographs of spider jumps taken in the late 1950's and 1970's respectively. The maximum available frame rate at these times was significantly lower than the 1000 fps video footage used in the 2013 study, which would have limited the accuracy of their observations.

This review is centred on salticid spiders, as their jumping mechanism is best understood, however the study by Weihmann, et al. [6] into the jumping kinematics of wandering spiders (*Cupiennius salei*) must also be considered, as they hypothesized that these spiders also use tension on their draglines for aerial righting. From the perspective of this paper, the most notable aspect of this finding is that the method remains effective despite the wandering spider being much larger and having a differently positioned centre of mass to the salticid species studied.

The jumps performed by spiders can be divided into two categories: prepared and unprepared. [6] In prepared jumps, the spiders arrange their legs into a set placement before jumping to optimize control and stability in flight. By contrast, unprepared jumps are performed in response to a sudden disturbance, and show very little uniformity in the animal's movement. [6] To simplify analysis, only prepared jumps will be discussed in this report. With the exception of Hill's work, the jumps studied were from horizontal surfaces to positions on the same level, or slightly lower, so these trajectories will be focussed on. As in the paper by Chen et al [1], the motion of the spider will be considered in a single two-dimensional plane, with pitch being the only rotational movement.

Take-off

In prepared jumps, spiders begin by touching their abdomen to the substrate, anchoring their dragline with a sticky disc of silk. Wandering spiders were found to jump from a posture very similar to the one used by salticids [6]. The rear leg pairs provide the thrust for the jump – either the fourth pair, the third pair, or both, depending on the species [3] [4] [6]. The first and second pairs do not contribute to the thrust, and may be raised before jumping [6].

The magnitude and direction of the initial velocity determines the range of the jump: for longer jumps, the spider accelerates faster and leaps at a higher angle relative to the horizontal substrate [10]. Jumps toward prey are also generally faster than jumps from one position to another [10].

As the spider pushes away from the surface, it takes on an initial rotation. Salticids tend to pitch backwards (abdomen down) [1] [10] [4] while wandering spiders rotate forward [6]. Differences in the center of mass position due to body shape, or the direction of the ground reaction forces due to their slightly different leg extension mechanisms could account for the change in direction of rotation between these species [6]. The rotational velocity tends to be greater for faster (and therefore more distant) jumps [10].

Aerial phase

Once in the air, the spider spreads its legs out and lifts them dorsally, assuming a posture which resembles a badminton shuttlecock [6]. Although there is some small relative motion between the cephalothorax and abdomen, the effects of this movement on the dynamics of the jump were neglected. Chen et al. did however adjust the calculation of the aerodynamic drag force at each point to account for the slight differences in body posture [1].

Three forces act on the spider during this phase: gravity, the pulling force from the dragline (F_S) and aerodynamic drag (F_D). The silk force can be regarded as a combination of a braking force (the component parallel to the body) and a moment (the perpendicular component) which causes its rotation [1] [10].

Parry and Brown did not address drag in their analysis of the jump [4] and Hill did not observe any aerodynamic effects [10]. The more recent examination of the dynamics conducted by Chen et al. showed that drag has negligible effect in the vertical direction, but cannot be neglected in the horizontal direction [1]. It was also suggested that the spider's 'shuttlecock' pose could help stabilize it aerodynamically [6].

In a shallow sub-horizontal jump, salticids were observed to reverse their pitch between one and three times, with two reversals being the case for most jumps [1].

The first pitch reversal occurs about 31% of the way through the air time, once the pitch has rotated the abdomen (Θ_A) from 180˚ to around 220˚. At this time, the angle between the silk and the abdomen ($\Theta_{S\text{-}A}$) will be approximately 140˚ [1]. Silk force is at its maximum (about 40% of the spider's body weight) from take-off until the abdomen returns to 180˚. Roughly 80% of the magnitude of the combined resistive force ($F_S + F_D$) can be attributed to the dragline at this stage [1].

Rather than stopping at 180˚, the spider's forward pitch continues, but a slower rate: the moment has reversed direction, so it is now acting against the direction of pitch. The silk force has decreased slightly, and the dragline is now more in line with the abdomen, so the moment is greatly reduced and the braking component dominates [1]. The second pitch reversal occurs about 72% through the aerial phase, when the silk is at more or less 150˚ to the abdomen. Shortly after it begins, the silk force falls away rapidly, until it makes up around 20% of the resistive force acting on the spider. The body continues to pitch backwards until it returns to 180˚ (or slightly less) just before landing [1].

The diagram below illustrates the key points in a jump where two pitch reversals take place:

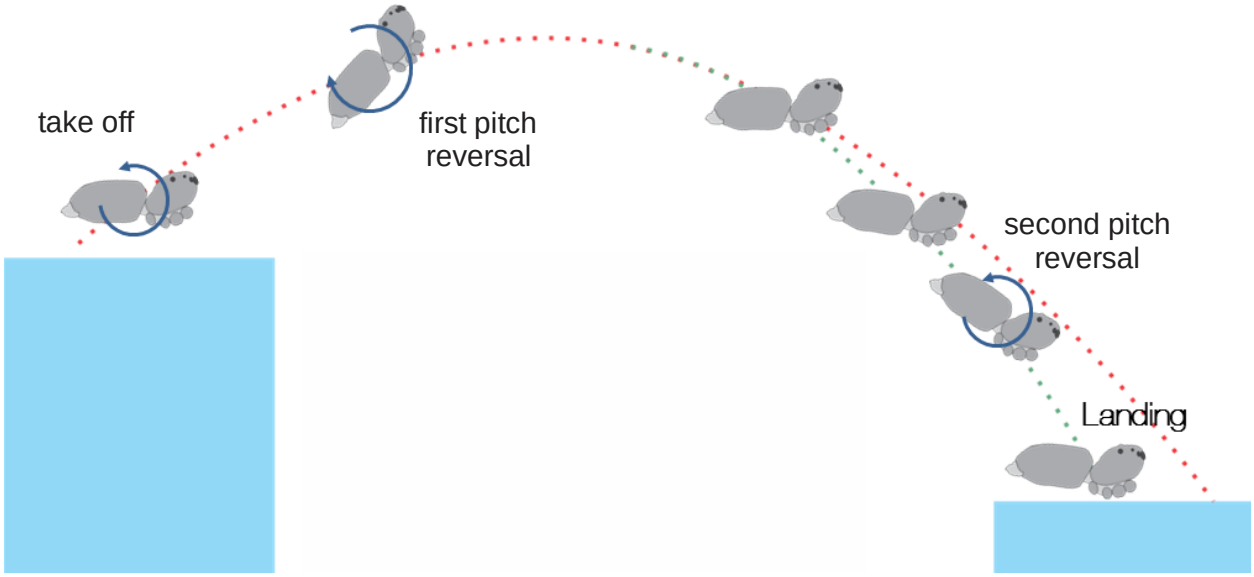

Figure 1: illustration of the motion of a jumping spider performing a sub-horizontal jump during which it reverses its pitch twice. The dashed red curve represents the ideal ballistic trajectory while the green curve is the actual trajectory followed.

In spiders which jump without a dragline, the initial rearward pitch continues throughout the jump, so the body is at its steepest angle as it lands [1]. This is also true of silk-jumping spiders where the line breaks before the first pitch reversal can occur. If the initial rotational velocity is large, the spider may lose stability completely and flip over backwards in the air [4], as shown int the following figure:

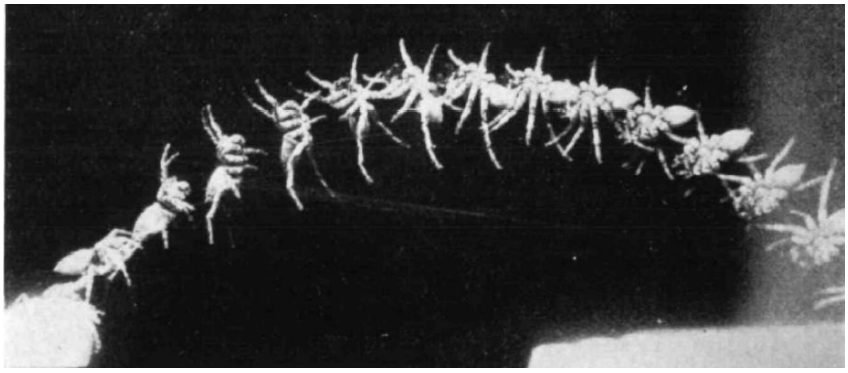

Figure 2: multi-image photograph of a jumping spider flipping backwards in the air following the breaking of its dragline [8]

Landing

The landing phase of the jump is the time between the first leg touching down and the spider reaching a stable position with all eight legs on the surface. For a 'good' landing, the duration of landing should be as short as possible, and the spider should maintain the same body orientation throughout. There must also be no bouncing – once a leg makes contact with the ground, it must not lift off again. [1] A comparison between footage of a spider making a safe landing and an uncontrolled landing is shown in Figure 3.

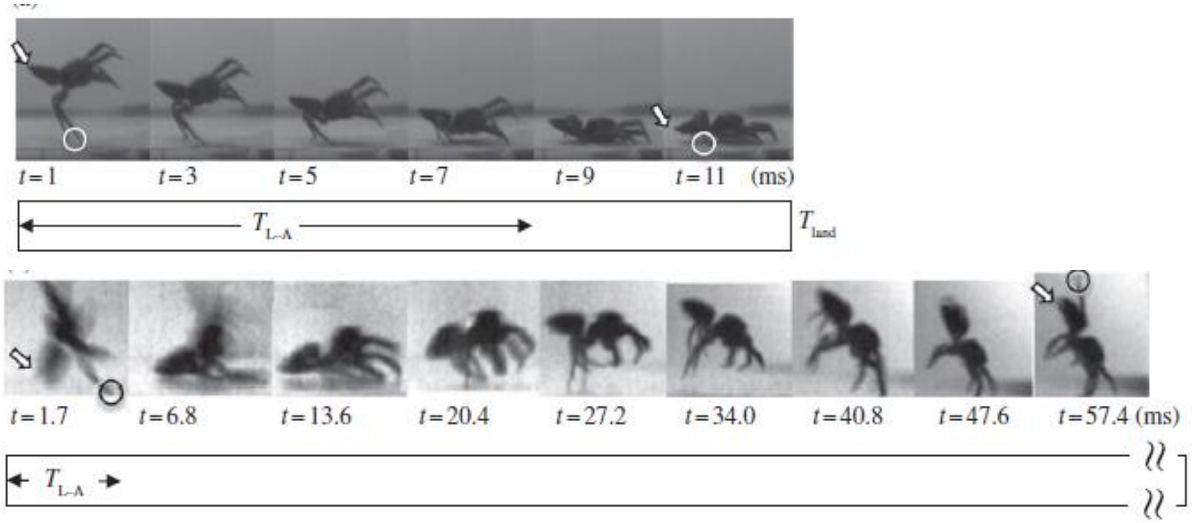

Figure 3: frames from video footage showing a spider making a safe landing (top) and tumbling during an uncontrolled landing (bottom) [1]

To make a 'good' landing, both the angle and velocity of the spider are important. This can be seen through comparison between the jumps of similar non-silk and silk-jumping spiders:

Silk-jumpers were able to bring their body approximately parallel to the surface before landing, and maintain this orientation throughout the landing phase, [1] [10] but non-silk spiders approached the landing at a steep body angle and pitched forward rapidly after first touch-down [1].

The horizontal velocity of non-silk spiders was also much greater. With only air resistance to slow them down, these spiders lost only 33% of their initial mechanical energy, compared to the 76% dissipated by silk spiders [1]. They were also exposed to much larger impact forces [1]. In some cases, the large deceleration required during landing was sufficient to cause overpitch for

these spiders: unable to maintain leg contact and control their forward pitch, they tumble until they have lost enough energy to right themselves [1]. Because of their instability, the duration of landings for non-silk spiders was greater than that of silk spiders by a factor of five [1].

2.2.2 Dragline braking mechanism

To understand how spiders apply tension to their draglines during the jump, it is necessary to have a basic understanding of the silk production process and the structures which facilitate it.

The silk production pathways vary widely from species to species, depending on their individual requirements for the silk. Although eight different types of silk gland have been classified, only the most sophisticated spinners – the orb weavers - possess all eight [3].

Dragline silk is produced from the Ampullate glands [3]. New silk is secreted as a liquid, which then forms into threads due to the alignment of its molecules under tension [7]. Contrary to the idea that they can 'shoot' web, popularized by Spider Man, the spider does not produce sufficient hydrostatic pressure to forcibly extrude silk – it must be drawn from the body, either under its body weight, or with the assistance of a leg [3] [7] [8].

It has been shown that spiders can actively control the tension required to draw silk from their bodies [8]. Within the normal range of spider behaviour, the force applied is thought to range from less than 10% of its body weight up to 2.2 times the body weight used to bring the spider to a dead stop while descending on its line [8]. Though it has been suggested that hair-like structures on the spinneret may perform this function by acting as a 'tension gate' [10], it is now generally accepted that the spider achieves this control through some combination of its internal pressure, and a control valve near the end of the silk gland [1] [10] [11] [12].

The structure and function of this control valve was investigated by Wilson in the 1960's [7] [11] [9]. He described it as a ring which can swell up to occlude the silk duct or deflate to open it under the action of two muscles, the valve-tensor and the duct-elevator muscles [9] [7]. His diagrams of the valve in its open and closed position are shown in Figure 4. Wilson's hypothesis that this valve can act as a brake to control the descent of the spider on its dragline was supported by a later study, which confirmed that the forming silk threads would have sufficient strength to support the spider at the point where they pass through the valve [12].

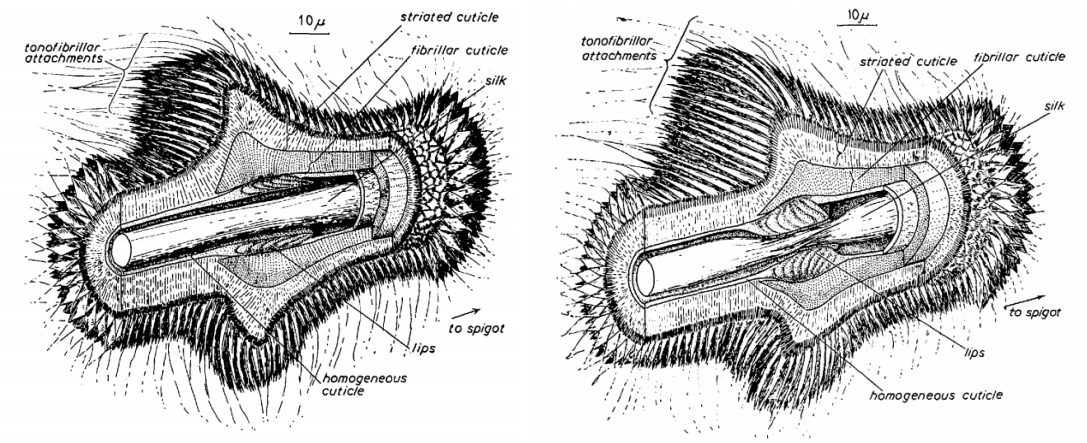

Figure 4: diagrams of the silk valve of the garden spider *Araneus diadematus* in the open (left) and closed (right) positions, as studied by Wilson [18].

While these studies give an idea of how the jumping spider may control the tension on its dragline, determining the exact mechanism would require study specifically into the silk pathways of salticids. The existing literature has focussed almost entirely on silk production in orb-weavers [7] [11].

Salticids belong to the collection of families known as the RTA clade, consisting of those species which have largely lost the use of silk for trapping prey [11]. While RTA clade spiders do have control valves resembling those described, they are less well-developed than those of orb-weavers, generally lacking the duct-elevator muscle [7]. It has therefore been hypothesized that they may have reduced ability to control the tension on their draglines during descents, or utilize some alternative method to slow themselves down [11].

2.2.3 Mechanical Properties of Spider Silk

Precisely quantifying the mechanical properties of spider silk is difficult, as these properties vary widely - not only from species to species, but also for individual spiders, as factors such as temperature, drawing speed, spinning direction and diet also affect them [12]. There are, however, some general characteristics which should be noted in relation to the function of the dragline.

Spiders are capable of producing several types of silk to perform different functions [3] [12]. The silk draglines are formed from is called major ampullate silk, and is one of the stiffest and strongest biomaterials known [16].

In mechanical terms, strength refers both to the ability of the silk to resist breaking under the application of a large force (tensile strength) and under a large increase to its length (extensibility) [10] [16]. ‘Stiff’ means that a large force is required to produce a given extension in the material [10].Compared to synthetic fibres such as Kevlar, spider silk is not as stiff or as strong in terms of tensile strength, but it is more extensible and also tougher – it requires much more energy to break the thread [16].

Spider silk is a viscoelastic material, meaning its properties also depend on the rate of strain [10] [11] [16]. Its strength, stiffness and toughness have been shown to increase with the rate of strain, so for strain occurring over a short time scale, such as a jump or drop on the dragline, the amount of energy and force required to stretch the line would be very large [16].

Other important characteristics of spider silk are its torsional and damping properties. It has been found to have a torsional shape ‘memory’ – when twisted, it will return to its original position without an external stimulus [17]. Its hysteretic properties cause it to dissipate most of its kinetic energy as heat and it also has a large damping coefficient [10] meaning that, when it is disturbed, it will return to rest quickly and without oscillation about its equilibrium point [17]. In combination, these properties are the reason that the spider can descend on its dragline without appearing to twist [17].

2.3 Alternative methods of aerial righting

The jumping spider is just one of a broad range of terrestrial animals which require mechanisms for righting themselves in the air. Many different solutions to this problem can be found throughout the diversity of the animal kingdom, as well as a variety of man-made solutions.

2.3.1 Aerial righting in nature

The following techniques are some of the commonly observed methods that have been used by terrestrial animals to right themselves in the air:

Modifying angular momentum prior to leaving the ground

During take-off, an animal can use its last moments of contact with the substrate to give itself an initial angular momentum that will be maintained throughout the jump, if no external forces act. This technique has been observed in frogs, as well as being applied in some gymnastics skills [6].

Modifying angular momentum during flight by changing body posture

By moving their body segments relative to each other in the air, animals change their instantaneous moments of inertia. Because, in the absence of external forces, angular momentum is conserved, this action can induce or modify a rotational velocity [22].

In mammals, this is generally achieved by twisting of the spine or rotating limbs [22] [6]. The falling cat is probably the most popular example, but rodents, monkeys and even humans have been observed to right themselves in this way [22].

Because their tails are larger and more massive relative to their bodies, reptiles are able to rotate themselves in the air by rapidly spinning their tails [6] [22]. This technique in particular has piqued the interest of the robotics community, with several studies showing that a rotating tail is an effective means of achieving aerial manoeuvrability in a robot [23] [24] [25].

Inducing an aerodynamic torque

Animals which are capable of flapping flight, and terrestrial gliders such as flying squirrels are capable of using aerodynamic lift and drag to induce a torque on their bodies, for instance by moving their left and right wings asymmetrically [22].

2.3.2 Artificial solutions to aerial righting

In aerospace applications, spacecraft and satellites are usually stabilized either by applying torques from thrusters or through angular momentum-based methods such as flywheels and gyroscopes [26] [24]. In the context of a small robotic platform, however, the use of thrusters is generally not feasible so only momentum-based methods will be discussed.

Besides purpose-built flywheels, the robot's driving wheels can also be used for attitude righting. Off-road motorcyclists have been observed to modify their pitch during jumps by accelerating or braking their wheels [6], and a study by Davis, et al. [27] showed that this same method can be applied to achieve aerial righting in a small, four-wheeled vehicle.

2.3.3 The dragline method vs. other pitch righting strategies

Compared to the other natural methods of pitch righting discussed, the dragline method is unique in that it does not rely on changing body posture or manipulation of the aerodynamic forces acting on the body [1]. This makes it feasible for use in robots where the body cannot articulate.

In the case of wheeled robots, the advantage of using momentum-based righting is that it could potentially be implemented using the driving wheels, without the need for additional purpose-

built structures [27]. There has, however been increasing interest in developing legged robots, as legs are a more efficient form of locomotion on soft or uneven ground [2]. For legged robots and wheeled robots where the driving wheels cannot sufficiently alter the pitch, flywheels and active tails have been shown to be effective methods of achieving righting [27] [24] [23], with the dragline method being a possible alternative to these. While further research into the implementation of the dragline is necessary to evaluate its feasibility, some advantages and disadvantages in relation to these other methods are immediately apparent.

The dragline is not size-dependent

The angular momentum of a tail or reaction wheel needs to be large enough relative to that of the body to bring about rotation. This requires it either to be spun at a high speed, or to have a large moment of inertia [28]. If the mechanical power needed to achieve fast rotation cannot be provided, the tail or wheel will have to be either large or heavy, as the moment of inertia is proportional to the mass and the square of the radius of an object [28].

Although using the dragline approach would require the addition of a spool to store the line and an actuator to control the spool, in robots where minimizing the weight or size is a priority, these components could have a lower cost than a tail or wheel. Additionally, assuming that the tension necessary to rotate the robot will be small in relation to its body weight, as was observed in the spider [1], the actuators required to apply this force will be less powerful than those needed to drive a tail or flywheel.

The dragline also acts as a brake and safety line

In addition to landing at a favourable angle, reducing the landing velocity may also be necessary for the robot to avoid damage. While the tail and flywheel can affect the attitude of the body, they cannot decelerate it linearly, unlike the dragline which was also shown to act as a brake on the spider [1].

In the event of a fall, the dragline could act as a safety line to prevent the robot from hitting the ground altogether. Besides reducing the chance of damage, the robot could ascend the dragline and return to its original position after such an event, as spiders can in the case of a failed jump [10]. It could even use the dragline to intentionally descend from a solid surface, allowing it to move around its environment more efficiently [29].

Jump planning, attachment and storage considerations

A difficulty associated with the use of the dragline is that it must be attached to the substrate before the spider jumps [24] [10] [8] [10]. This means the robot will need to be able to predict an impending ballistic action early enough to anchor its line, which may not be feasible in the case of a sudden fall or unintentional launch. By contrast, flywheels and tails can be activated once the robot is already airborne [22] [6]. The robot will also need some means of attaching the line which is quick, secure and effective on a variety of surfaces.

The problem of storing the line must also be carefully considered. If a disposable line is used, the robot will need to be able to store enough thread to complete its mission. While reeling in and re-using the line could reduce the space requirement, it introduces the additional complication that the attachment method used must also be remotely detachable.

In terms of line storage, the spider’s ability to spin silk from a liquid feedstock as it is required is a major advantage. Recently, there has been an attempt to replicate this ability in a mobile

robot, using a heated thermoplastic material to form the dragline [29]. This study applied the mechanism specifically to lower the robot in a vertical descent, but with further development, a similar solution could provide an alternative to the spool and cable.

2.4 Summary and Conclusions

In response to the findings by Chen, et al [1] that jumping spiders use silk draglines to stabilize themselves in the air, this review aimed to investigate the possible applications of a similar mechanism in the field of mobile robotics, as well as presenting a summary of the associated biological knowledge.

This review provided some answers to the three research questions it addressed:

- The potential value of the dragline mechanism to the mobile robotics field lies in the need for robots navigating rough terrain to have a means of controlling their landings.
- It was found that spiders use an internal friction brake to apply an average tension of around 26 percent of their body weight to the dragline, and they generally reverse their pitch twice during the course of a jump [1].
- The dragline mechanism was specifically compared to tails and flywheels, as these were evaluated to be the most feasible alternative righting methods. It was found to have advantages in terms of size and multi-purpose applicability, but potential complications associated with its use and implementation were raised as initially apparent drawbacks.

These answers are far from complete, however, and the review revealed some significant gaps in the available literature. There has been very little research into the jumping motion of spiders, and although previous studies hinted at the use of the dragline in aerial control [10] [8] [10], Chen, et al [1] have been the first to study this mechanism specifically. Additionally, while their work illuminated *what* the spider does during the jump, there has not yet been any attempt to explain *why* it does it that way.

To answer that question, the jumping spider must be analysed from the perspective of biomechanics and control theory. This will also provide greater insight into the problem of implementing a dragline-based control system, and ultimately its feasibility and usefulness compared to existing aerial righting methods.

3 Theory Development

This chapter explains some theoretical concepts utilized throughout the report.

3.1 Lagrange Dynamics

In classical mechanics, the motion of bodies is determined by Newton's Laws [28]. While these laws can be used to model and solve problems involving mechanical systems, they can often be complicated and difficult to implement for multi-body systems or systems with many degrees of freedom, as they require precise knowledge of all the forces acting on the system [30] [31].

Lagrange dynamics is an alternative method of representing Newtonian mechanics, based around the conservation of energy [31] [32]. The advantage of this method is that it is often able to simplify the representation of systems which would be extremely complex to model using traditional Newtonian techniques [30].

The modelling of the jumping spider system using Lagrange equations will be described in chapter 0.

3.1.1 The Lagrangian

The Lagrangian is a scalar quantity given by the equation:

$$L = T - U$$

where T is the total kinetic energy in the system and U is the total potential energy [33] [32] [31] [30]. For a multi-body system, these quantities are given by

$$\sum_{i=1}^{N} T_i$$

$$\sum_{i=1}^{N} U_i$$

with T_i and U_i being the kinetic and potential energies of the individual bodies, and N being the total number of bodies in the system [33] [32] [31] [30].

3.1.2 Generalized Coordinate Systems

Another advantage of Lagrangian mechanics is that it does not require an inertial coordinate system, but can be applied using any convenient system which satisfies the following conditions [32]:

- **Completeness:** any possible state of the system can be described using the coordinate system [32].
- **Independence:** the system can move about its full range of motion in each coordinate, even if the position of all the other coordinates is held fixed [32].
- **Holonomicity:** the number of coordinates necessary to describe the motion of the system is equal to the number of degrees of freedom in which the system can move [32].

The coordinates used in Lagrangian dynamics are referred to as generalized coordinates. In a system with M degrees of freedom, the motion is described by a set of M equations of motion – one for each of the generalized coordinates, q_i [33] [32] [31] [30].

In terms of the Lagrangian, each equation of motion is derived by working out the expression corresponding to the following:

$$\frac{d}{dt}\left(\frac{\delta L}{\delta \dot{q}_i}\right) - \frac{\delta L}{\delta q_i} = Q_i$$

where Q is the generalized force acting in the direction of that component [33] [32] [31] [30].

3.1.3 Generalized forces

Because the Lagrangian method is based on the conservation of energy, only non-conservative forces need to be considered when evaluating the generalized forces. If the system is under the influence of only conservative forces, the generalized force will be zero [33] [32] [31] [30].

For a system acted on by N non-conservative forces, the generalized force in each coordinate is given by the sum of the dot products

$$Q_i = \sum_{j=1}^{N} \frac{\delta r_j}{\delta q_i} \cdot F_j$$

where F_j is the force vector, and r_j is a vector representing the position where the force acts [31] [32].

3.2 Euler Angles

In chapter 8.3.1, the use of a three-axis gyroscopic sensor for measuring the angular position of the robot is discussed. This device outputs the angular velocities in terms of a reference frame which moves with the body, however for the position to be interpreted correctly, these need to be converted to the static, inertial reference frame [34].

The rotation of the body frame relative to the inertial frame is given by three Euler angles [34] [35]:

- Roll ϕ
- Pitch Θ
- Yaw ψ

These angles can be used to convert from the inertial frame to the body frame by rotating the frame in a specific order. The Euler 3-2-1 sequence is a commonly used option [34]:

1. The system is rotated about the z axis by ψ
2. The system is rotated about the y axis by Θ
3. The system is rotated about the x axis by ϕ

The conversion from the inertial frame to the body frame can be represented by the matrix equation [35] [34]:

$$\begin{pmatrix} X_B \\ Y_B \\ Z_B \end{pmatrix} = \begin{bmatrix} \cos\theta\cos\psi & \cos\theta\sin\psi & -\sin\theta \\ \sin\varphi\sin\theta\cos\psi - \cos\varphi\sin\psi & \sin\varphi\sin\theta\sin\psi + \cos\varphi\cos\psi & \sin\varphi\cos\theta \\ \cos\varphi\sin\theta\cos\psi + \sin\varphi\sin\psi & \cos\varphi\sin\theta\sin\psi - \sin\varphi\cos\psi & \cos\varphi\cos\theta \end{bmatrix} \begin{pmatrix} X_I \\ Y_I \\ Z_I \end{pmatrix}$$

The values of the Euler angles used are obtained from the previous position of the system [34].

Provided the inverse of the rotation matrix exists, this equation can be reversed to give the conversion from the body frame to the inertial frame.

A matrix based on the Euler angles called the Direction Cosine Matrix (DCM) can be used to convert between angular velocities in the two frames [34].

The conversion from the angular velocities in the body frame to the inertial frame is given by [35]:

$$\begin{pmatrix} \dot{\varphi}_I \\ \dot{\theta}_I \\ \dot{\psi}_I \end{pmatrix} = \begin{bmatrix} 1 & \sin\varphi\tan\theta & \cos\varphi\tan\theta \\ 0 & \cos\theta & -\sin\varphi \\ 0 & \sin\varphi\sec\theta & \cos\varphi\sec\theta \end{bmatrix} \begin{pmatrix} \dot{\varphi}_B \\ \dot{\theta}_B \\ \dot{\psi}_B \end{pmatrix}$$

Expressions derived from this matrix equation were used to convert the gyroscope readings to the correct frame.

4 Project Plan and Methodology

This chapter outlines the process of research, design and implementation which will be used in this thesis to meet the stated objectives.

4.1 Dynamic investigation of the dragline mechanism

In accordance with the approach to bioinspired design followed in this project, it is necessary to thoroughly understand a biological feature before adapting it to an engineering application.

The first goal of this thesis is therefore to gain a robust understanding of how the dragline is used, and the different factors which affect the motion of the spider or robot during the jump. To do this, a dynamic model of the body and dragline system will be derived using Lagrange equations. The resulting model will then be simulated using MATLAB Simulink software, and the outcomes of varying different parameters of interest will be studied.

As this investigation will precede the design of the physical testing platform, the parameters used in the simulation will be based on rough predictions of the size of the platform and values which are found to give similar motion to that observed by Chen, et al [1]. Visualizations of the simulated motion will be compared to videos of the jumping spider, to validate the accuracy of the models used.

The results of the simulations will provide a base for adapting the dragline mechanism to a robotic platform. Analysis of the factors affecting the spider's motion will also be used to explain its observed behaviour by examining its jump as a control engineering problem.

4.2 Design of a line-equipped autonomous platform

Following the dynamic investigation, the next goal of the project is to design a line-equipped autonomous platform (or LEAP) which can be used to investigate the dragline mechanism through physical experimentation.

The design of the platform will be divided into three stages of increasing complexity. The first phase will be a simple testing model which can be used as a proof-of-concept to validate the role of the dragline in bringing about pitch rotation. The final phase will be able to actively control the tension in the dragline using a DC motor. In combination with sensors which can continuously track its angular position, this will make the platform suitable for testing controllers utilizing the dragline. The simulations produced in the previous phase of the project will be used to aid in design decisions where required.

4.3 Testing the LEAP design

The purpose of splitting the design phase into three stages is to prevent problems with the implementation of a complex design from holding back the testing process. The first stage represents the simplest possible testing system which can be used to demonstrate the ability of a dragline to induce pitch rotation in a mobile robot.

If time allows, each design stage will be tested on the same sub-horizontal jump as the simulations. Because the design of a controller falls outside the scope of this project, the goal of these tests is not to achieve an ideal landing, but rather to confirm that the dragline has the

expected effects on the pitch by comparing the results from jumps with and without tension in the line.

5 System Modelling and Simulation

In order to explain the motion of the spider observed in the literature, it was necessary to build up a dynamic model and simulation which could accurately capture the complexity of this system. Two different system models were ultimately used for this purpose.

5.1 Defining the System

The proposed final LEAP system is made up of three components: the robot body, the dragline and the launcher used to propel it into the air. The body consists of a chassis housing the electronics and a motor and spool system used to apply a pulling force on the dragline, and was modelled as a rectangular box of uniformly distributed mass. Simulation took place from the time the body leaves the launcher, so only the dynamics of the body and line were modelled.

The coordinates of interest are based on those used to document the motion of the spider in the study by Chen, et al [1] These are:

- the Cartesian coordinates of the centre of mass of the body, **x and y,** with the launch position taken as the origin,
- the abdomen angle $\boldsymbol{\Theta_A}$, the anticlockwise angle of the robot body axis relative to the x axis,
- the silk angle $\boldsymbol{\Theta_S}$, the anticlockwise angle of the dragline relative to the body angle.

These coordinates are shown in the diagram below:

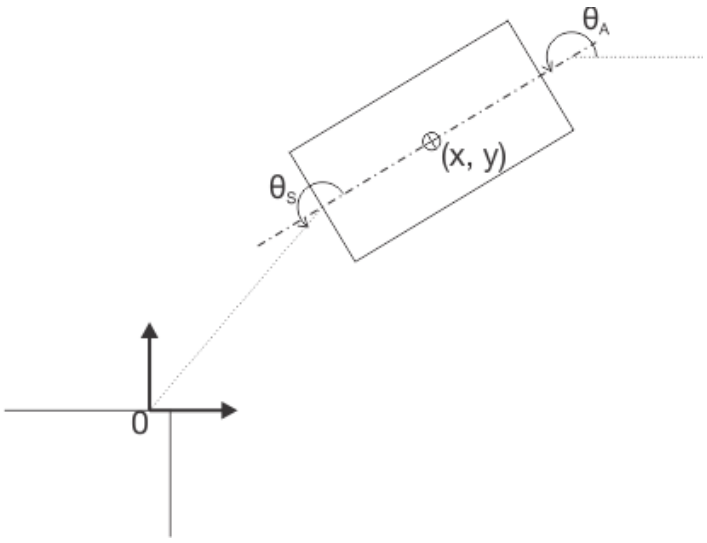

Figure 5: diagram showing coordinates of interest

In both models, the system was assumed to be confined to planar motion, therefore x, y and Θ_A represent the three degrees of freedom of motion available: translation in the x and y axes, and pitch rotation about the z axis.

5.2 Assumptions

The following assumptions and simplifications were common to both system models.

Moment of Inertia of the Body

The body was modelled as a rectangular box of uniformly distributed mass rotating about its centre of mass. Based on these assumptions, its moment of inertia can be calculated as [2]:

$$I = \frac{m}{12}(b^2 + l^2)$$

where m is the mass of the body, and b and l are the breadth and length respectively.

To minimize the force required to launch the platform, one of the design goals would be to keep the mass of the robot below 100 grams, so this value was used for the mass. The box was given dimensions of 10 x 5 x 5 centimetres, to match the size approximated from initial LEGO models of the chassis.

Calculation of Drag Force

The aerodynamic drag force was calculated using the equation:

$$F_D = \frac{1}{2}\rho c_d A v^2$$

where ρ is the mass density of air at 20˚C (1.2041 $kg.m^{-3}$) <ref>, c_d is the drag coefficient of a rectangular box (2.1) <ref>, A is the cross-sectional area of the body in the plane perpendicular to the direction of the velocity, and v is the magnitude of the velocity.

It was assumed that variations in the cross-sectional area due to changes in the body's angle of attack could be ignored without significantly impacting the accuracy of the model, so the drag force in the x direction (F_{Dx}) was calculated using the area of the front face of the body box (25 cm^2) while the drag force in the y direction (F_{Dy}) was calculated using the area of the top face (50 cm^2).

Simplifications of Spider Model

As this paper is focussed on the effects of the dragline, two other factors which could affect the aerial motion of the spider are neglected: the motion and position of the legs, and changes in the body posture (motion of the abdomen relative to the cephalothorax) during flight.

The spider does not flail its limbs, but rather elevates them dorsally throughout the jump [3], and the observed changes in body posture were small [1], so it is assumed that these factors are not part of the spider's active stability control mechanisms, but rather influence the drag force. The legs were neglected in the literature studied [1] [10] [3] and although Chen et al. did model the spider as two connected rigid segments, their relative movements were only taken into account through small adjustments of the drag coefficient [1]. It could therefore be assumed that the omission of these elements would not significantly impact the accuracy of the dynamic model, and would allow for the active control action of the dragline to be better isolated and studied.

5.3 Jump Parameters

All simulations were based on a scaled version of the experimental jump setup used by Chen, et al [1]. The supplementary material for this study included video footage of silk and non-silk spiders attempting this jump, so choosing these parameters would allow for this to be used as a direct visual comparison to validate the accuracy of the model.

The parameters of the jump are shown in Figure 6. Based on the average distance jumped by the spiders, the robot should land at a distance exceeding 1.25 metres, or 12.5 times its own body length. It would be launched from a height of 60 cm and an angle of 15 degrees to the horizontal.

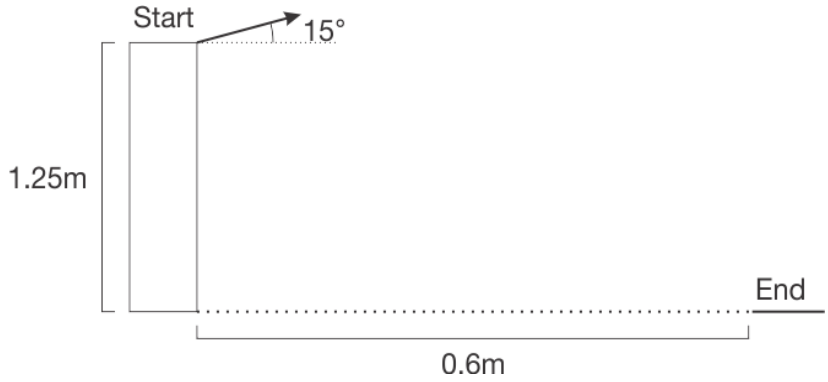

Figure 6: parameters of the jump on which the simulations were based

5.4 Model 1: Simple Model

The first attempt at modelling the system was a simplification of the model used by Chen, et al. [1] It modelled the system as a single rigid body – the robot body.

5.4.1 Assumptions

As in the study on the spider [1], it was assumed that three forces act on the body: gravity and aerodynamic drag (F_D) acting through the centre of mass, and the silk force (F_S) which acts at the point where the dragline attaches to the body. This point was taken to be in line with the centre of mass on the rearmost face of the body box. The direction of this force always pointed back to the origin, as this was taken to be where the silk connected to the substrate.

This free body diagram shows these forces.

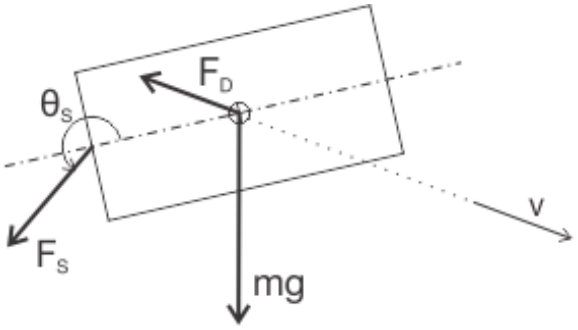

Figure 7: Free body diagram showing the forces acting on the robot body in Model 1

5.4.2 Equations of Motion

Lagrange dynamics was used to determine the equations of motion for this system, which could then be simulated using the Simulink software platform.

Three generalized coordinates were necessary to describe the motion: **x, y and θ_A.** These coordinates have the following characteristics:

- They can describe any possible position of the robot body, and are therefore *complete.*
- If any of the coordinates is held fixed, the others can still move through their full range. They are therefore *independent.*
- They are as many coordinates as there are degrees of freedom in the system. They are therefore *holonomic.*

The chosen coordinates therefore satisfy the requirements of a generalized coordinate system necessary for Lagrange dynamics to be used [32].

The gravitational force acting on the system is a conservative force, and therefore included within the potential energy term [31]. The silk force and drag force are non-conservative, and were hence taken into account as generalized forces [31].

Based on these parameters, the following equations were derived to describe the motion of the system:

$$m\ddot{x} = \pm F_{Dx} - F_S \cos(\theta_S + \theta_A) \tag{1.1}$$

$$m\ddot{y} + mg = \pm F_{Dy} - F_S \sin(\theta_S + \theta_A) \tag{1.2}$$

$$I\ddot{\theta_A} + mg = -\frac{1}{2} F_S l \sin(\theta_S) \tag{1.3}$$

where F_S is the magnitude of the silk force. The direction of the drag force varies as it must act opposite to the velocity.

5.4.3 Simulation Model

The equations of motion were simulated using MATLAB Simulink. V-Realm Builder, a Virtual Reality Modelling Language (VRML) editor, was used to produce animations of the robot body including the directions of the silk force and its components normal and tangential to the body axis. The virtual reality model representing the robot is shown in Figure 8.

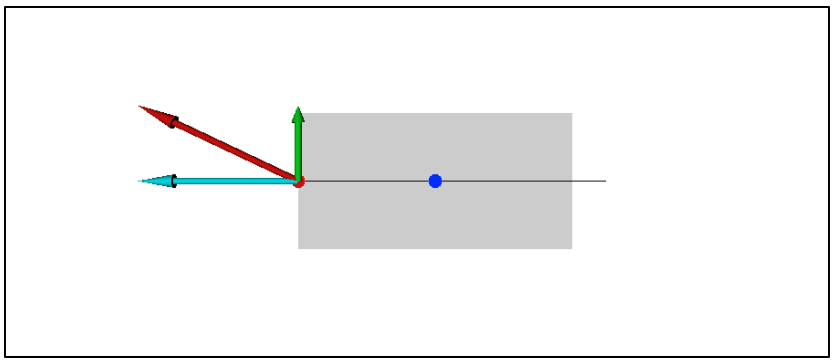

Figure 8: Virtual reality model representing the robot body in flight. The directions of the silk force (red) and its normal (green) and tangential (cyan) components relative to the body axis (black line) are shown.

Graphs of the changing position, velocity and acceleration of the body in terms of its x, y and Θ_A coordinates were also generated, as well as a graph of the silk angle over the course of the jump.

Figure 9 shows a simplified block diagram of the Simulink model used to simulate the robot. The vector of input constants contained the parameters of the robot body and the constants used in the calculation of the drag force. The generalised coordinates were grouped into a single vector $q = [x, y, \theta_A]$. Together with the constants in C, the initial values of the position (q_0) and the velocity ($\dot{q_0}$) were the inputs required to run the simulation.

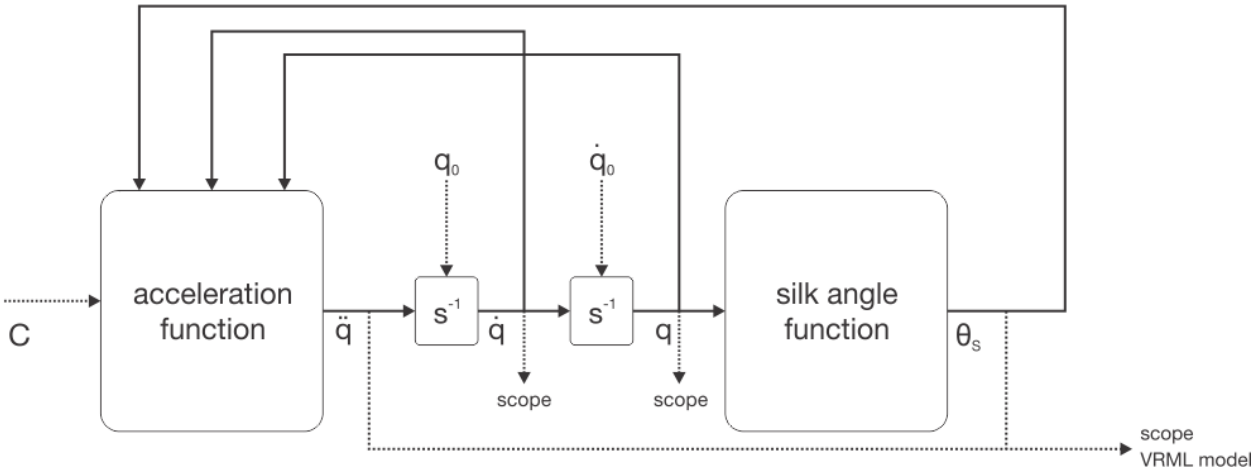

Figure 9: simplified block diagram of the simulink model representing Model 1. C is a vector of the input constants, and q is the vector of generalized coordinates.

Embedded MATLAB functions were required to calculate the silk angle from the current position and to calculate the acceleration vector ($\ddot{q_0}$). The velocity and position vectors were obtained by integrating the acceleration vector.

5.4.4 Purpose and Limitations

The role of this first model was to investigate the rotation of the body under varying magnitudes of silk force, and the ability of the line to affect the motion at different positions of the body relative to the substrate. These insights were required to give an initial idea of the control problems associated with this system.

In order to design the control mechanism for the LEAP, however, information about not only the force on the dragline, but its feed rate was required. As this model omitted the line entirely, a second, more complex model including the line was needed.

5.5 Model 2: Modified Double Pendulum Model

This model represents the dragline and body as two interacting rigid bodies in a similar configuration to the double pendulum system.

5.5.1 Assumptions

Rigid body assumption for the dragline

During the initial research phase of this project it was found that there are two different approaches to understanding the spider's use of the dragline.

The first approach focusses on the force which acts on the body due to the dragline. It forms the basis of the first model, where the body's motion is studied in isolation, and the dynamics of the line ignored.

The alternative is to regard the velocity of the line, rather than the force, as the controlling agent. This idea is illustrated in Figure 10. Assuming the line is inelastic and does not snap, the body can only reach positions within the range of the line. If the line can lengthen at a sufficient rate to accommodate it, the body will follow its ballistic trajectory without being affected, as in A. When the velocity of the line is constrained, however, the body will be forced to rotate or deviate from this trajectory, as in B.

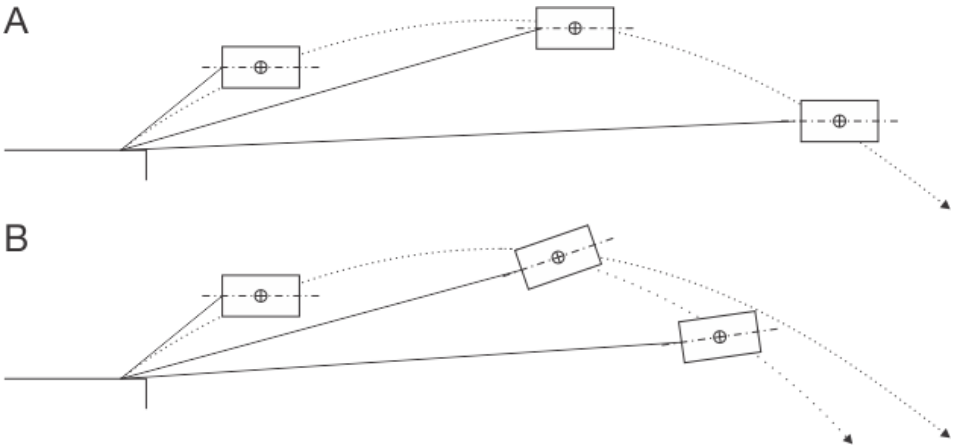

Figure 10: Diagram showing the effect of unconstrained (A) and constrained (B) line velocity on the motion of the robot body

The motion in A corresponds to the rate of extension at which the line ceases to exert a force on the body, as well as the highest rate at which it can feed out without overrunning and becoming slack. Therefore, in any situation where the line is exerting a controlling force on the body, it must be taut. Assuming that the line applies some force, however small, throughout the jump, the line will be taut over the full duration and can hence be modelled as a rigid body.

Under this condition, the dragline-body system can be represented as a double pendulum in planar motion, with the length of the first pendulum being variable rather than fixed. Because the mass of the line is very small in relation to the robot body, it was taken to be negligible.

Forces acting on the system

In this model, the aerodynamic and gravitational forces still act through the centre of mass of the robot body, but the silk force is now represented as a tensile force opposing the lengthening of the dragline. These forces are shown in the free body diagram below.

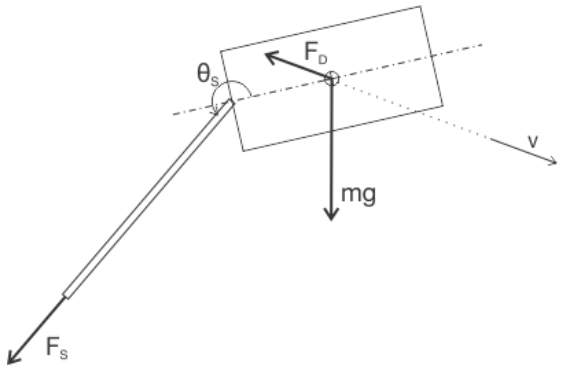

Figure 11: Free body diagram showing the forces acting on the robot body and dragline in model 2

Motor Model

For the purpose of the dynamic investigation, the tension in the dragline could be modelled as a constant force, but to aid in the design of the LEAP, it was necessary to incorporate a model representing the inherent constraints of the DC motor.

Assuming the motor operates within its constant power region, the relationship between the velocity of the shaft (ω_m) and the torque acting on it (τ_m) is:

$$\omega_m = \frac{V_t}{K} - \frac{R_a \tau_m}{K^2}$$

where V_t is the terminal voltage, R_a is the armature resistance and K is a constant depending on the geometry of the motor [5].

The force on the line is related to the torque by $F_m = rN\tau_m$ and the line speed is related to the shaft speed by $\dot{L} = \frac{r\omega_m}{N}$ where r is the radius of the spool and N is the gear ratio of the motor. The force acting on the dragline due to the motor at a particular speed and voltage was therefore evaluated using the equation:

$$F_m = \frac{KNr}{R_a} V_t - \frac{K^2 N^2}{R_a} \dot{L}$$

5.5.2 Equations of Motion

The double pendulum can be modelled more effectively using Lagrangian dynamics rather than Newtonian mechanics, so this approach was again used to derive the equations of motion.

Although x, y and Θ_A are still ultimately the coordinates of interest for the system, an alternative set of generalized coordinates was found to simplify the modelling process:

- The angle of the silk at the origin, $\boldsymbol{\Theta_0}$**,** anticlockwise from the horizontal.
- The silk angle $\boldsymbol{\Theta_s}$**,** anticlockwise from the body axis as defined previously.

- The length of the dragline, **L**.

These coordinates also satisfy the requirements of completeness, independence and holonomicity. The two coordinate systems could be related by the following equations:

$$x = L\cos(\theta_0) - \frac{1}{2}l\cos(\theta_0 - \theta_S)$$

$$y = L\sin(\theta_0) - \frac{1}{2}l\sin(\theta_0 - \theta_S)$$

$$\theta_A = \theta_0 - \theta_S$$

Both systems are represented in the following diagram.

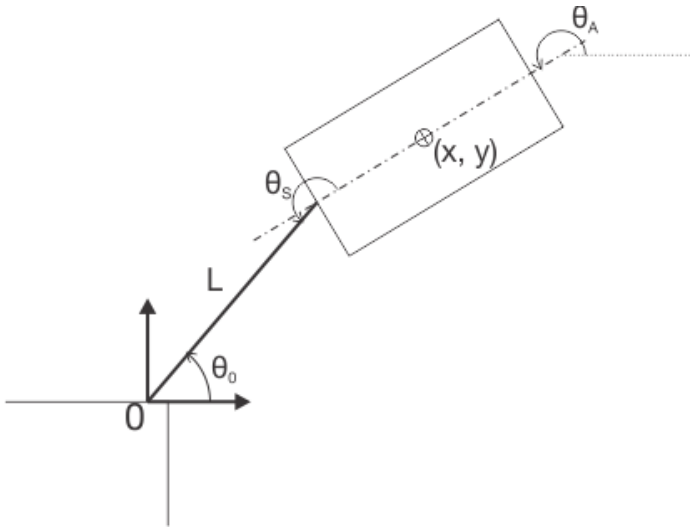

Figure 12: Diagram showing the two coordinate systems applied to Model 2

As in the previous model, the silk and drag forces were taken into account as generalized forces, while the gravitational force was included within the potential term of the Lagrangian.

Because the Lagrangian for this system was evaluated to be a much more complex expression than that of the previous model, the MATLAB Symbolic Math Toolbox was used to derive the equations of motion to reduce the high chance of computational errors associated with performing these calculations by hand.

This produced the following equations of motion for the model:

$$I(\ddot{\theta}_0 - \ddot{\theta}_S) + mL^2\ddot{\theta}_0 + \frac{1}{4}ml^2(\ddot{\theta}_0 - \ddot{\theta}_S) + mgL\cos\theta_0 - \frac{1}{2}mgl\cos(\theta_0 - \theta_S) + 2mL\dot{L}\dot{\theta}_0$$
$$-\frac{1}{2}ml\ddot{L}\sin\theta_S - mlL\ddot{\theta}_0\cos\theta_S + \frac{1}{2}mlL\ddot{\theta}_S\cos\theta_S - ml\dot{L}\,\dot{\theta}_0\cos\theta_S - \frac{1}{2}mlL\dot{\theta}_S^2\sin\theta_S + mlL\dot{\theta}_0\dot{\theta}_S\sin\theta_S \qquad (2.1)$$
$$= \pm F_{Dx}\left(-L\sin\theta_0 + \frac{1}{2}l\sin(\theta_0 - \theta_S)\right) \pm F_{Dy}\left(L\cos\theta_0 - \frac{1}{2}l\cos(\theta_0 - \theta_S)\right)$$

$$I(\ddot{\theta}_S - \ddot{\theta}_0) + \frac{1}{4}ml^2(\ddot{\theta}_S - \ddot{\theta}_0) + \frac{1}{2}mgl\cos(\theta_0 - \theta_S) + \frac{1}{2}ml\ddot{L}\sin\theta_S$$
$$+\frac{1}{2}mlL\ddot{\theta}_0\cos\theta_S + ml\dot{L}\dot{\theta}_0\cos\theta_S - \frac{1}{2}mlL\dot{\theta}_0^2\sin\theta_S = \pm\frac{1}{2}lF_{Dx}\sin(\theta_0 - \theta_S) \pm\frac{1}{2}lF_{Dy}\cos(\theta_0 - \theta_S) \quad (2.2)$$

$$m\ddot{L} + mg\sin\theta_0 - mL\dot{\theta}_0^2 - \frac{1}{2}ml\ddot{\theta}_0\sin\theta_S + \frac{1}{2}ml\ddot{\theta}_S\sin\theta_S + \frac{1}{2}ml\dot{\theta}_0^2\cos\theta_S + \frac{1}{2}ml\dot{\theta}_S^2\cos\theta_S$$
$$- ml\dot{\theta}_0\dot{\theta}_S\cos\theta_S = -F_M \pm F_{Dx}\cos\theta_0 \pm F_{Dy}\sin\theta_0 \quad (2.3)$$

5.5.3 Simulation Model

In order to simulate these equations, the coefficients of the acceleration terms in each equation were grouped into a 3x3 matrix A, while the coefficients of the velocity and position and the constant terms were grouped into the 3x3 matrices B_1, B_2 and the 3x1 matrix B_3 respectively. The acceleration at each instant was then determined by solving the matrix equation

$$A\begin{bmatrix}\ddot{\theta}_0\\ \ddot{\theta}_S\\ \ddot{L}\end{bmatrix} = B_1\begin{bmatrix}\dot{\theta}_0\\ \dot{\theta}_S\\ \dot{L}\end{bmatrix} + B_2\begin{bmatrix}\theta_0\\ \theta_S\\ L\end{bmatrix} + B_3$$

or in compact form,

$$A\ddot{q} = B_1\dot{q} + B_2 q + B_3$$

As before, the simulation was implemented in MATLAB Simulink, with a virtual reality model created in V-Realm builder used to visualize the motion of the dragline and robot body. This model is shown below.

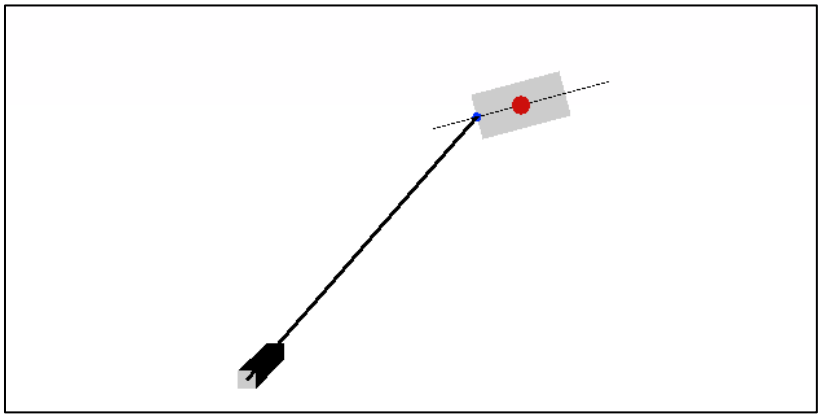

Figure 13: Virtual reality model representing the double pendulum model of the robot body and dragline

The acceleration, velocity and position values were also graphed in terms of both coordinate systems considered.

Figure 14 shows a simplified block diagram of the Simulink model used to simulate this system. The input constants vector C includes the parameters of the robot body, and the constants required for the drag and motor force calculations. The initial position and velocity values were defined in terms of their [x, y, Θ_A] values and mapped to the [Θ_0, Θ_S, L] system prior to the simulation being run.

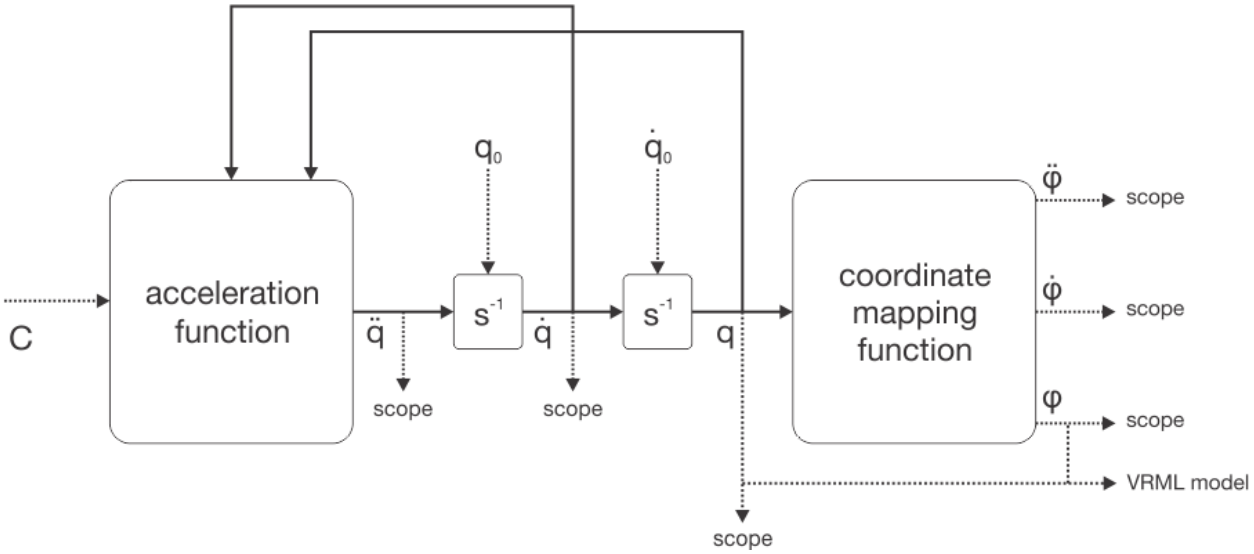

Figure 14: simplified block diagram of the Simulink model representing Model 2. C is the vector of input constants, q is the vector of generalized coordinates [Θ_0, Θ_S, L] and φ is the mapping of q to the [x, y, Θ_A] coordinate system.

As before, an embedded MATLAB function (the acceleration function in the figure) was used to work out the vector of acceleration values, which was then integrated to give the velocity and position vectors. Another embedded function (the coordinate mapping function) was used to convert these to φ and its derivatives – the position, velocity and acceleration vectors in terms of [x, y, Θ_A] coordinates.

5.6 Effects of Inaccurately Approximated Parameters

In the previous chapter, it was stated that the dynamic models and corresponding simulations were intended as tools for both the analysis of the dragline and the design of the LEAP. To achieve the first of these, it was beneficial to simplify the system as far as possible without compromising accuracy so the effects of the dragline could be isolated. In reality, however, the robot is unlikely to conform to its approximation as a uniform rectangular box of the stated size.

If the robot is larger, smaller or shaped differently to the approximated box, its moment of inertia will be inaccurate, and consequently the force required to achieve a particular rotational acceleration will be different to that shown in the simulation. Its coefficient of drag will also be increased or decreased. To account for this, any design decisions based on the simulation must be shown to give acceptable results for ±20% variation in the moment of inertia of the body and its drag coefficients.

Because of the different densities of the various components housed within the robot body, its centre of mass may be shifted from the geometric centre. One result of this could be that the robot tends to rotate backwards or forwards following launch. As the spiders were observed to jump with some initial pitch velocity [1] [6] [3], the effects of this initial condition will be studied as part of the system description phase, and velocities of up to ±π will be accommodated in the design phase. A more problematic result would be that the unbalance produces yaw or roll, as these cannot be accounted for in the existing simulation models. The robot body will therefore have to be carefully balanced during construction to ensure that it does not tend to rotate about the x and y axes.

5.6.1 Summary

Two different dynamic models were developed to simulate the effects of the dragline on the motion of the body. The first modelled the robot as a single rigid body, while the second modelled the dragline and robot as two rigid bodies interacting in a similar manner to a double pendulum. This chapter discussed the development of these models, and how their equations of motion were derived and simulated. Assumptions and simplifications made while modelling the system, and their potential impacts on the system identification and design phases, were also stated.

6 Dynamic Analysis of Dragline-Assisted Pitch Righting

6.1 Testing Methodology

To meet the objectives of this project, it was first necessary to gather information about the factors affecting the spider's motion. To do this, the two dynamic models derived were used to simulate the effects of varying the following parameters on the jump:

- The magnitude of the silk force applied
- The magnitude and angle of the launch velocity
- The magnitude of the initial pitch rotation

Based on the characteristics of a 'good' landing defined in the literature, the experiments concerned their impacts on the range of the jump, the velocity at the time of landing and the changes in the abdomen angle throughout the jump.

Rather than running for a fixed time, the simulation was configured to stop automatically when the body reached the designated landing y position of 0.6 meters below the starting point.

Trends were obtained by running multiple simulations using nested *for loops,* and plotting the relevant outputs on a graph. Each test consisted of sweeping the silk force and another parameter of interest, to obtain different output vs. silk force curves for each value of that parameter.

Although the spider tended to decrease the force on the dragline towards the end of the jump [1], to isolate the role of the magnitude specifically, this force was held constant for the duration of each individual simulation.

6.1.1 Test Values

Unless otherwise stated, values over the following ranges were used for each of the testing parameters:

Silk force was swept from zero to the proposed body weight of the robot, using a step size of 0.1 times the body weight. Zero force represents the non-silk condition, while a force equivalent to the body weight is around half of that required to bring the spider to standstill while descending a vertical line [1]. Some tests were also run with the force held constant at 0.26 and 0.4 times the body weight. These values represent the average and maximum forces observed for aerial righting during jumps [2].

Launch velocity (v_0) was swept between 2.5 and 5.5 meters per second, with a step size of 0.5 m/s. This range was selected because, for the step size used, 2.5 m/s was found to be the smallest velocity for which the non-silk robot would reach the target distance of 1.25 metres, while 5.5 m/s was found to be the smallest velocity where the robot would clear this distance over the full range of forces tested. It does not correspond to the values of initial velocity observed in the literature, as scaling the average value recorded by Chen, et al [2] to the body length of the robot would give a velocity of around 16.2 m/s, which appeared unrealistically large.

When tests required a constant velocity, a value of 4 m/s was used as this was found to give outputs relatively close to those observed in the spider for similar magnitudes of silk force.

The angle of the launch velocity (Θ_L) was swept between 0 and 45 degrees (anticlockwise from the horizontal) at 15 degree intervals, as this was the range generally observed in the literature [3]. An angle of 15 degrees was used when this parameter was held constant, as this is close to the average launch angle observed by Chen, et al [2].

Initial pitch velocity ($\dot{\theta}_A$) was swept between zero and π radians per second, using a step size of π/4 rad/s in both clockwise and anticlockwise directions. The maximum value of π rad/s was selected as, when combined with zero silk force, this gave a similar near-vertical landing posture to that observed in non-silk spiders [2]. In tests not directly concerned with the initial pitch, the body was given no initial rotation.

The test values discussed are summarized in the table below:

Table 1: Experimental parameter values used in simulations

	Sweep				
Parameter	**start**	**step**	**end**	**Constant**	**Unit**
Silk force	0	0.1	1	0.26 or 0.4	n x BW
Launch velocity	2.5	0.5	5.5	4	m/s
Launch angle	0	15	45	15	deg (ccw)
Initial pitch	-π	π/4	π	0	rad/s (ccw)

6.2 Factors affecting jump range

The set of tests focussed on the range of the jump – the final x value output from the simulation.

As would be expected, increasing the launch velocity was found to increase the range of the jump. Model 2 showed a near-linear decrease in range for increasing silk force at each velocity. The results for Model 1 were similar, but at some velocities, the range increased slightly when a small silk force was applied (0.1 BW's) compared to the non-silk condition. These results are shown in Figure 15.

The tendency for jump range to decrease with increasing silk force would continue throughout the tests conducted.

Figure 16 shows the results for varying the angle of the launch velocity. Both models showed that a steeper launch angle tends to increase the range of the jump for smaller magnitudes of silk force, but decrease the range when more force is applied.

The initial pitch velocity appeared to have little effect on the range of the jump. Model 2 showed near-identical plots for different values, and the plots from Model 1 also tended to converge at larger magnitudes of silk force. These plots are given in Figure 17.

To establish the relationship between the initial pitch velocity and range for smaller silk forces (i.e. forces below 0.3 BW) in Model 1, additional tests were run sweeping the clockwise and counter-clockwise directions separately. For backward rotation, increasing the pitch velocity

appears to increase the range, but there appears to be no correlation between pitch velocity and range for forward rotation. The results of these tests are shown in Figure 18.

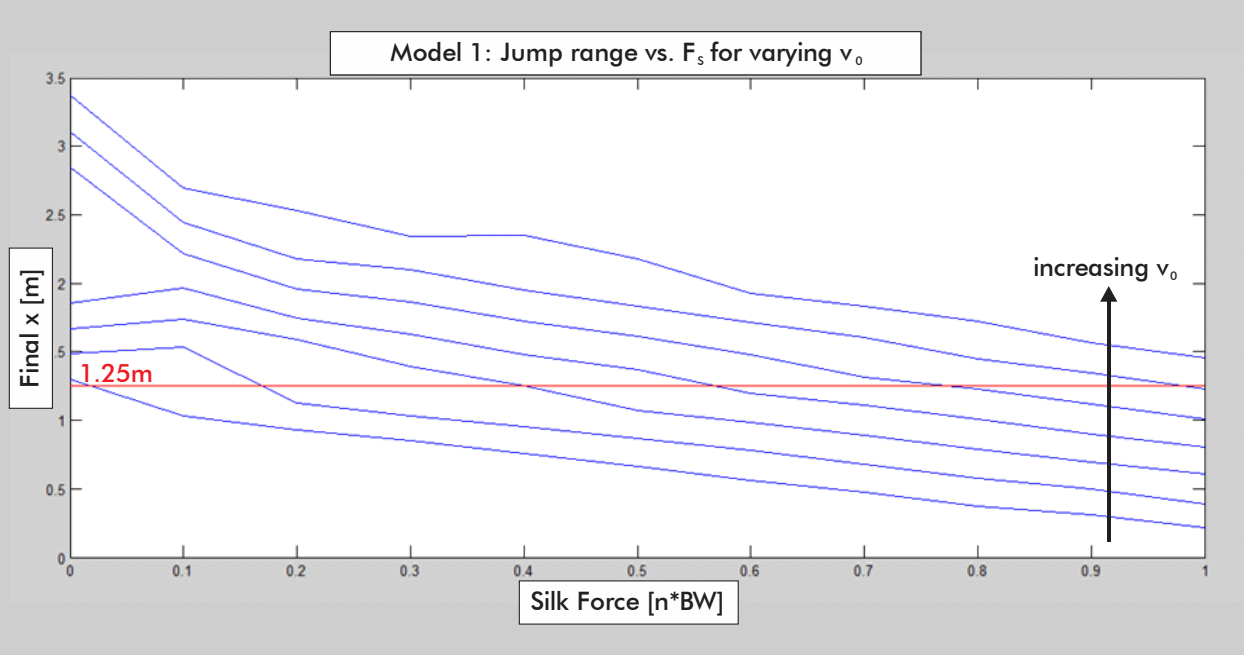

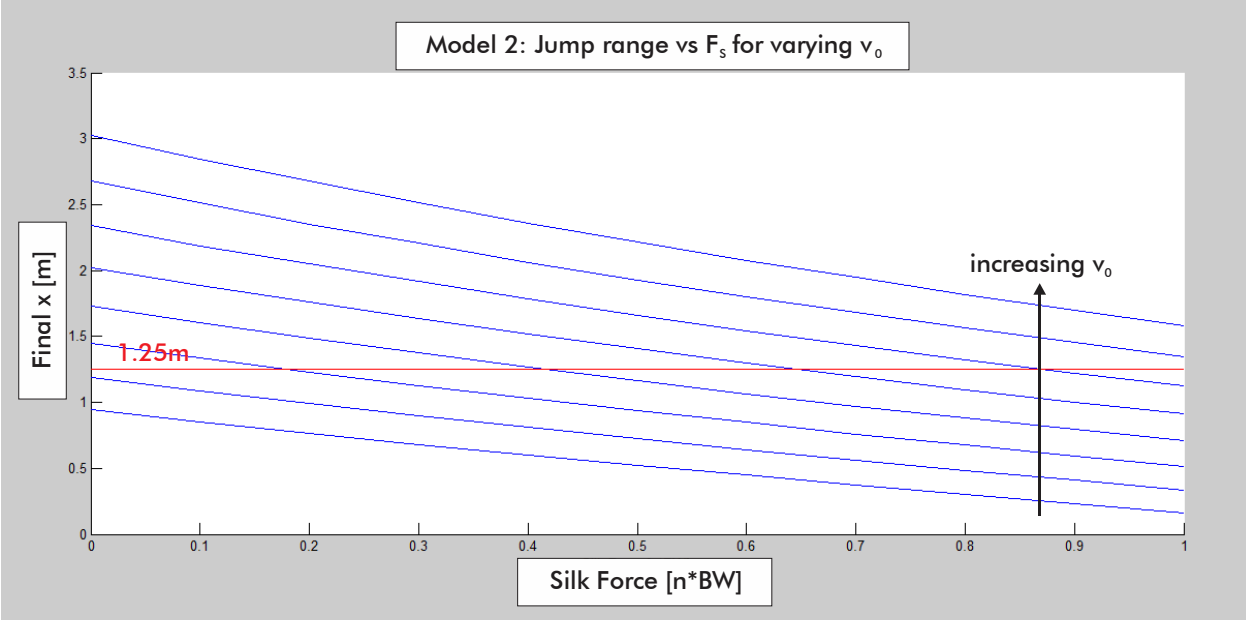

Figure 15: Results for jump range vs. silk force for varying launch velocity. Range increases with launch velocity, and tends to decrease with the magnitude of the silk force applied.

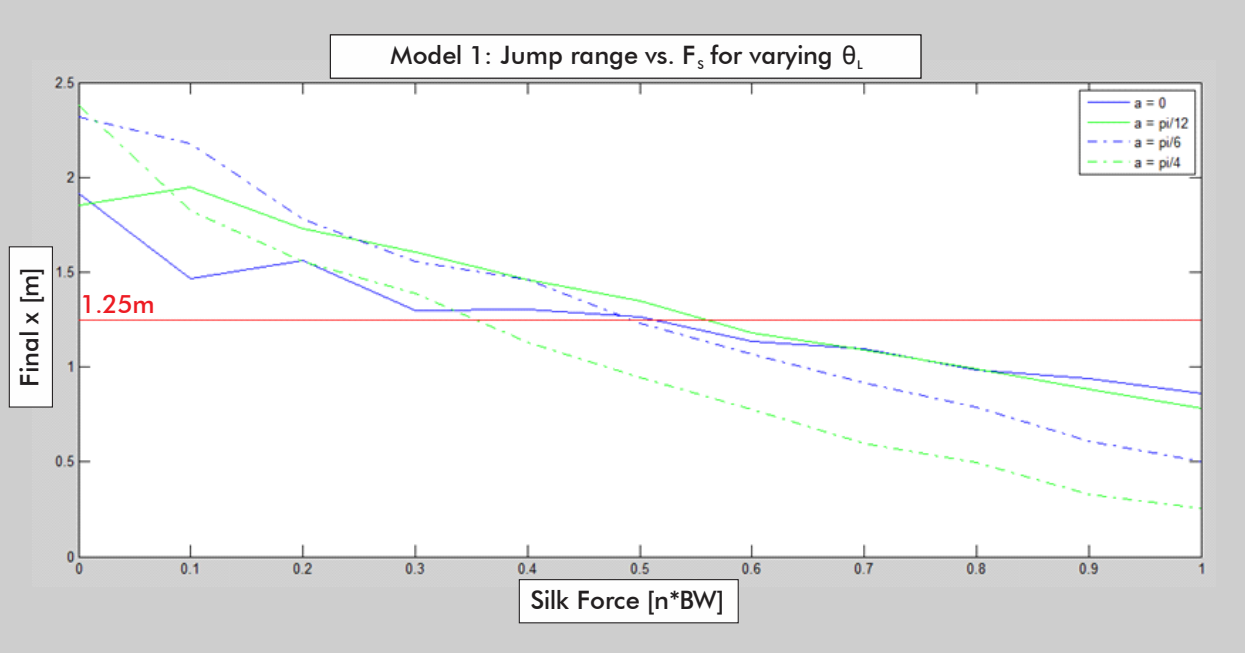

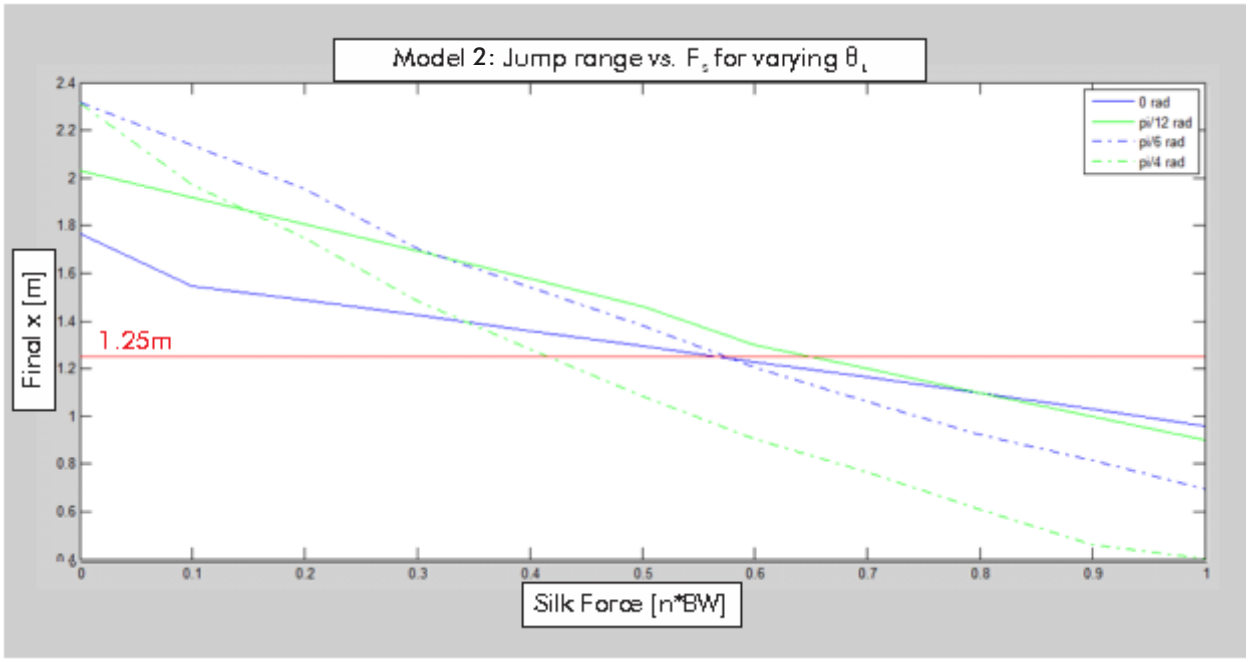

Figure 16: Results for jump range vs. silk force for varying launch angle. At lower magnitudes of silk force, increasing launch angle tends to increase range, while steeper angles reduce the range for larger silk forces.

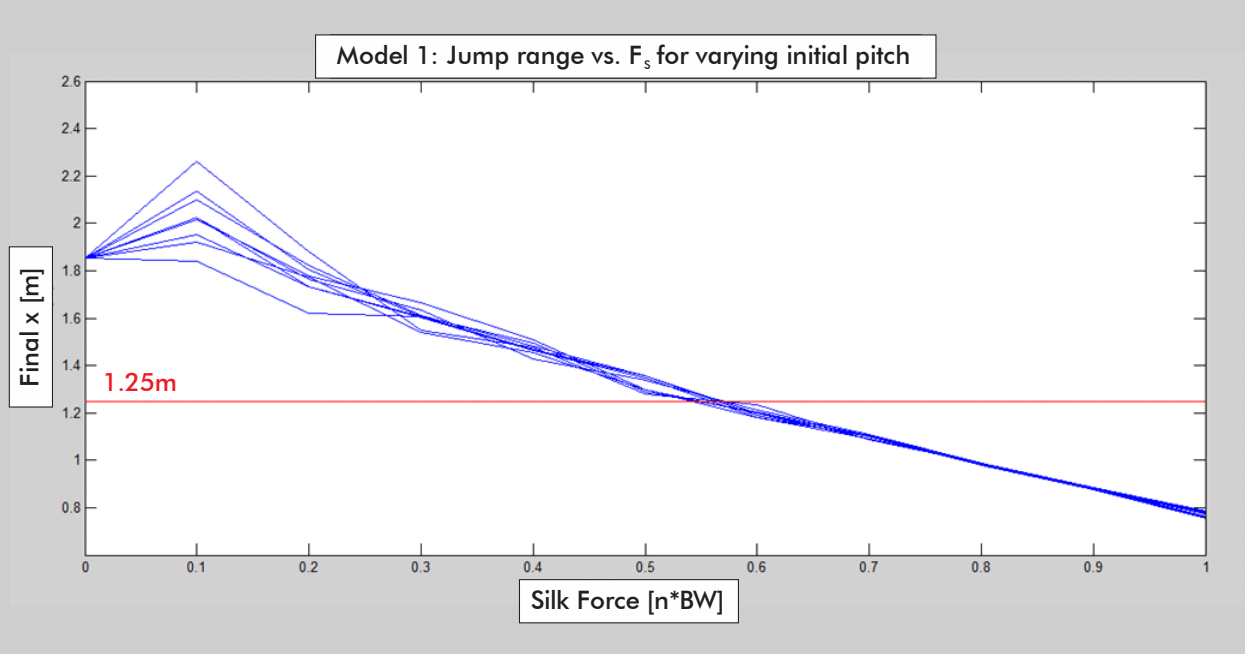

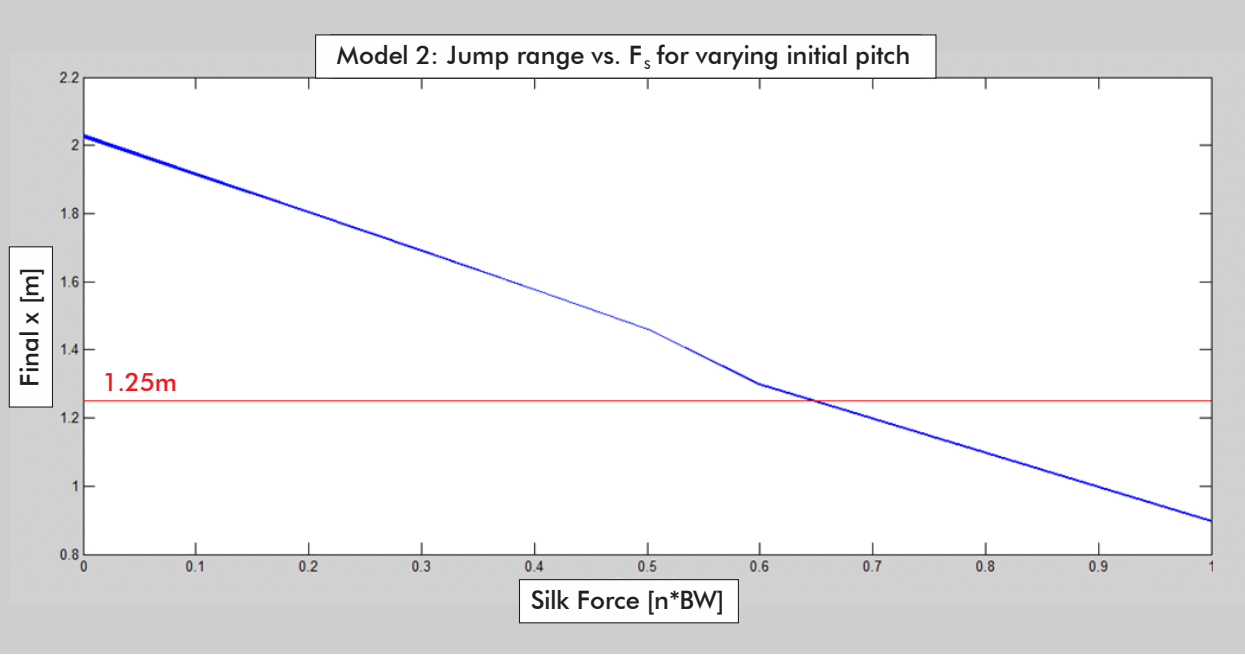

Figure 17: Results for jump range vs. silk force for varying initial pitch velocity. For both models, initial rotation had little impact on the range at larger magnitudes of silk force.

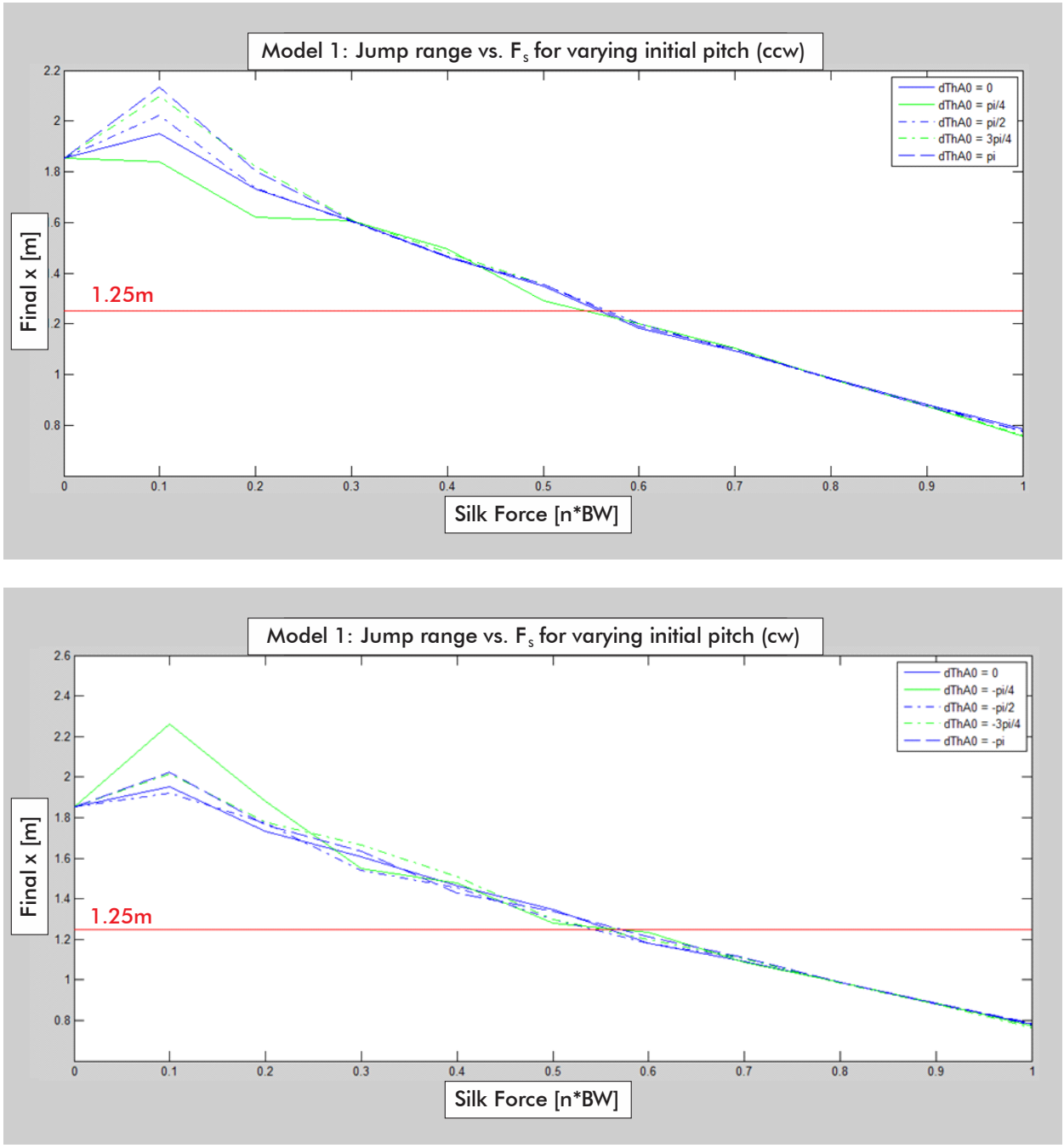

Figure 18: Model 1 results for jump range at varying initial pitch isolated by direction of rotation. For backward (ccw) rotation, increasing the pitch velocity increases the range, but for forward rotation, there appears to be no correlation between the rotational velocity and the range.

6.3 Factors affecting final horizontal velocity

The next set of tests addressed the final velocity in the horizontal direction. The purpose of this test was to establish the role of the silk force combined with the other parameters considered in braking, so rather than actual the magnitude of the velocity, the concern was its reduction as a percentage of the initial velocity.

Because the simulation does not capture the aftermath of the landing, a benchmark value for the braking had to be assumed based on the observations in the literature. In the study by Chen et al [1], the silk spiders were found to decrease their x velocity by an average of 37%. This value was used as the target, but from the range of values observed in this study, it can be assumed that a reduction of more than 30% would be sufficient to prevent overpitch on landing.

The reductions in velocity from different initial velocities are displayed in Figure 19. For both models, larger initial velocities were observed to lead to a smaller relative decrease in the final velocity. At velocities below 5 m/s, the negative output values indicate that larger magnitudes of silk force would eventually cause the direction of the x velocity to reverse and the robot to swing back towards its starting point.

As can be seen in Figure 20, steeper launch angles were also found to cause greater reduction in the x velocity over the course of the jump.

In addition to having little effect on the range of the jump, the initial pitch does not appear to have a significant impact on the deceleration. The plots from both models do not vary significantly for different rotational velocities, as displayed in Figure 21.

Throughout these tests, increasing the magnitude of the silk force caused greater reductions in the velocity. The target amount of braking tended to occur for magnitudes of silk force between 0.2 and 0.4 times the body weight.

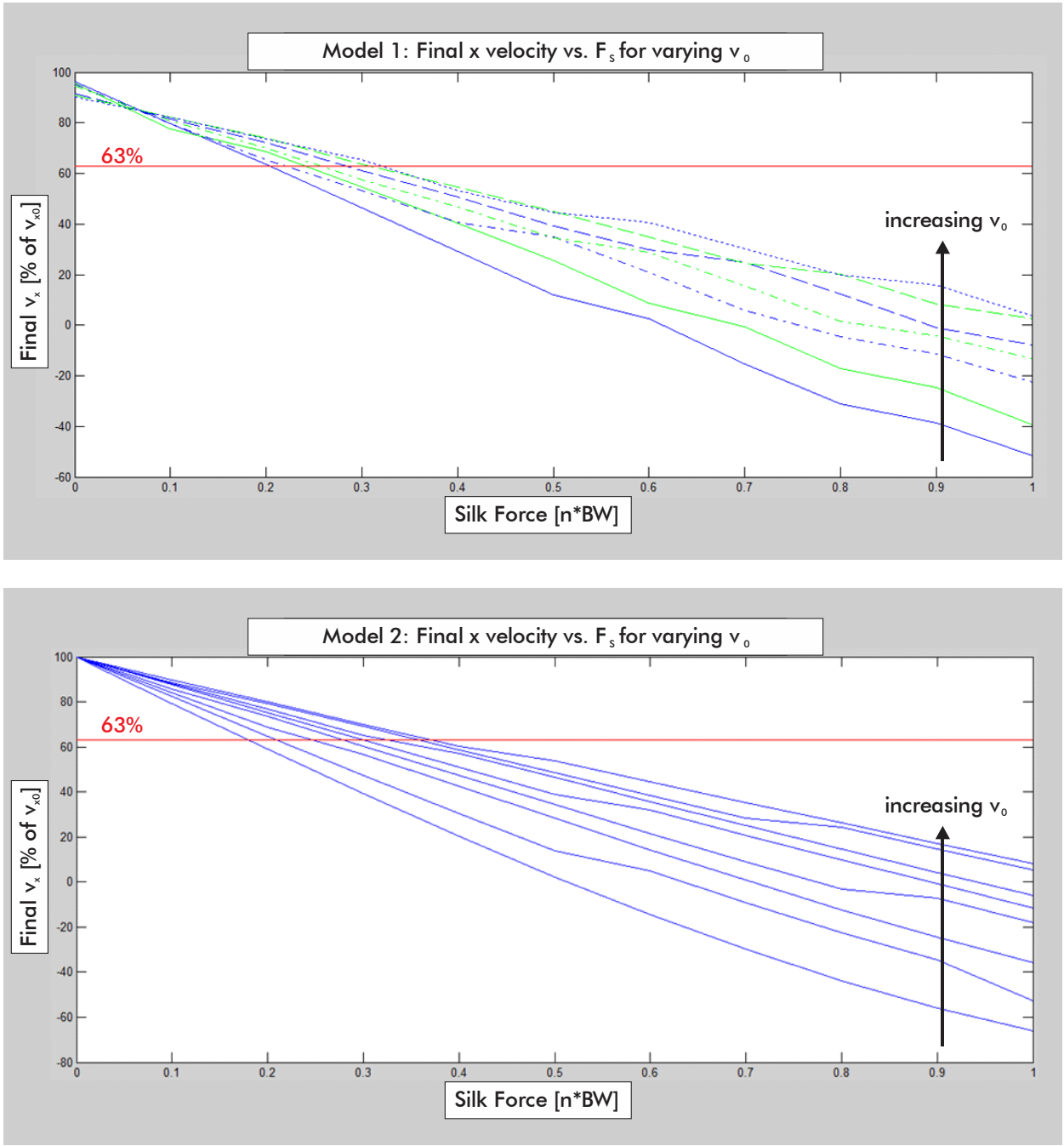

Figure 19: Results for the final x velocity (as a percentage of the initial velocity) at varying launch velocities. Increasing launch velocity results in less relative reduction in the x velocity. Negative values indicate a reversal in the direction of motion.

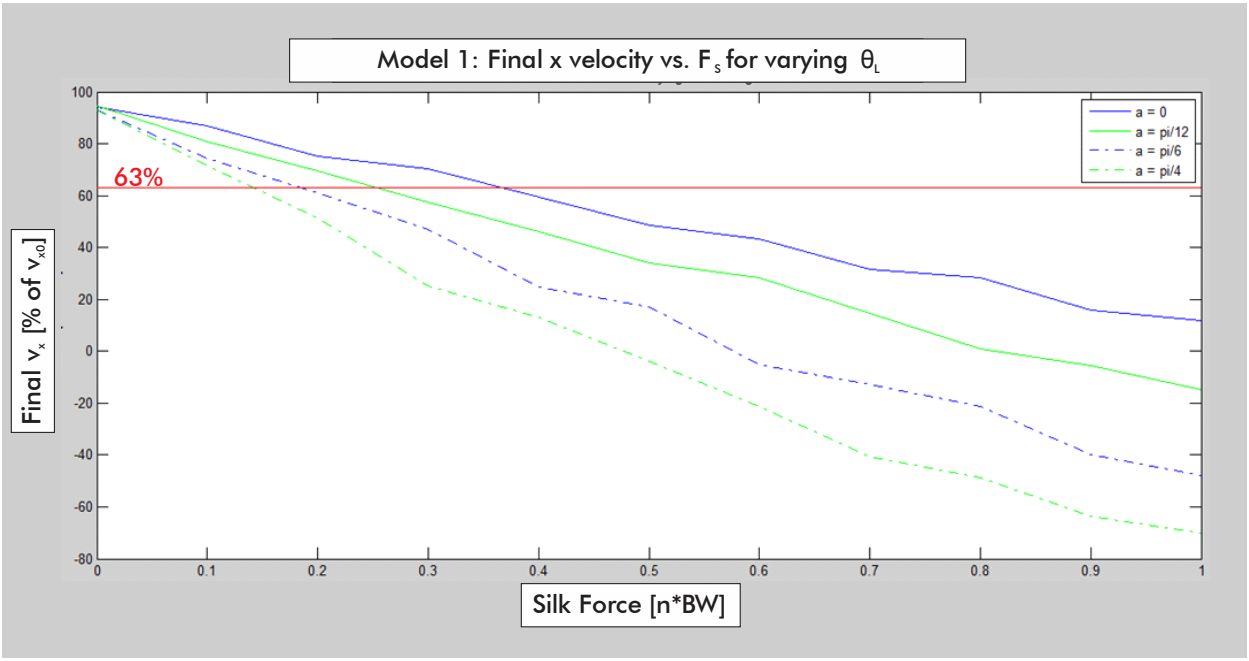

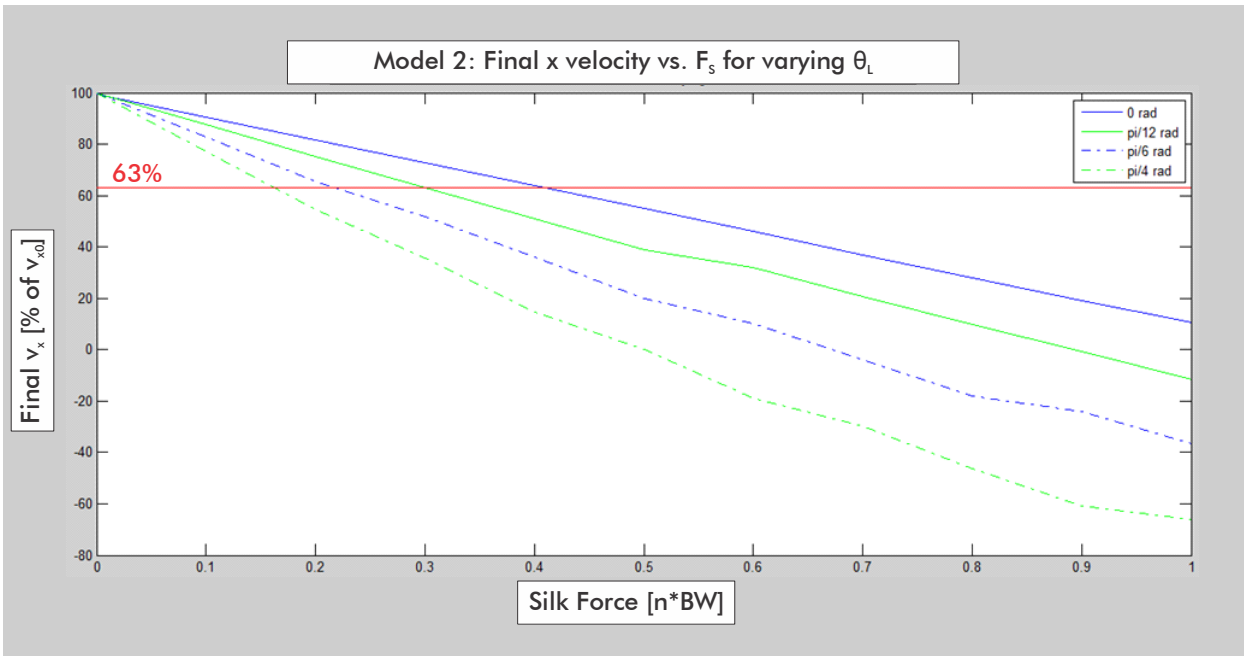

Figure 20: Results for the final x velocity (as a percentage of the initial velocity) at varying launch angles. Increasing launch angle results in greater reduction in the x velocity over the course of the jump.

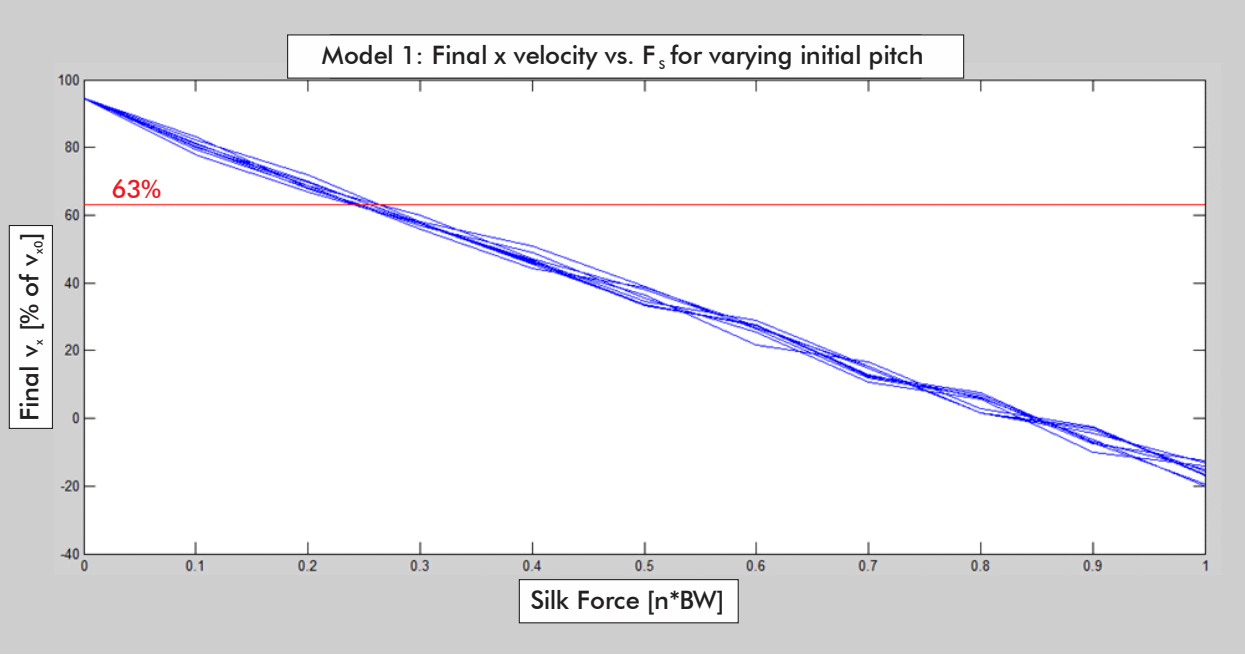

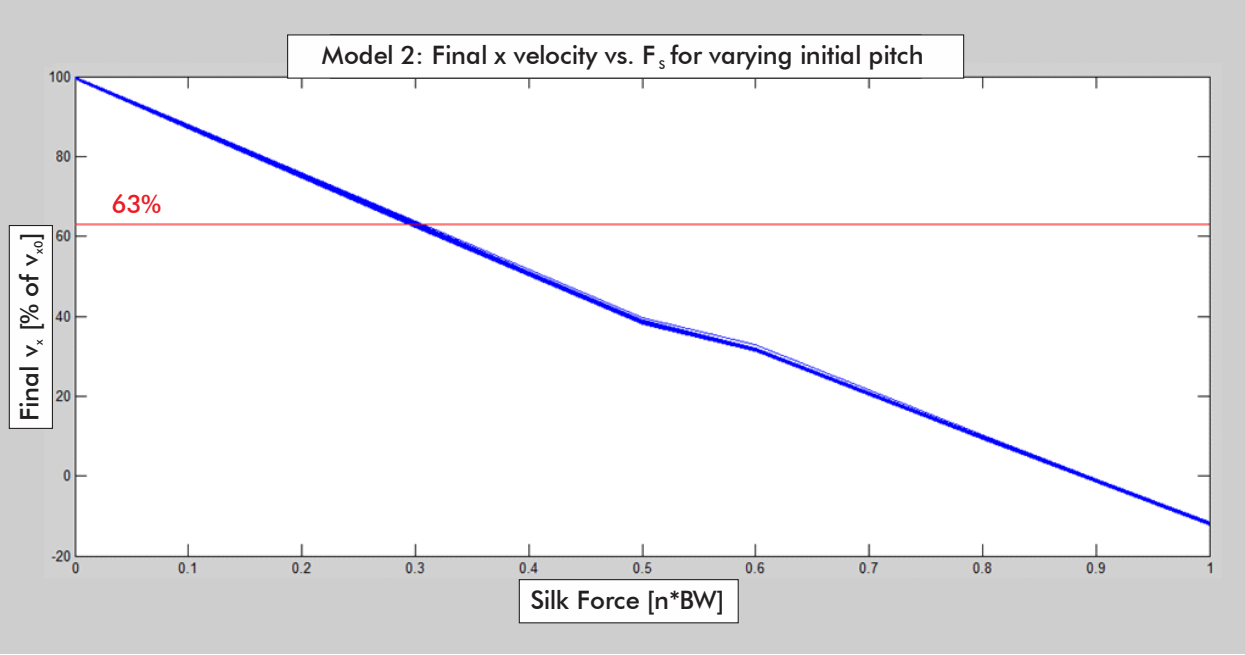

Figure 21: Results for the final x velocity (as a percentage of the initial velocity) at varying velocities of initial pitch. The initial rotation appears to have no significant impact on the final velocity.

6.4 Factors affecting abdomen angle response

The final set of tests was concerned with the changes in the abdomen angle throughout the jump. Besides the proximity of the final angle to the target of 180 degrees, other features of interest included the number of pitch reversals, the angles at which these reversals occurred and the number of 180 degree crossings.

Unlike the previous tests, where silk force had been varied together with other parameters, for these tests, it was considered in isolation. The simplest test utilized Model 1; the position of the centre of mass was held constant, and a constant silk force was applied. This was repeated for silk forces in the same range of magnitudes used in previous tests, and gave the results shown in Figure 24. It can be seen that the application of a constant silk force at constant position produced sinusoidal oscillation in the abdomen angle. Increasing the magnitude of the force increased the frequency of the sinusoid, but not its amplitude – the turning points occurred at the same angles.

Figure 25 shows the results from both models for varying silk force in the context of the moving robot. Again, the basic form of the response is sinusoidal, but consecutive pitch reversals now occur at different angles. When this same experiment was allowed to run for two seconds, rather than being stopped at the designated y value, the curves given in Figure 26 were produced. From these, the sinusoid seems to remain at constant magnitude, but be shifted by a value which tends asymptotically to 90 degrees. A possible mathematical representation of this is the function:

$$\theta_A = A\cos\left(\frac{2\pi t}{\omega} - \Phi\right) + Be^{-\frac{t}{\Omega}} + \frac{\pi}{2}$$

The parameters of this equation are illustrated in the figure below:

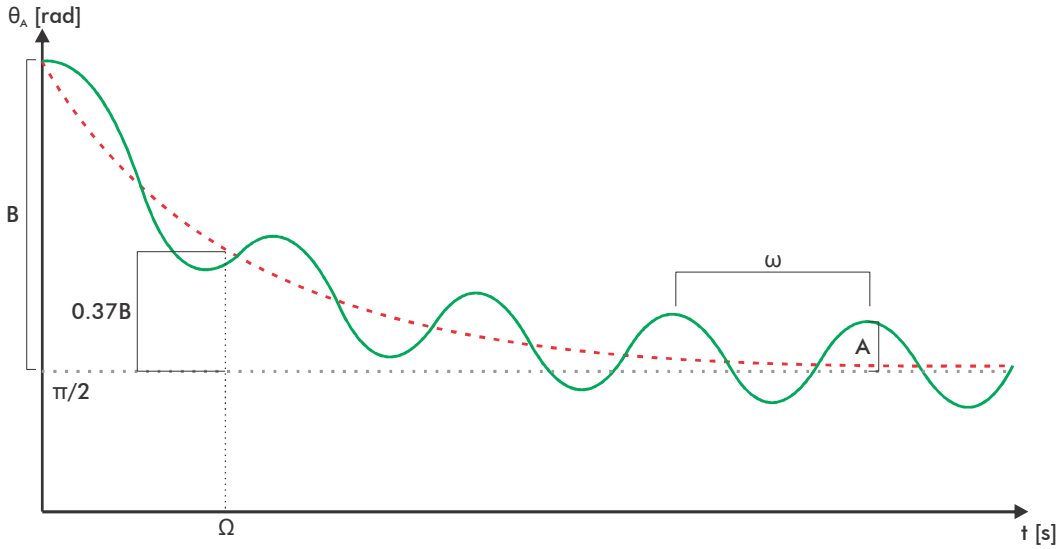

Figure 22 diagram of the approximated abdomen angle response for zero phase shift. The red dashed line represents the exponential term and the dotted line indicates pi/2.

As observed in the first test, the frequency of the sinusoidal term (ω) appears to increase with the magnitude of the silk force.

Figure 26 gives the curves produced over a two second period for varying launch velocity and a constant silk force of 0.4 body weights. Based on these results, the time constant of the exponential term (Ω) seems to decrease with increasing launch velocity. When the results for different launch velocities are plotted on the same axis, as in Figure 27, it can be seen that this has the effect of increasing the angle at which the latter turning points take place. For the applied silk force, Model 2 indicates that a launch velocity of at least 7 m/s is required to produce a second 180 degree crossing within the course of the jump.

Because the models were configured such that the initial position of the body axis is parallel to the launch direction, the launch angle determines the starting angle for the jump. Using the stated mathematical representation, this means increasing the launch angle increases the amplitude of the exponential term (B).

The launch angle also appears to affect the amplitude of the sinusoidal term (A). According to Figure 28 which shows the responses over a two second period for different launch angles, and Figure 29 which plots them on the same axis, the amplitude will first decrease with increasing launch angle up to some turning point, and then begin to increase as the launch angle increases beyond this point. At the turning point angle, the amplitude will be close to zero. The plots for 30 and 45 degrees for Model 1 and Model 2 respectively show little sinusoidal oscillation, so it is assumed that these values are close to the turning points for the each model.

The amplitude of the sinusoid also appears to depend on the initial pitch. Figure 30, which shows the results for different magnitudes of backward pitch, indicates that faster initial rotation increases the amplitude of the sinusoid. For forward rotation, it was necessary to generate plots for a range of velocities up to 2π radians per second to see the true trend: based on the plots generated by Model 1, for rotation of less than π rad/s (shown in blue in Figure 31) the amplitude decreases with increasing pitch, but for faster rotation (shown in green), the amplitude begins to increase with the velocity. Model 2 produced similar results, but the turning point velocity appears to occur between 1.25π and 1.5π rad/s.

The plots for forward rotation also show that the initial pitch influences the phase of the sinusoid (Φ). As the pitch increases in the clockwise direction, negative phase shift occurs – the sinusoid shifts to the right.

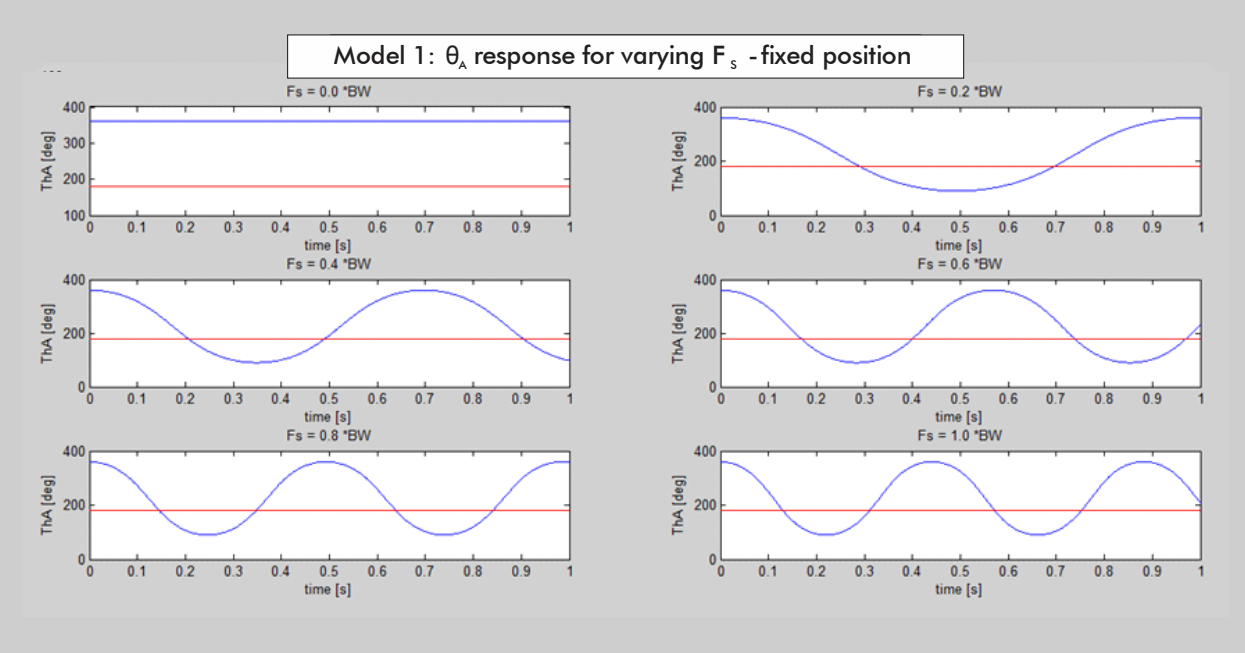

Figure 23: Plots of the abdomen angle response for different magnitudes of silk force and fixed centre of mass position. The responses take a sinusoidal form, and their frequency increases with increasing force. (red line = 180 degrees)

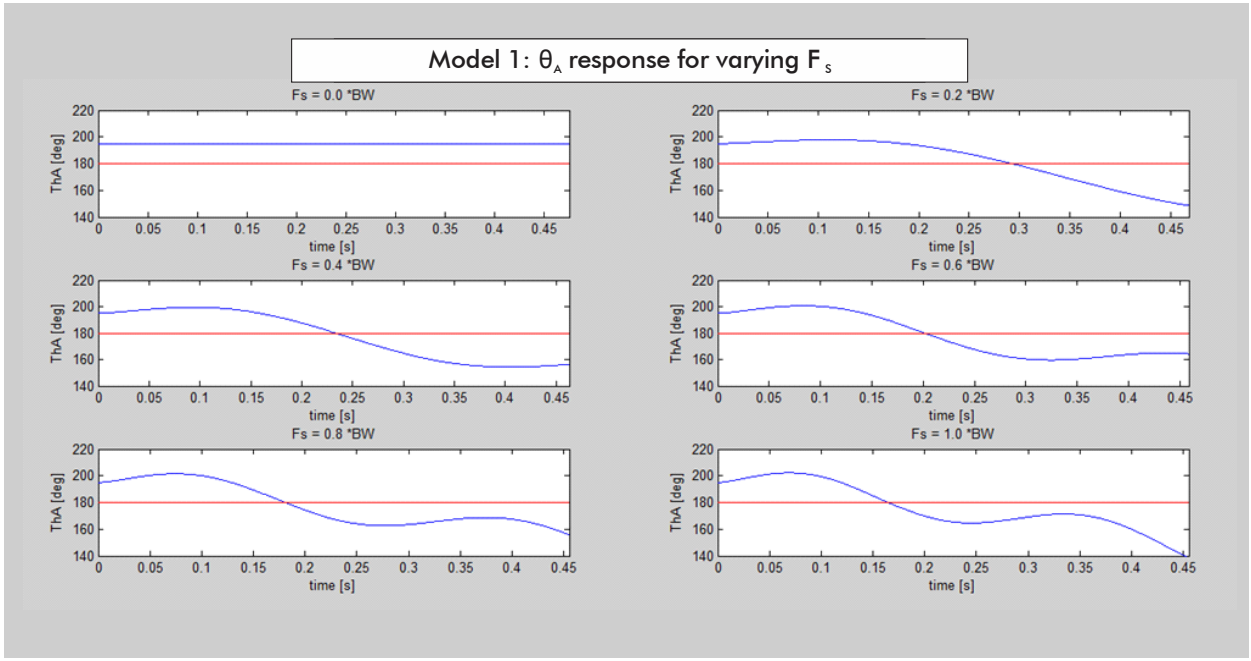

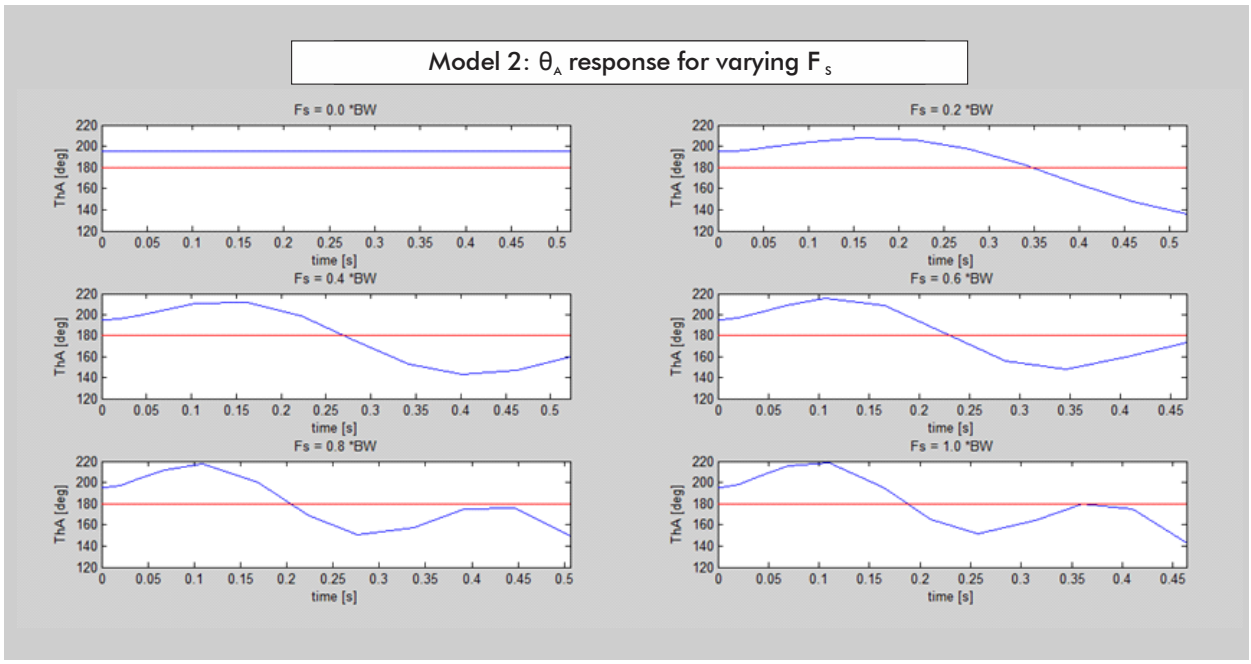

Figure 24: Abdomen angle responses for varying magnitudes of silk force. The responses are basically sinusoidal in form, with the frequency increasing with the silk force. (red line = 180 degrees)

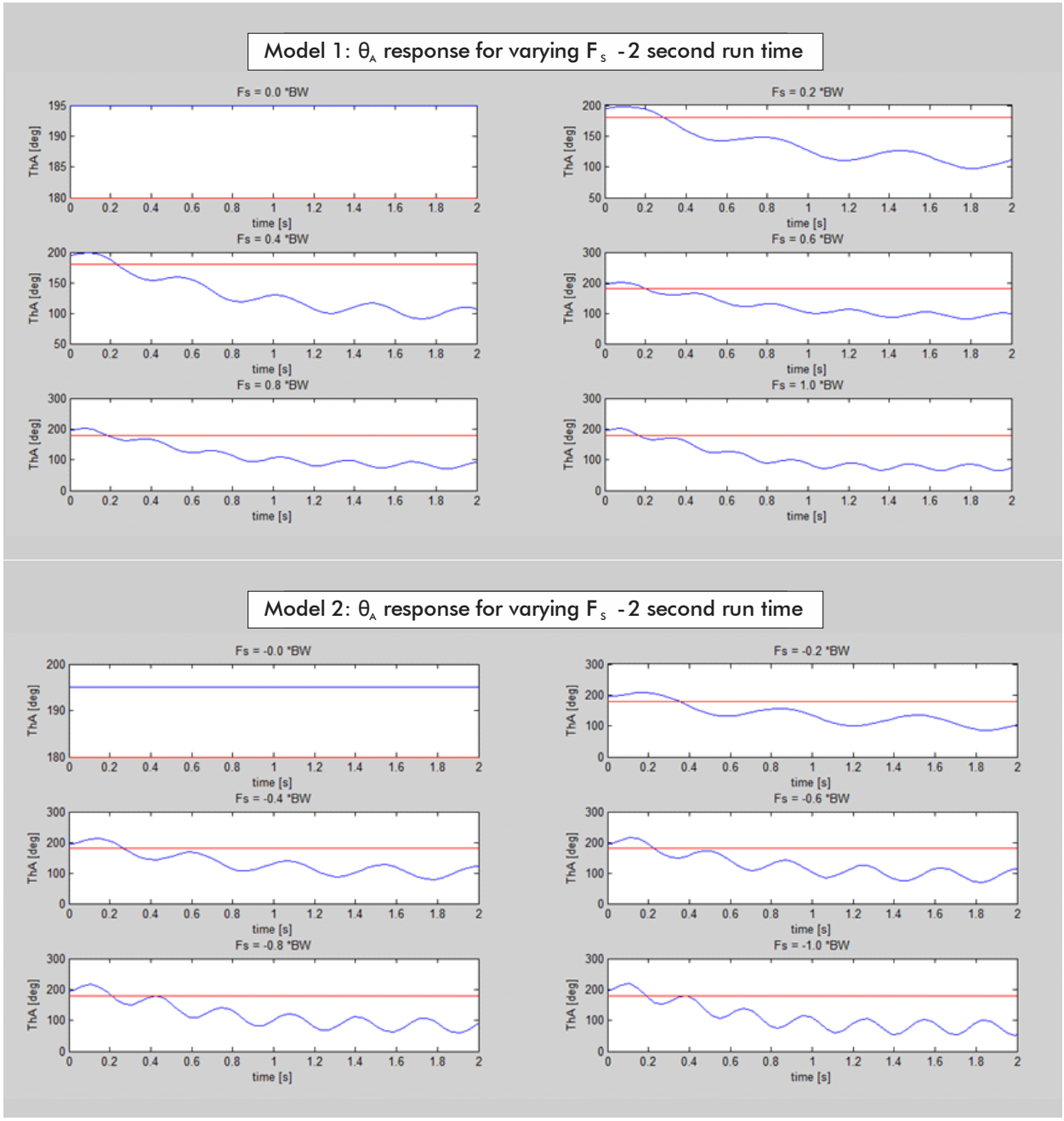

Figure 25: Abdomen angle responses for varying magnitudes of silk force, tested over two seconds. The response takes the form of a sinusoid shifted by a value tending exponentially to 90 degrees (red line = 180 degrees)

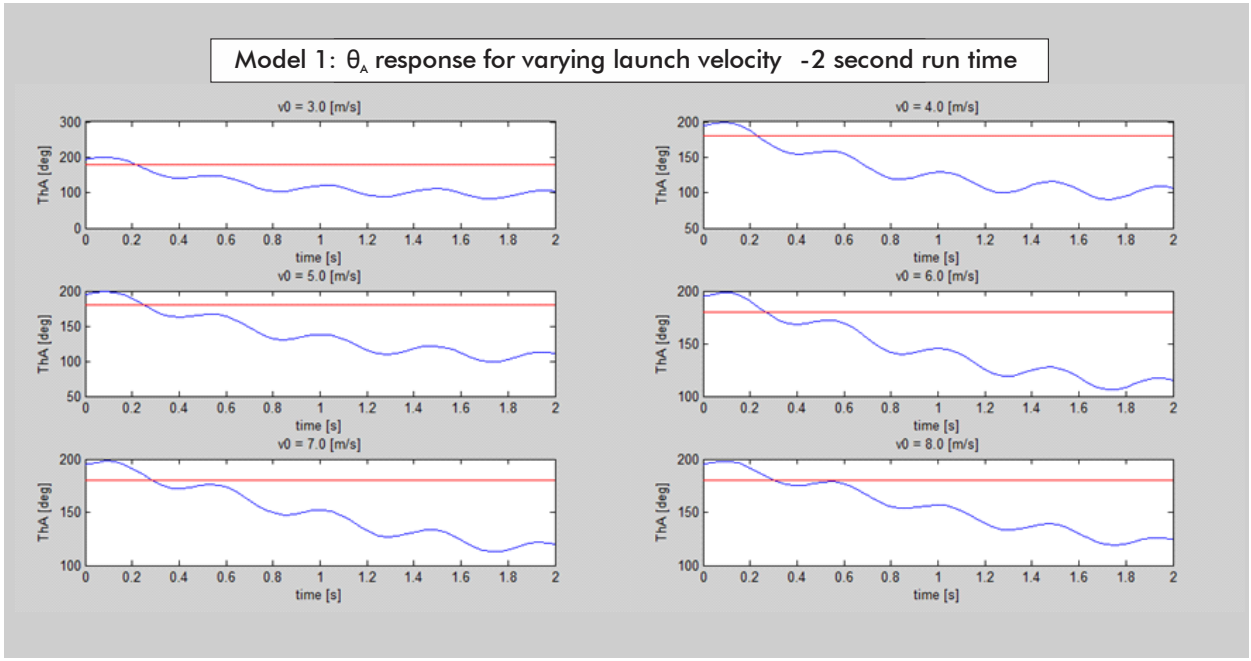

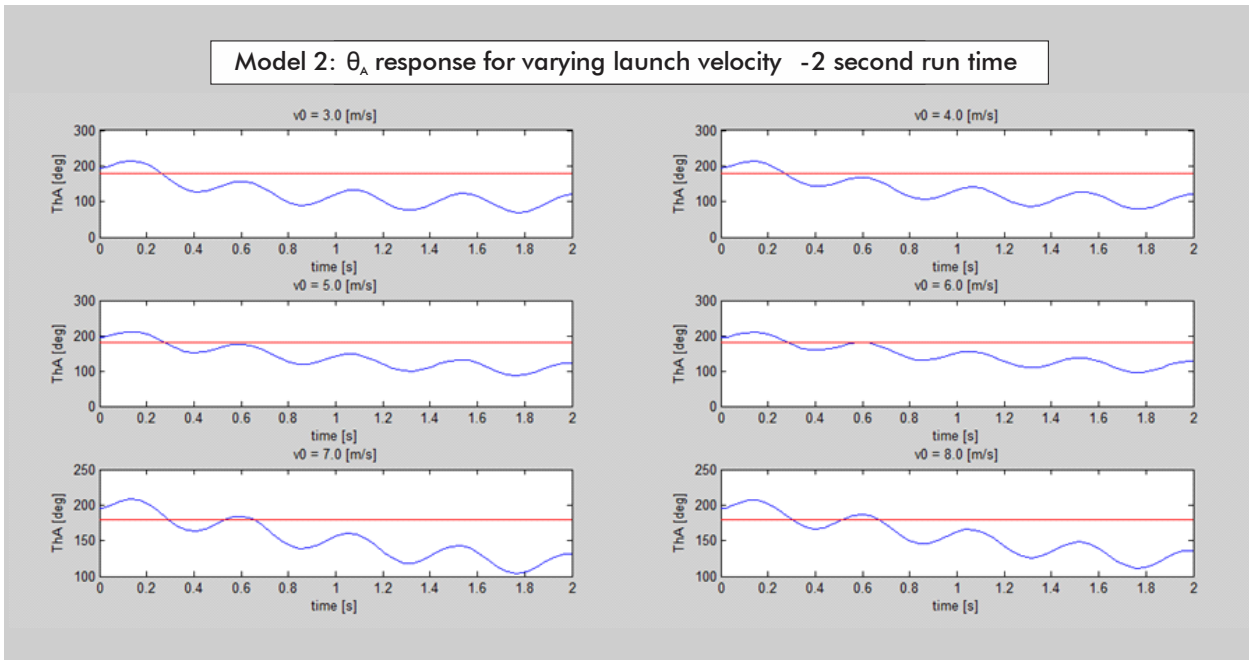

Figure 26: Abdomen angle responses for varying launch velocity, tested over two seconds. The time constant of the exponential term shifting the sinusoid increases with increasing velocity. (red line = 180 degrees)

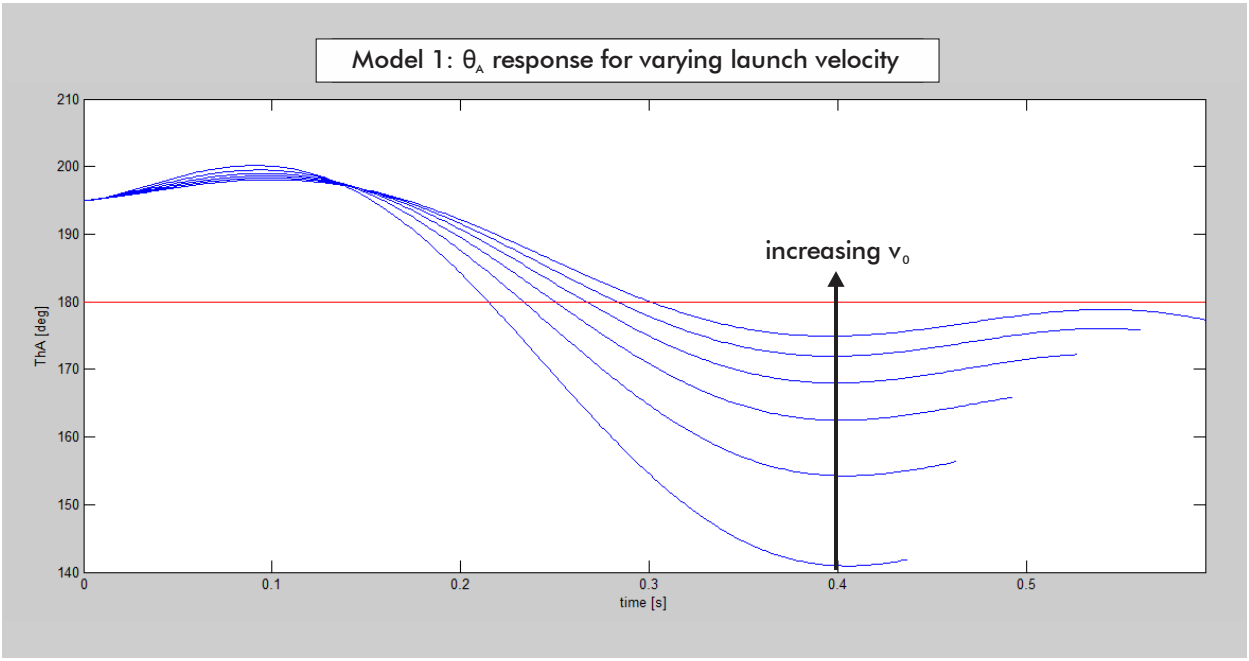

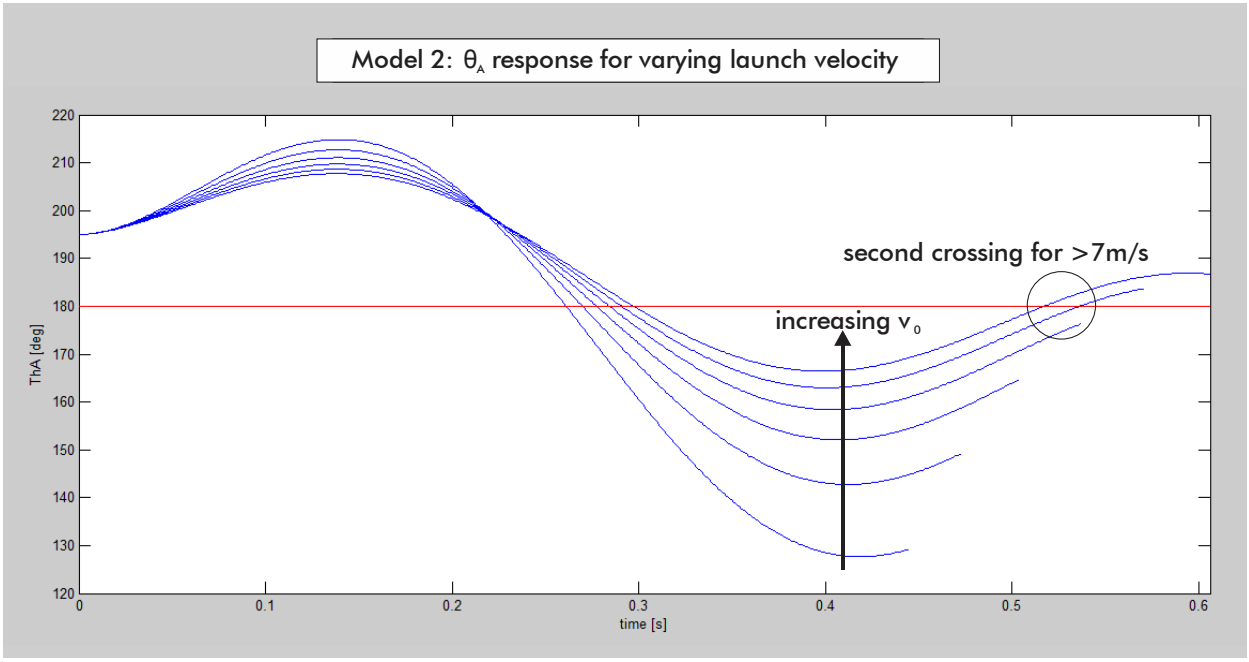

Figure 27: Abdomen angle response for varying launch velocity. The angle at which the second pitch reversal occurs increases with the velocity. Based on Model 2, a velocity of 7 m/s is required to produce a second 180 degree crossing.

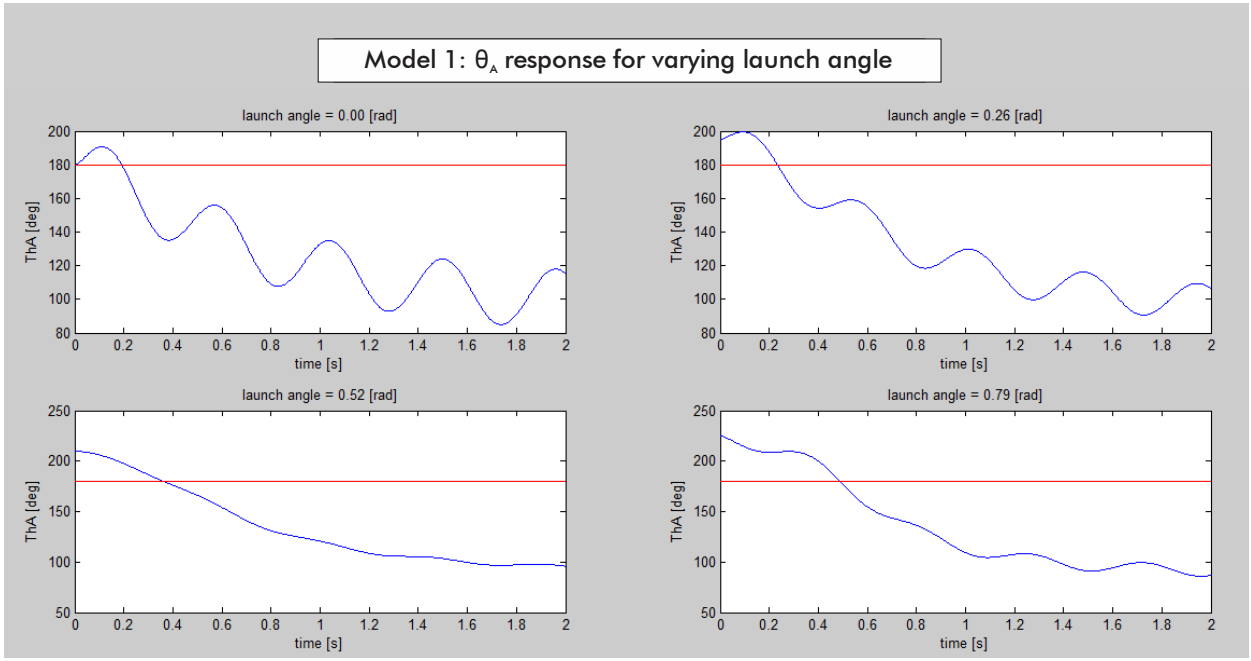

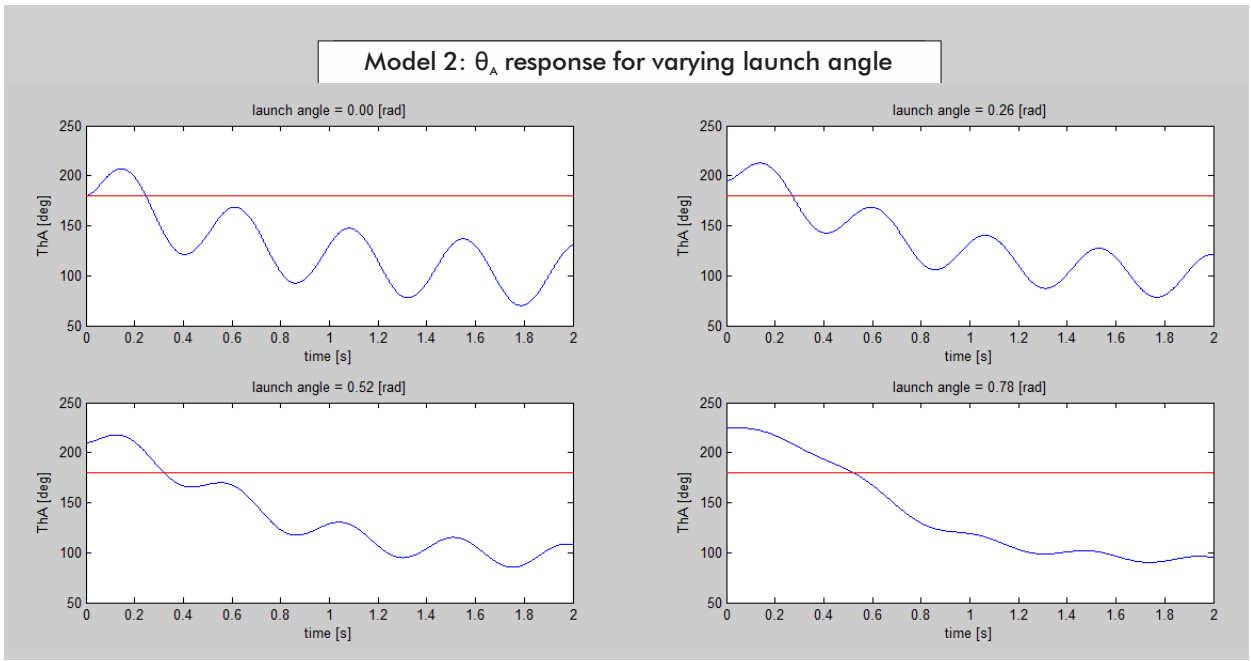

Figure 28: Abdomen angle response for varying launch angle. (red line = 180 degrees)

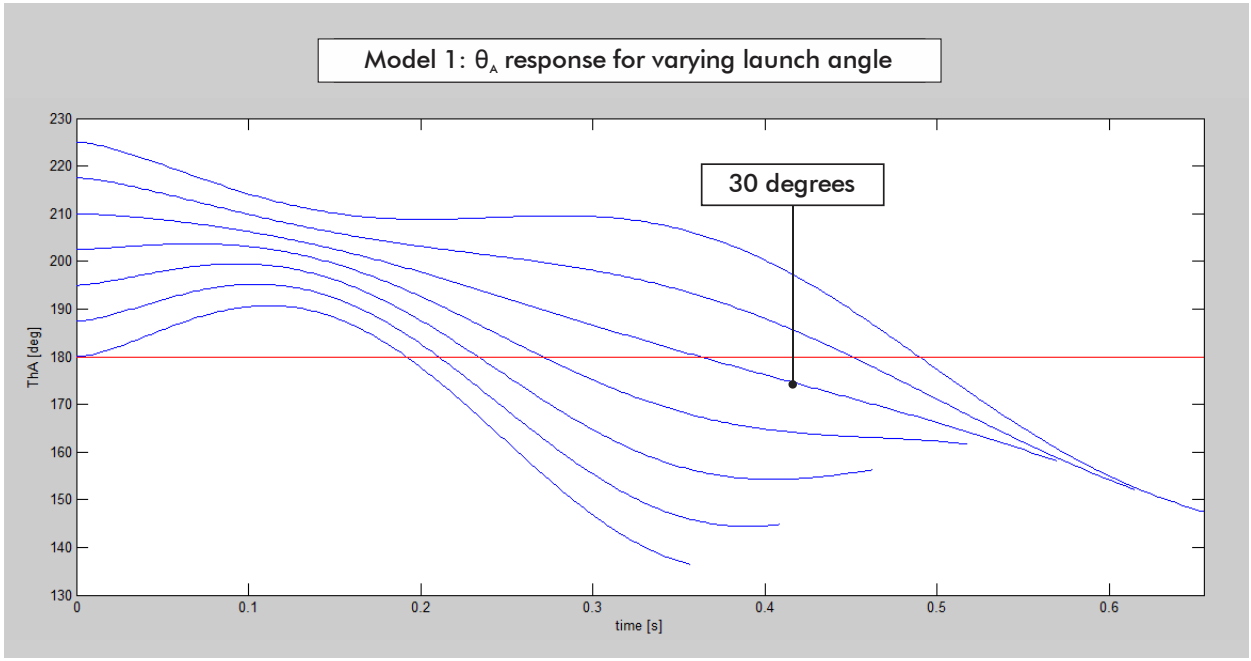

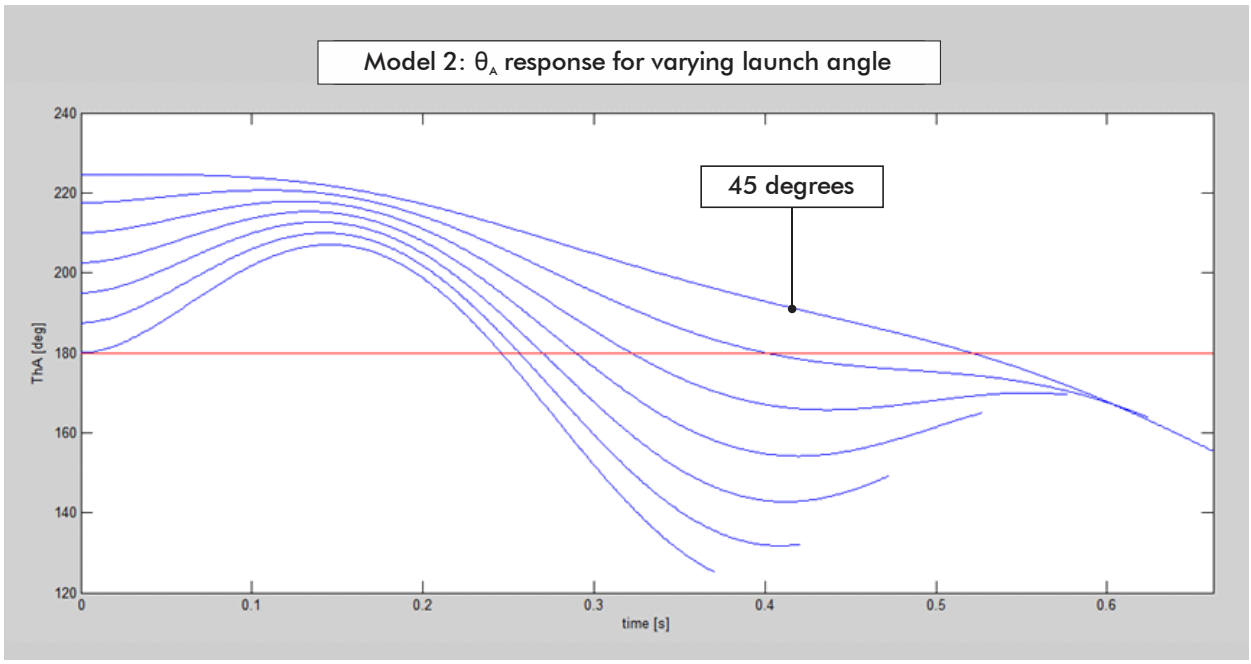

Figure 29: Abdomen angle response for varying launch angle. For Model 1, the amplitude of the sinusoid decreases with increasing launch angle until it reaches a turning point at approximately 30 degrees, and begins increasing. For Model 2, the amplitude of the sinusoid decreases with increasing launch angle until 45 degrees.

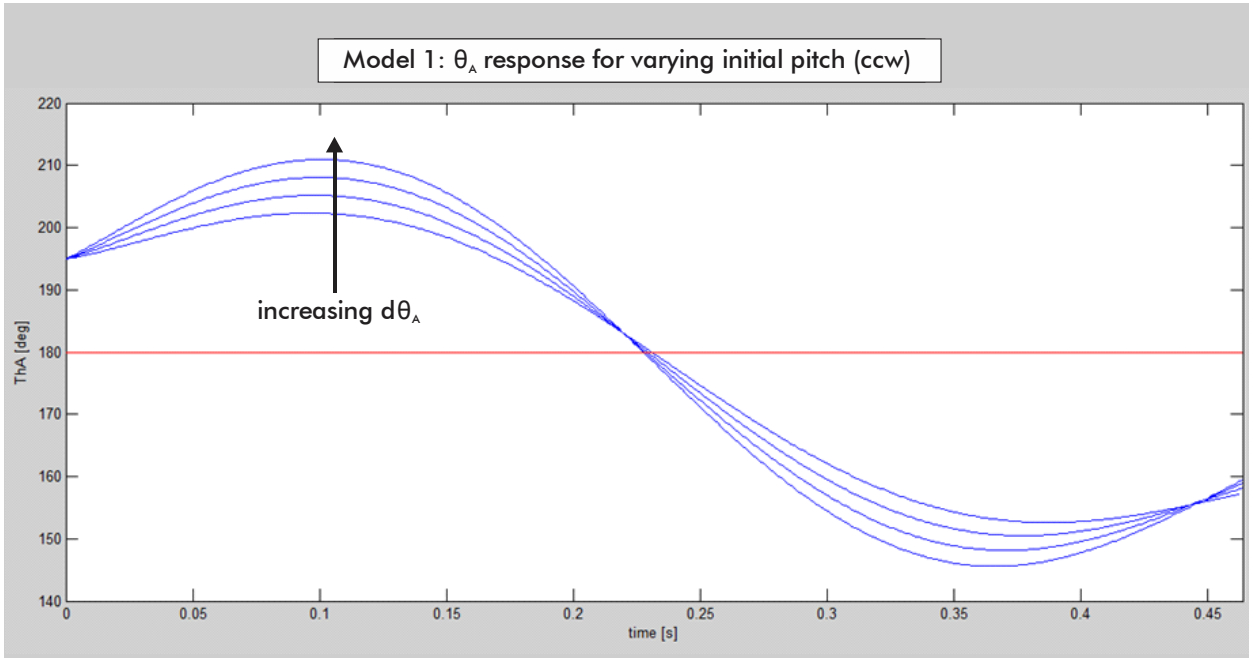

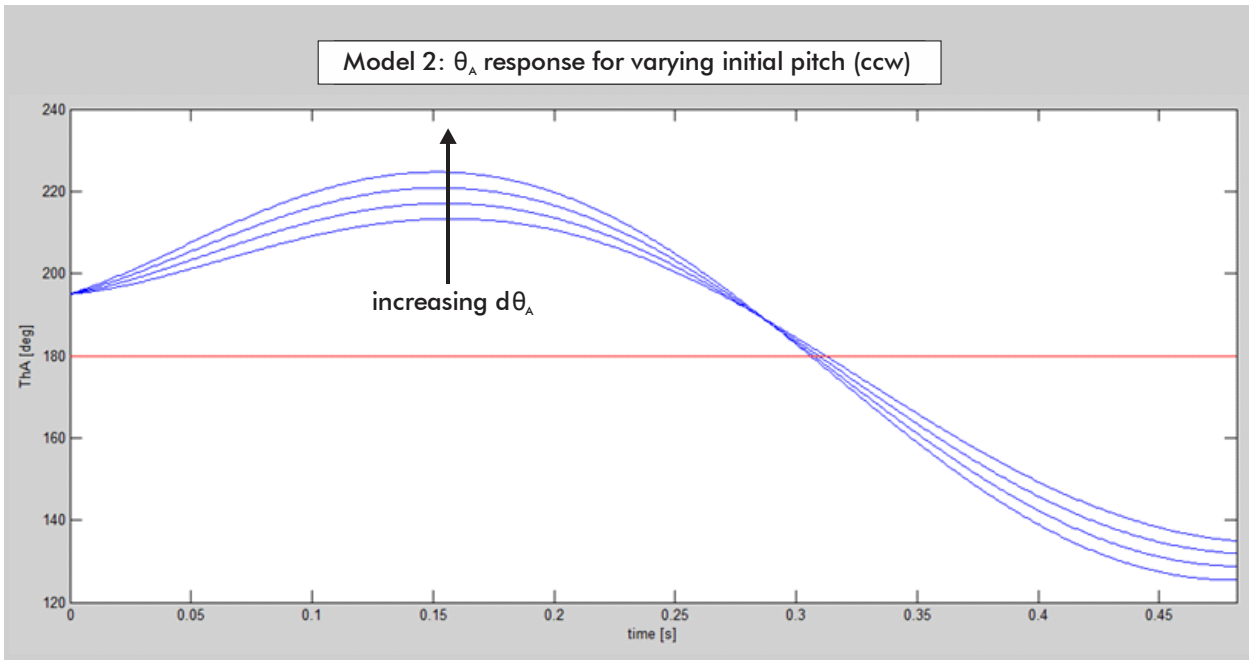

Figure 30: Abdomen angle response for varying velocities of backward intial pitch. The amplitude of the sinusoid increases with the speed of rotation.

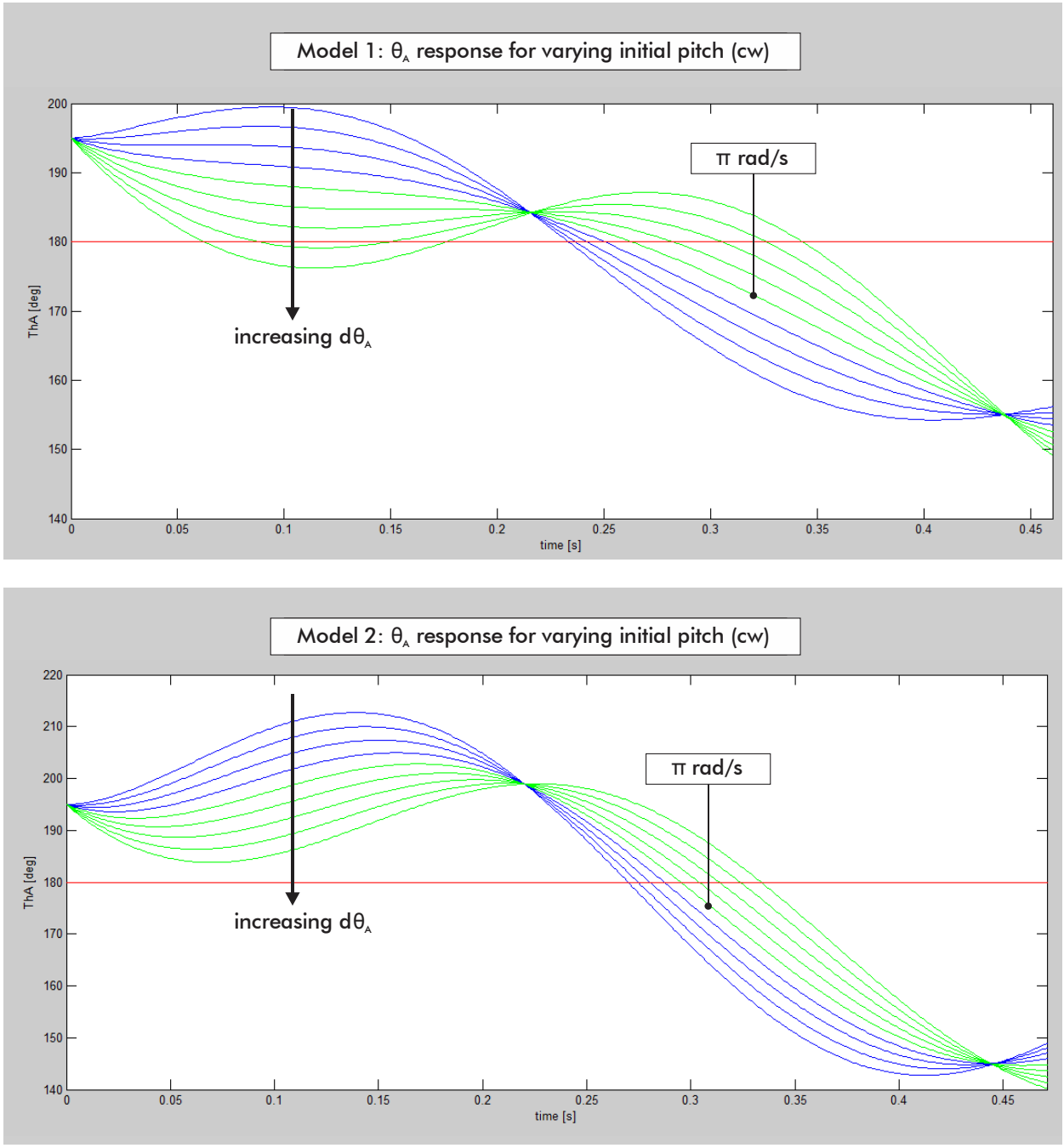

Figure 31: Abdomen angle response for varying velocities of forward initial pitch. The blue plots are those corresponding to a rotation of less than π rad/s. The amplitude of the sinusoid decreases for increasing pitch up to a turning point velocity (π for Model 1, between 1.25 and 1.5π for Model 2) and then increases with the magnitude of the pitch above this value. Increasing the rate of clockwise rotation shifts the sinusoid to the right.

6.5 Phase plane analysis of abdomen angle response

To validate the observations made in previous experiments, both dynamic models were used to plot rough phase portraits from the abdomen angle response.

This was achieved by running ten simulations with randomized initial values for the abdomen angle and pitch velocity, with all other parameters fixed. The starting angles could range from 90 to 270 degrees, and the velocities up to π radians per second in either direction. The resulting abdomen angle responses were then plotted against the pitch velocity responses to give the state trajectories over a ten second period.

Figure 32 shows the phase portraits that resulted. A colour gradient was used to give the direction, with points in a more saturated red being closer to the endpoint of the trajectory. In both portraits, the trajectories converge to circle around the point representing an abdomen angle of 90 degrees and zero pitch. This indicates that this point is a vertex [37], and confirms the observation that the body will always eventually fall into a pendulum-like oscillation about an equilibrium point at 90 degrees.

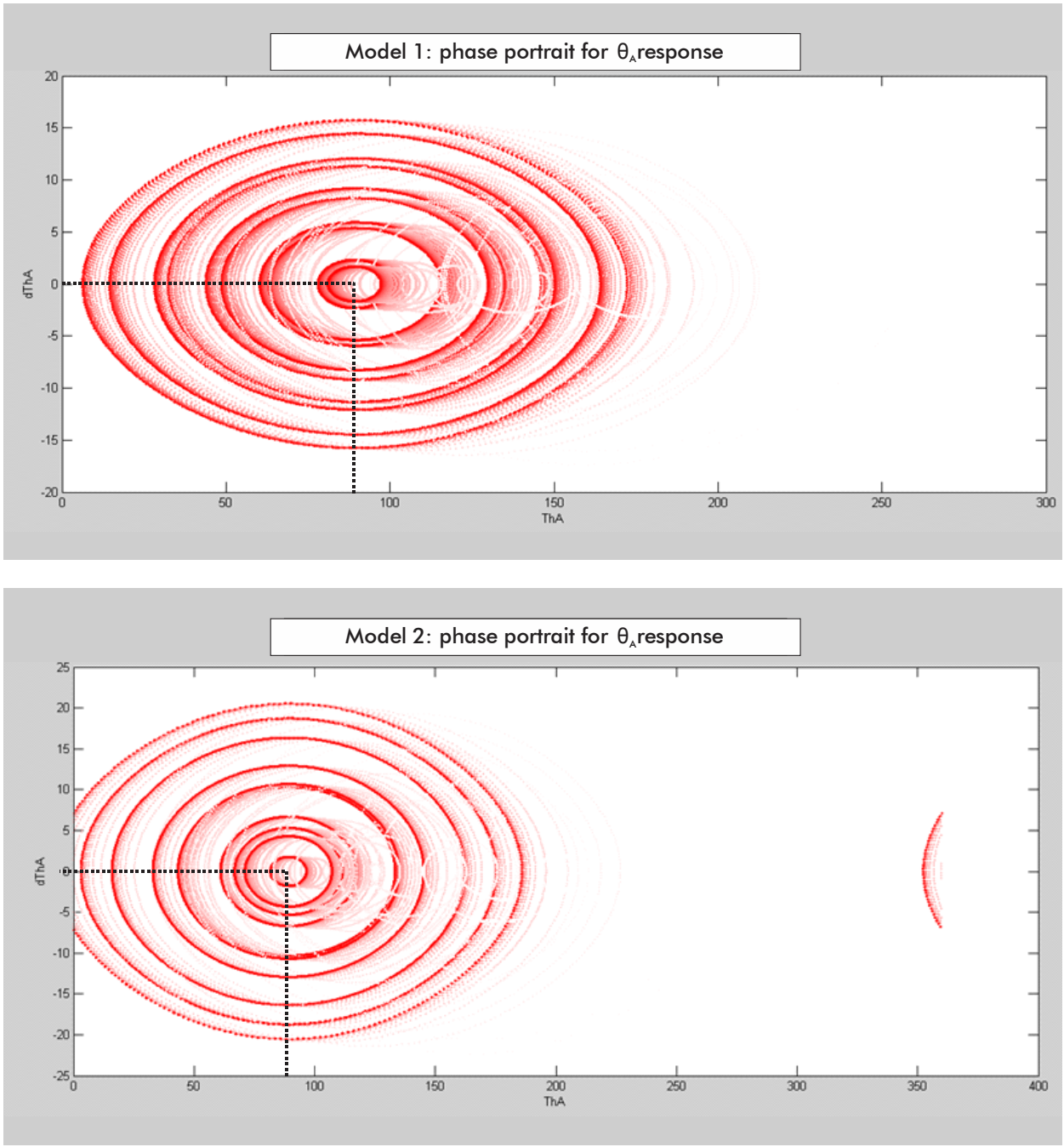

Figure 32: Phase portraits representing the abdomen angle response. Points closer to the end of each trajectory are shown in a more saturated red. The trajectories converge to rings around the point representing an abdomen angle of 90 degrees and zero pitch, indicating that this point is a vertex.

6.6 Comparison between simulated model and footage of spider

In order to validate the dynamic models, simulations were performed using initial parameters drawn from those documented in *More than a Safety Line…* [1]. The results could then be compared to the video footage of silk and non-silk spiders jumping supplied as supplementary material for this study.

The parameters used are listed in the table below:

Table 2: Experimental parameter values based on study by Chen, et al [1]

parameter	value	Unit
Body mass	20	mg
Body length	6.1	mm
Launch velocity	1	m/s
Launch angle		deg. (ccw)
Silk	11.4	
Non-silk	5	
Initial pitch*	4π	rad/s (ccw)
Silk force	0.42	Body weights
Drag coefficient	1.5	

*This value was not stated in the text, but was found to give a landing angle similar to that observed for the non-silk spiders

Figure 33 shows the abdomen and silk angle curves retrieved from the simulations compared to those recorded for the silk spider in the text [1]. Video footage of non-silk spiders jumping is compared to the animations produced from the two models simulating the non-silk condition in Figure 34. The same comparison is made for silk spiders in Figure 35.

Despite the application of a constant silk force, rather than one which varied as observed in the study, and the approximation of many parameters not stated in the text, it can be seen that both models accurately captured the basic motion of both the silk and non-silk spiders.

6.7 Discrepancies between the models

Although the results produced by the two models were largely similar and showed the same general trends, they were not identical. In cases where the differences are significant, conclusions will be drawn based on the results of Model 2, as this is a less idealized model and therefore assumed to represent the real system more accurately.

Comparisons between the results from the two models and the observations by Chen, et al [1] show that Model 2 gives results which are slightly closer to the behaviour of the spiders studied.

Plots of Θ_A and Θ_S vs. time from *More than a Safety Line: jump-stabilizing silk of salticids* by Chen, et al [1]

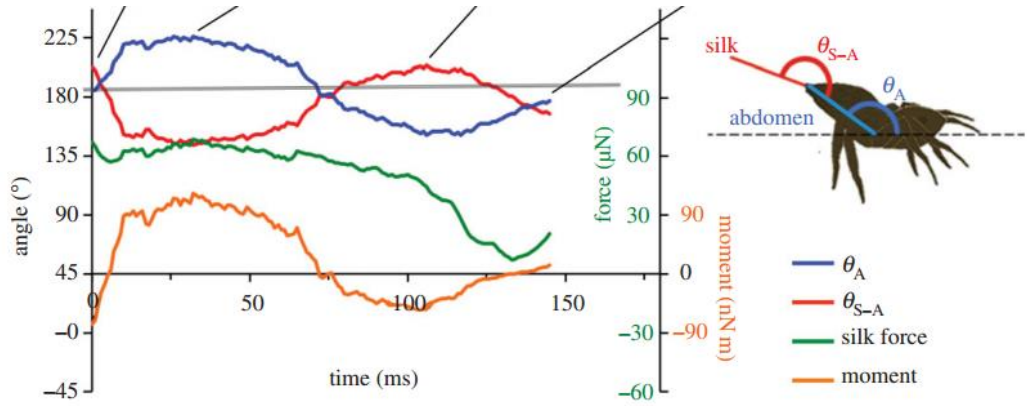

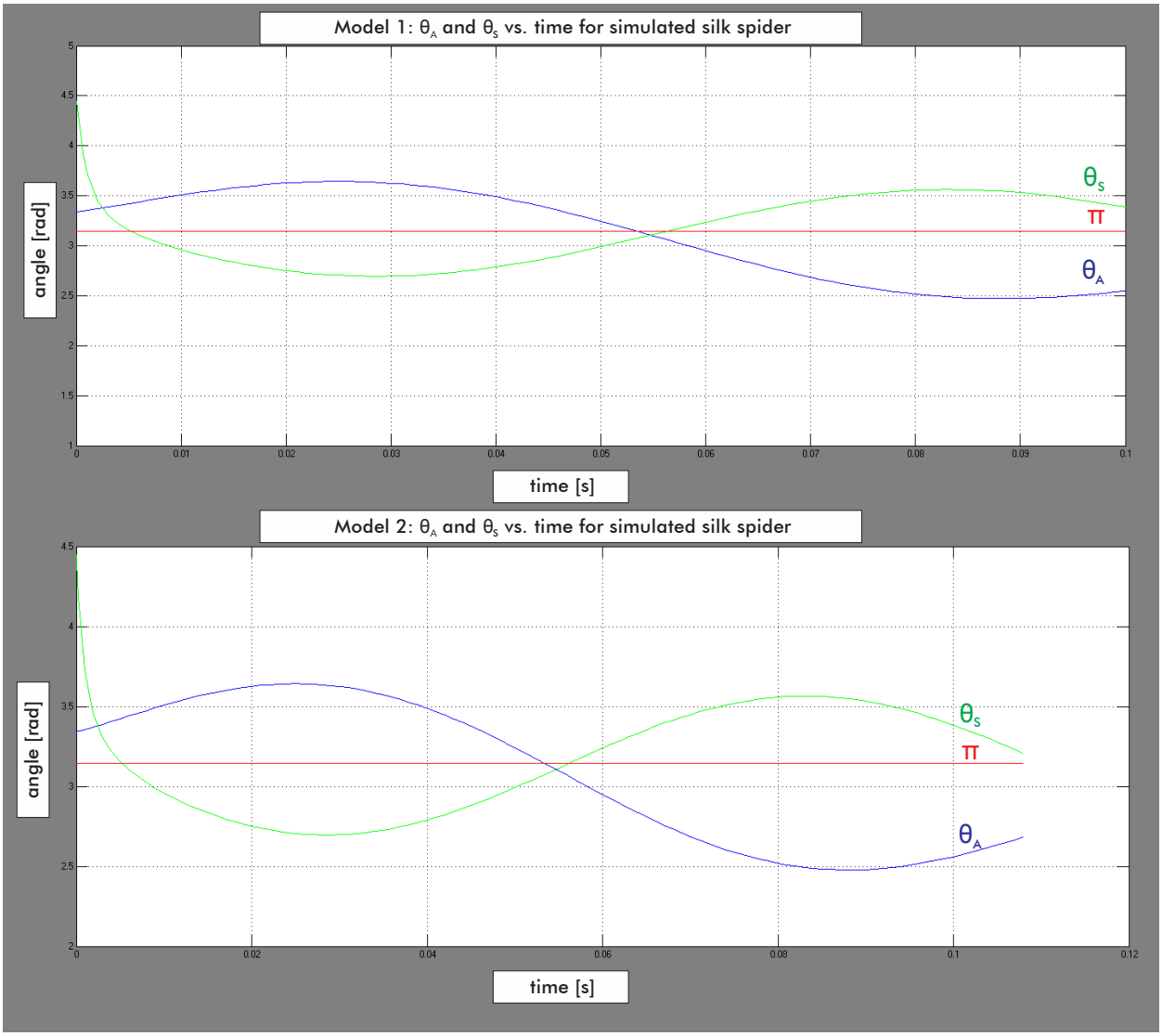

Figure 33: comparison between the silk and abdomen responses observed by Chen, et al, and those produced in simulations with parameters imitating the silk spider. Although the final angles differ, the simulation accurately captures the general form of the response.

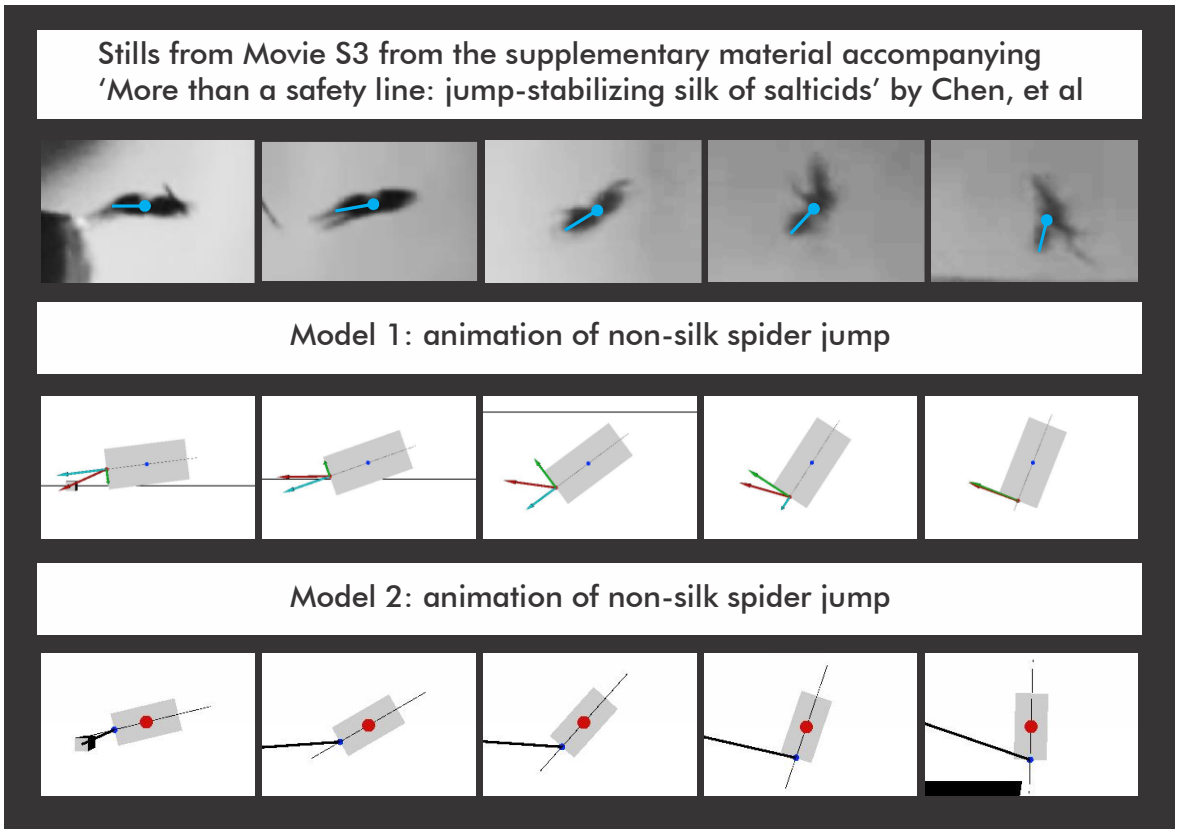

Figure 34: comparison between video footage of a non-silk spider jumping and the animations produced from the dynamic models

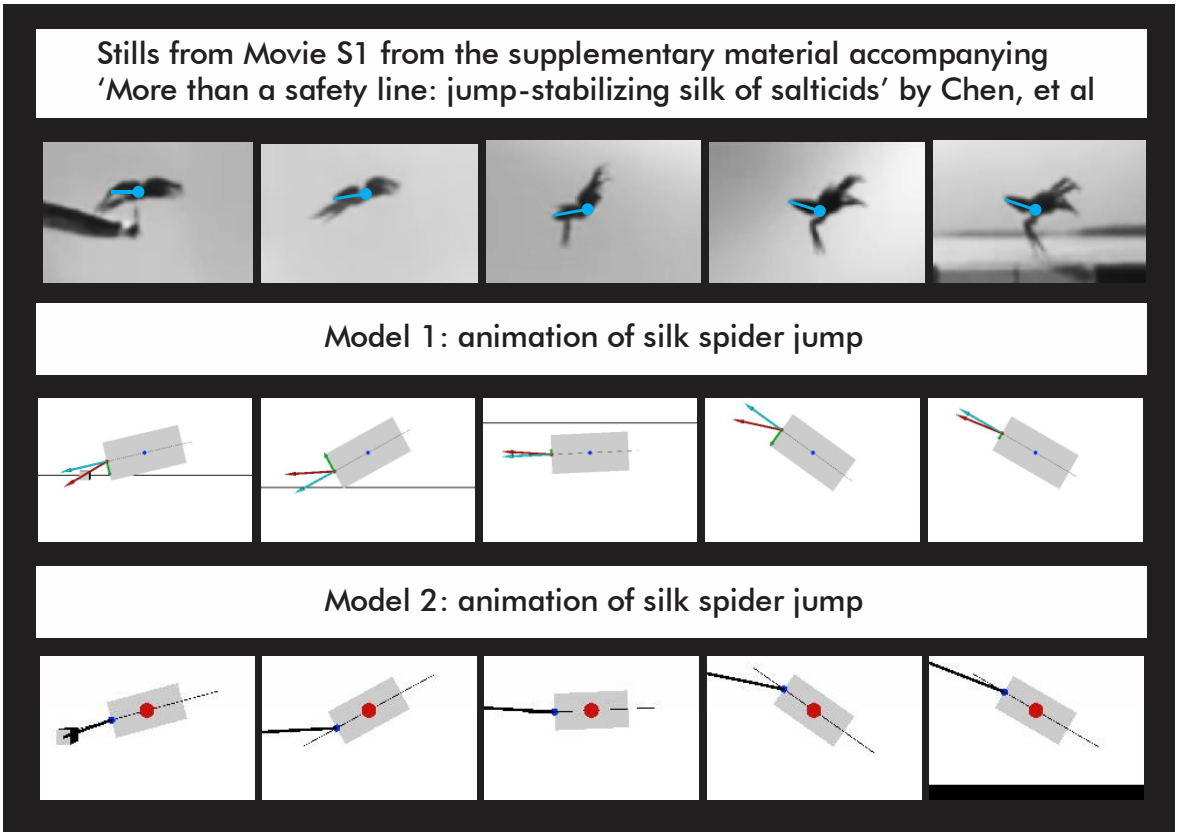

Figure 35: Comparison between video footage of a salticid spider jumping and the animations produced from the dynamic models

6.8 Summary

Simulations based on the two dynamic models of the system were used to determine the effects of different parameters on the characteristics of the spider's jump. Factors affecting the range and landing velocity were established, as well as the abdomen angle response, which was found to be a sinusoid of the form:

$$\theta_A = A\cos\left(\frac{2\pi t}{\omega} - \Phi\right) + Be^{-\frac{t}{\Omega}} + \frac{\pi}{2}$$

Plots of the response over time and phase plane analysis both suggest that the equilibrium angle for the body is 90 degrees, and the robot will eventually fall into oscillation about this position.

The table below summarizes the effects of various parameters on the motion of the robot:

Table 3: Effects of varying jump parameters based on simulation tests

Increasing Parameter	Effect
Silk force	• decreases jump range • greater reduction in horizontal velocity • abdomen angle oscillates at higher frequency
Launch velocity	• increases jump range • smaller reduction in horizontal velocity • increases angles at which latter turning points occur in the abdomen angle response by increasing the time constant Ω of the exponential term
Launch angle	• increases jump range for smaller magnitudes of silk force, but decreases it for larger forces • greater reduction in horizontal velocity • increases the starting body angle, and hence the magnitude B of the exponential term in the abdomen angle response • increases or decreases the amplitude A of the sinusoid in the angle response. For the testing parameters used, it decreased A up to around 45˚, then increased A
Initial pitch	• increases or decreases the amplitude A of the sinusoid in the angle response. For the testing parameters used, it increased A for velocities above approximately -1.25π rad/s (taking ccw rotation as positive) • backward pitch shifts the sinusoid to the left, forward pitch shifts it to the right

7 Discussion of the Motion of the Jumping Spider as a Control Problem

The first objective of this study is to gain an understanding of the spider's motion and attempt to explain the observations made in previous studies. Based on the results of the simulations performed, some of the questions raised by the literature review can be answered, and a clearer idea of the control problems faced by the spider can be established.

7.1 Implications of system instability on control objectives

Based on the experiments regarding the abdomen angle response, the system is marginally stable – it will tend to equilibrium oscillating about 90 degrees, but it will not settle at a particular angle. When analysing the forces involved, it can clearly be seen why this is the case:

For the silk force to accelerate the spider in a clockwise direction, the body must be in the position shown in diagram A of Figure 36 for the normal component to create the required moment. When it has rotated to the position in B, with the silk force in line with the body axis, there is instantaneously no moment acting, so the clockwise rotation will continue past this point. This causes the normal force to act in the opposite direction, as in C, and hence a counter-clockwise acceleration to be produced. Eventually, this acceleration will cause the body to rotate in the counter-clockwise direction, moving back to A in the same way and beginning the cycle again.

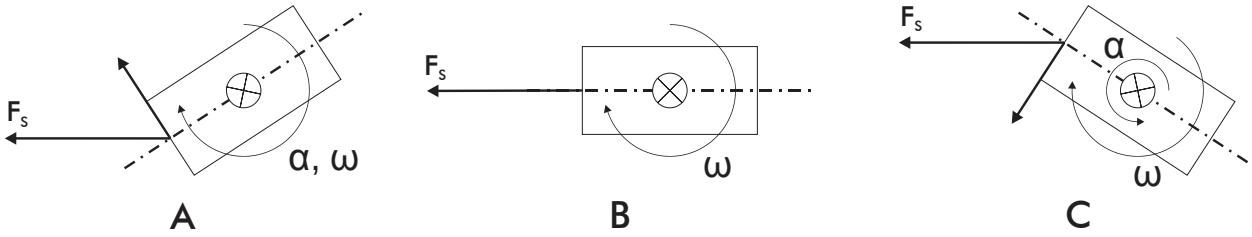

Figure 36: diagrams showing the changing position of the silk force relative to the body as it rotates, and the corresponding directions of rotational velocity and acceleration

This analysis is done from the perspective of a stationary centre of mass, but still applies when it is in motion.

The spider may not be able to prevent itself from oscillating, but as demonstrated in the simulation, it can alter the characteristics of the angle response by adjusting its launch velocity, silk force and initial pitch. Rather than attempting to get the system to settle quickly at the desired value, its control problem is therefore to adjust the response such that a suitable angle will coincide with the landing time.

7.2 Benefits of multiple pitch reversals

Having explained the general form of the abdomen response, the next question was why jumps with multiple pitch reversals were observed to be more common than those where the pitch reversed once [1].

The explanation most likely relates to the different parameters the spider must optimize for an ideal landing. Besides reaching an angle close to 180 degrees, the spider also needs to find the correct balance of braking which will slow it sufficiently to prevent rolling on landing, but not compromise the range of the jump.

Based on the experiments assessing the influence of different factors on the final x velocity, jumps with larger initial velocities require more silk force to achieve the same relative velocity reduction. Since the frequency of the abdomen angle response was also found to increase with the silk force, the spider should hence reverse its pitch more often in jumps with larger initial velocities.

The various simulations performed indicate that the spider should be able to achieve similar landing conditions either by jumping with a slower initial velocity and applying a smaller average silk force, or by jumping faster and applying more force. Considering the relationship between the number of pitch reversals and the launch velocity, the question of why multiple reversals are preferable therefore becomes a question of why a greater initial velocity would be beneficial for the spider.

In nature, salticids use their jumps for locomotion, prey capture and escaping predators [2]. With this in mind, it is assumed that range is the most important concern for the spider, as the cost of underestimating the distance and falling is likely greater than the cost of an unsteady landing at the correct position.

Figure 37 provides a comparison between the range and final x velocity curves for varying silk force at different launch velocities. It shows that, despite the additional force required to decelerate to a specific final velocity, increasing the launch velocity still yields a significant increase in the range. Although this considered the specific case of 4, 5 and 6 m/s, the final position and velocity curves were found to have a similar slope for all launch velocities studied, so it can be assumed that this would hold for arbitrary increases.

The corresponding abdomen angle plots in Figure 37 show that, from a range perspective, there is a clear advantage to jumping with the velocity corresponding to three pitch reversals, however Chen, et al found that jumps with two, and even one reversal occurred more often [1]. Since the majority of the jumps had two reversals, these observations suggest that overestimation of the launch velocity is beneficial, but only up to a limit.

Determining what this limit is would require considering influences outside of the dynamics, such as the need for the spider to conserve its energy and the costs of a significant overshoot for the particular situation. To get a better understanding of the factors which determine the optimal velocity, it may be beneficial to extend the study documented in *More than a Safety Line…* [1] to include jumps at shorter and longer distances.

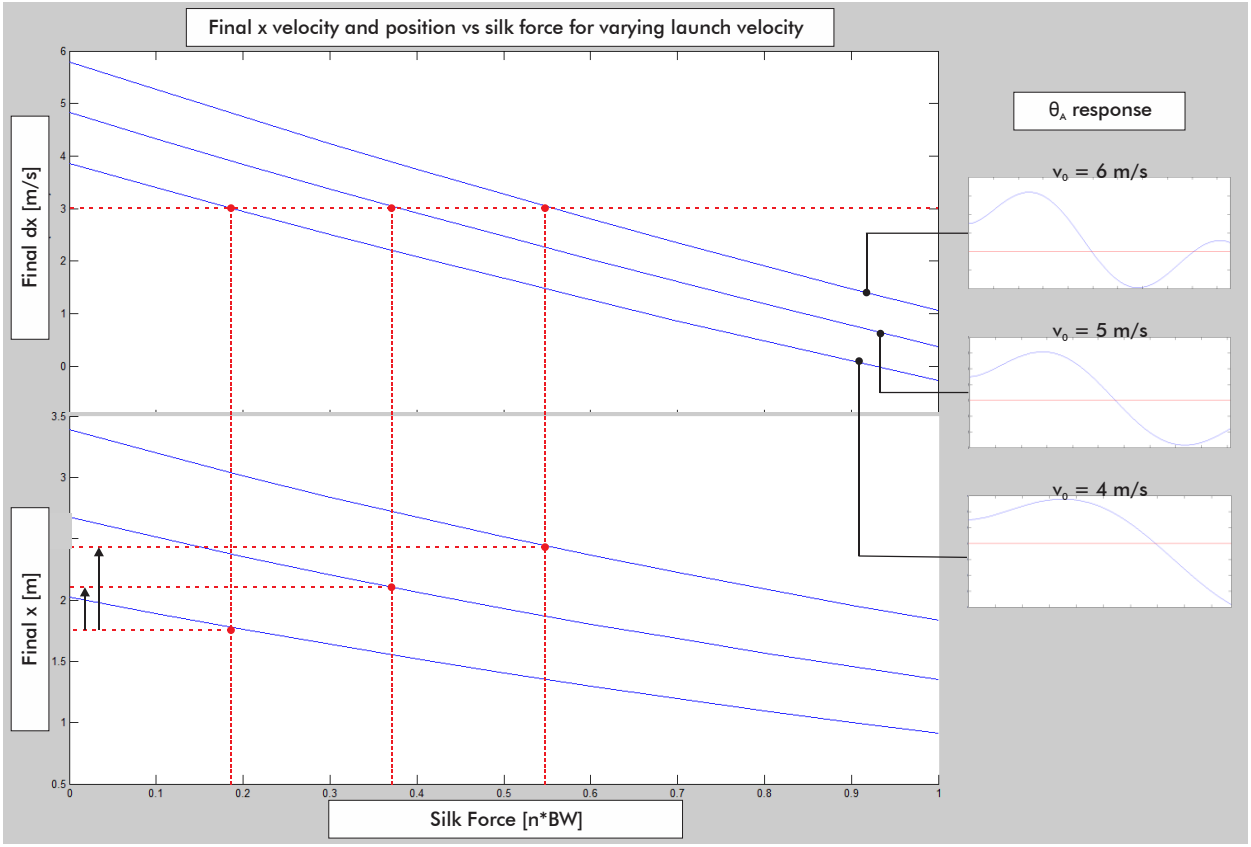

Figure 37: comparison between the graphs of final x position and velocity vs. silk force for varying launch velocity. Despite the additional force required to brake to the same final velocity, there is still an increase in the range achieved at an initial velocity of 5 m/s compared to 4 m/s.

7.3 Comments on the controllability of the system

As a control mechanism, the dragline has the complication of its results being determined by the time and position at which they are applied. The ability of the controlling variable – the silk force – to influence the future body angle is dependent on the current body angle. If the difference between the current angle and the set point of 180 degrees is taken as the error, applying the silk force could either act to decrease the error, increase it or at some instants, have no effect. Examples of positions which would produce these different results are illustrated in A, B and C of Figure 38 respectively.

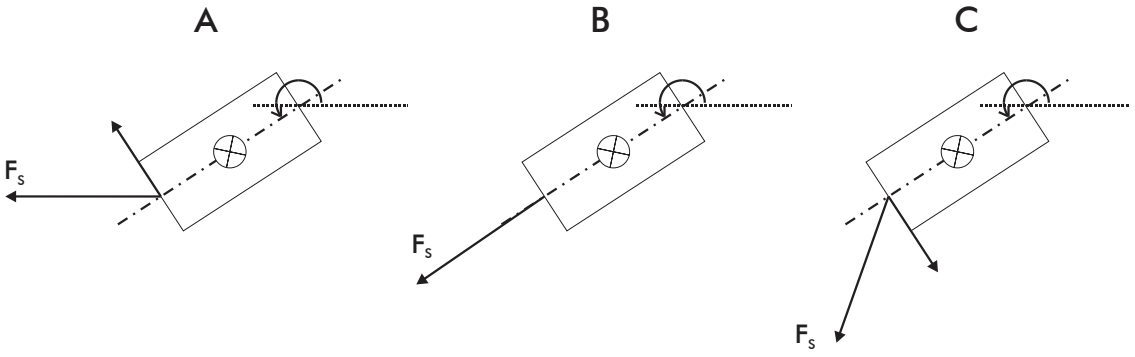

Figure 38: Diagrams illustrating three positions in which applying tension to the dragline will have different outcomes with regards to the error in the abdomen angle. In A, it will decrease the error, B will decrease it and C will have no effect.

The position of the centre of mass also affects the angle of the silk relative to the body, meaning the silk force will produce a different result depending on where the robot is along its flight trajectory.

The relationship between the time and position is just one timing problem that has to be considered. The other is that, due to the unstable nature of the system discussed previously, once a control action sets it in motion, the angle will continue to change until the end of the jump. A force applied at the start of the jump will therefore have a different final result to one applied later.

Because of these dependencies, any feedback controller used to stabilize the abdomen angle would need to take all the relevant positional information into account when calculating the control action. It is therefore only feasible to apply the dragline as a control method if the current centre of mass position, body angle and silk angle can be measured.

8 Design of a LEAP

In addition to understanding the motion of the jumping spider through theoretical models, the purpose of this thesis was to design a small robotic platform which could be used to analyse it experimentally.

Considering the spider, the hardware design could be broken down into the following components:

- the chassis forming the basis of the robot body
- a propulsion mechanism to get the robot off the ground
- the dragline itself
- a means of applying tension to the dragline
- the electronic system required to control the dragline and log the data

The design of these individual elements will be discussed for three design stages of increasing complexity.

8.1 Base design

The chassis design, launcher and dragline formed the base of the system, and were expanded on in each design stage.

8.1.1 Chassis

To minimize the force necessary to launch it into the air, the chassis was required to be as small and light as possible, but also strong enough to withstand the impact of landing and protect the electronic components it houses.

Rather than specially designing and fabricating parts, the chassis was built using components from the *LEGO Technic* range of construction toys. Besides facilitating rapid prototyping, this option was selected because the plastic the parts are made from is both strong and light. Additionally, if the robot does sustain damage on landing, it will almost certainly fail at the joins between individual pieces, rather than the pieces themselves failing. It can therefore be repaired quickly without the need for replacement parts.

The diagram below shows the features of the chassis:

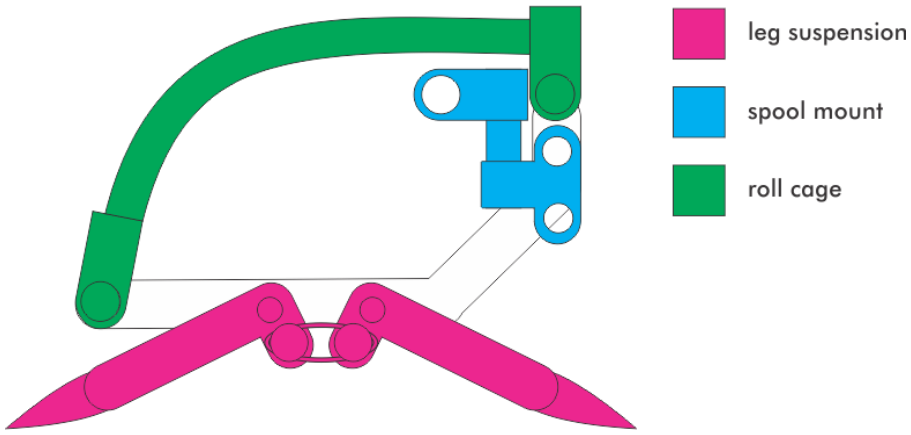

Figure 39: diagram of the chassis from the side view showing its significant features

Suspension

The chassis was supported on simple legs which could flex outward, allowing the body to dip down, under resistance from elastic bands. This formed a simple suspension system to protect the body during hard landings.

The action of the suspension system is illustrated below:

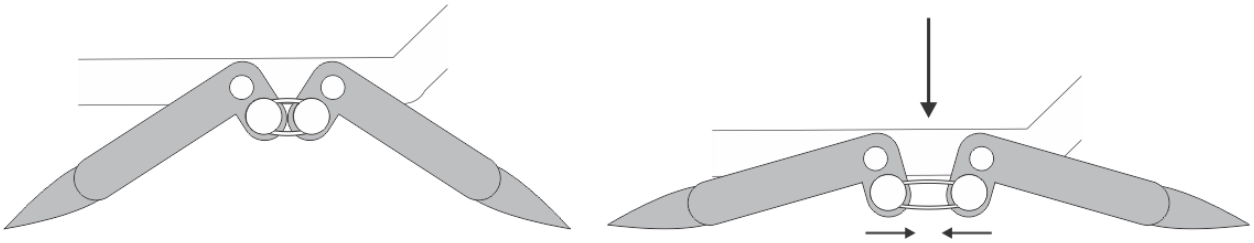

Figure 40: diagram showing the suspension system of the robot in its normal state (left) and under the action of a downward force (right)

Roll cage

In the literature, the spiders were sometimes observed to flip over during landings [1] [2]. Assuming the robot may do the same, a role cage was added to protect the electronics from upside-down impacts. Rather than a rigid cage, slightly flexible plastic tubes were used, as this would provide some cushioning.

Spool housing

The spool was mounted such that it could rotate freely. It was positioned as close to the rear of the body as possible, so that in the case of overrun, the line would not become tangled in the electronics. The line is fed through a narrow eyelet, to ensure that it exits from a constant point relative to the body.

Dimensions

Photographs of the chassis with the dimensions indicated are shown in Figure 41. With the spool and dragline included, it was found to weigh around 50 grams.

A list of the LEGO parts used to build the chassis is provided in Appendix B.

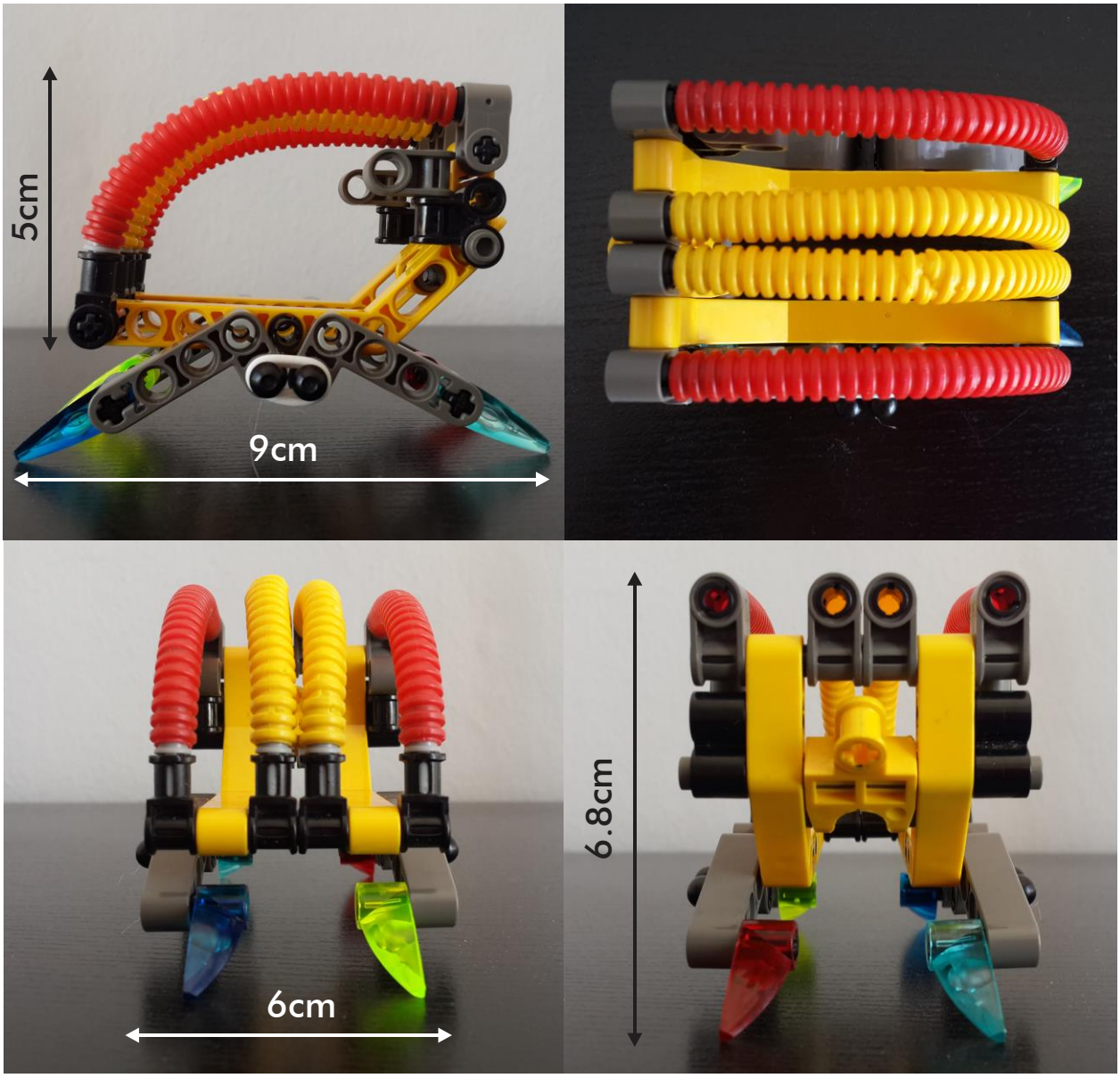

Figure 41: photgraphs of robot chassis showing dimensions. Clockwise from top left: side, top, rear, front

8.1.2 Dragline

The thread used for the dragline needed to be fine and light, but strong enough not to break under tension. It also had to be smooth enough to slide through the eyelet without friction, and it could not be made from a material which would tend to retain the shape of the spool. Braided fishing line was selected as it satisfies all these requirements.

8.1.3 Launching Mechanism

The robot will be launched into the air from a static launcher based on a catapult. The alternative was to have a propulsion mechanism on the robot itself, but this option was rejected as adding the necessary actuator to the robot would increase its weight and the complexity of the design. Additionally, the static launcher provides greater flexibility for varying the initial velocity and direction of the jump.

To ensure that the robot is launched straight, it is pushed along a narrow track by a slider. The propulsive force is provided by elastic bands, and the launch velocity can be increased by attaching more bands to the slider or by pulling it back further. The front of the track can be supported at different heights to change the launch angle. The operation of the launcher is illustrated in Figure 42.

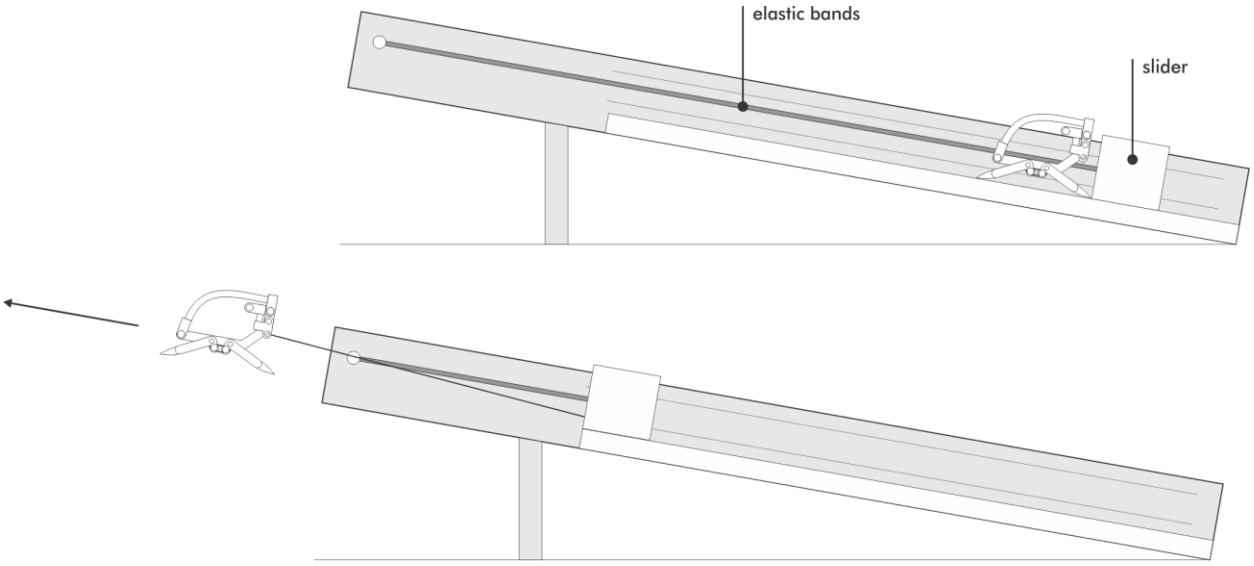

Figure 42: diagram showing the operation of the launcher

A tracking board mounted on the front of the launcher is used to determine the initial velocity of the robot from video footage of the jump. It is painted with black and white stripes of known width, and combined with the known frame rate of the footage, the velocity is given by the formula:

$$v_0 = \frac{w f_f}{n_f}$$

where w is the stripe width, n_f is the number of frames the robot takes to cross a single stripe, and f_f is the frame rate.

8.2 Stage 1: no active dragline control, video tracking

The first design is intended as a simple proof-of-concept to illustrate the ability of the dragline to bring about rotation.

8.2.1 Friction-based dragline control

In this design, tension is created in the dragline by using friction to restrict the motion of the spool. This is achieved by positioning two wheels attached to the axel of the spool such that they drag against the roll cage. The tension in the dragline using this method was approximated by measuring the maximum weight the line could hold before the spool began to turn. It was found that it could hold around 12 grams, or a tension of 0.118 Newton. This value corresponds to around 24% of the weight of the robot, close to the average force in bodyweight units applied by the spider [1].

8.2.2 Electronic system

This design does not require any electronics on board the robot itself. The motion of the robot is recorded externally from a video camera. A GoPro Hero3 (Silver Edition) camera was selected, as, despite being much lower than the frame rate used to study the spider [1], its maximum frame rate of 120 frames per second is assumed to be high enough to capture the essential motion of the spider.

8.3 Stage 2: no active dragline control, gyroscopic tracking

This design uses the same friction-based method as the first stage to control the dragline, but in addition to video footage, a gyroscopic sensor is used to monitor the pitch of the robot throughout the jump.

8.3.1 Electronic system

To record the angular position throughout the jump, the robot needs a system consisting of three components: a gyroscopic sensor to measure the pitch, a computer to process the data and a means of communicating between the two.

iNEMO-M1 inertial module

The iNEMO-M1 is an inertial module containing a 3-axis gyroscope and 6-axis e-compass. It can therefore completely describe the motion of the robot in the air, and record its linear motion. Besides its sensing capabilities, this module was selected because it is a complete system-on-board: since it is also a microprocessor, it can be used to process its sensor data and implement a controller. This saves the cost and complication of having to purchase and combine separate sensors and processor. More importantly for this design, it also saves space, as the iNEMO is an extremely small package.

Callen Fisher designed a development board which allows the iNEMO to be programmed via an STM32F4 Discovery microprocessor. With this board, its dimensions are 42 x 50 millimetres, which fits easily within the chassis of the robot.

XBEE Pro radio frequency modules

Because a tether would interfere with the motion of the robot, it was essential that the sensor module be able to communicate wirelessly with the computer. XBEE Pro radio frequency modules were selected to facilitate this, as they are small and can interface with the iNEMO and computer via a UART connection.

Another important consideration was the transmission rate, as the connection would need to be able to send data quickly to maximize the number of data points which could be acquired over the short time period of each jump. The XBEEs can accommodate a rate up to 115200 baud [31], which would allow them to send around 2880 four byte floating point values per second, assuming each byte is sent as a ten bit package. This is more than sufficient for the requirements of the project.

The operating range of these modules also far exceeds the requirements: indoors, they can transmit up to 90 metres [31]. They require a supply voltage of 3.3 volts and a current of 250 milliamps when transmitting, which can be provided by the iNEMO [31].

ZIPPY Flightmax 350mAh 2S 20C battery

A battery supplying at least five volts was required to power the iNEMO. Because the duration of each test would be short, the capacity of the battery was less of a priority than minimizing its size and weight.

For this reason, a pair of 3V Lithium coin cells with a capacity of 500 milliamp-hours initially considered, as these would give a total weight of less than 15 grams. There was a concern, however that these batteries would not supply sufficient current, and therefore a ZIPPY Flightmax Lithium Ion rechargeable battery pack was instead selected. This pack supplies 7.4 volts, but as it is intended for use on remote controlled helicopters and quadcopters, it is very small and weighs around 20 grams. This battery would also provide sufficient current to facilitate the future inclusion of a DC motor.

8.4 Stage 3: active dragline control, gyroscopic tracking

While the previous designs and the models used in the simulations applied an approximately constant level of resistance to the spool, the spider was shown to vary the force on the dragline throughout the jump [1]. The final model is intended to enable investigation into the effects of varying the force, and provide a platform on which controller designs can be tested.

As in the previous model, it tracks the position of the robot using both video footage and gyroscopic data.

8.4.1 DC Motor-controlled spool

Two methods for making the resistance on the spool controllable were considered:

Like the approach used in the previous designs, the first used friction to restrict the rotation of the spool. It involved turning a cam with a servomotor, such that it could be brought in and out of contact with the spool. This would create a bang-bang controller – a controller where the output switches between two discrete states.

The option of using a DC motor to control the spool was selected instead, as it would enable the output of the controller to be varied over a range of values. The motor is coupled to the spool such that its direction of turning opposes the unreeling of the line. Increasing the terminal voltage of the motor would therefore increase the resistance applied to the spool.

Regulation of the voltage over the motor would also be relatively simple to implement: as it only has to operate in one direction, it can be controlled by a single transistor rather than an H-bridge circuit. The iNEMO can produce a pulse-width-modulated (PWM) signal to drive the transistor.

For the purpose of studying the dragline mechanism, it does not matter whether the tension is applied from a brake on the body of the robot itself, or from one at the stationary anchor point. The possibility of mounting the motor and spool on the launcher was therefore considered, as this would remove the constraint on its size. It was, however rejected because implementing a controller would then require the microprocessor to transmit the control action wirelessly, which could potentially introduce the complication of dead time.

8.4.2 Specifying the motor

Having determined that a DC motor would be an effective method of driving the spool, simulations were performed using Model 2 to evaluate the most suitable type of motor.

Because of the large range of motors available, it was not feasible to simulate every individual model. Instead, the intention was to determine the general category of motor that should be used. The following types of motor were considered:

Sub-miniature geared motors: extremely small, light motors with high gear ratios. They turn slowly but output a large torque for their size.

Sub-miniature gearless motors: extremely small, light coreless motors commonly used in miniature quadcopters. They spin very fast and deliver small amounts of torque.

Toy motors: inexpensive, fast, low power motors typically used in toys. Although they are still relatively small, they are much larger than the more specialized sub-miniature models.

Geared motors: larger, heavier motors which turn slowly with a large torque.

Torque and speed requirements

To get an idea of the torques and speeds required from the motor, a parameter sweep was performed to determine the relationship between the torque applied to the spool and the speed of the line. Assuming the motor is directly coupled to the spool, the torques tested corresponded to forces ranging from zero to the weight of the body. A launch velocity of 4 meters per second at 15 degrees, without any initial rotation was used for all the simulations, and the diameter of the spool was taken to be five millimetres. The dependent variables were the maximum and average line speed, converted to the angular velocity of the spool.

The results of this test are shown in Figure 43: maximum and mean spool velocity for different values of torque. The spool velocity decreases with increasing force. The magnitudes indicate that the spool must turn at a very high speed, but that a small torque is sufficient to apply the line forces considered.Figure 43. As would be expected, considering that the torque opposes the motion of the spool, larger torque values correspond to slower rates of rotation.

Looking at the order of magnitude of the torque compared to the speed, it is clear that a high speed, low torque motor would be required. This test therefore eliminated the geared motors from consideration, as these are designed to output large torques at low speed.

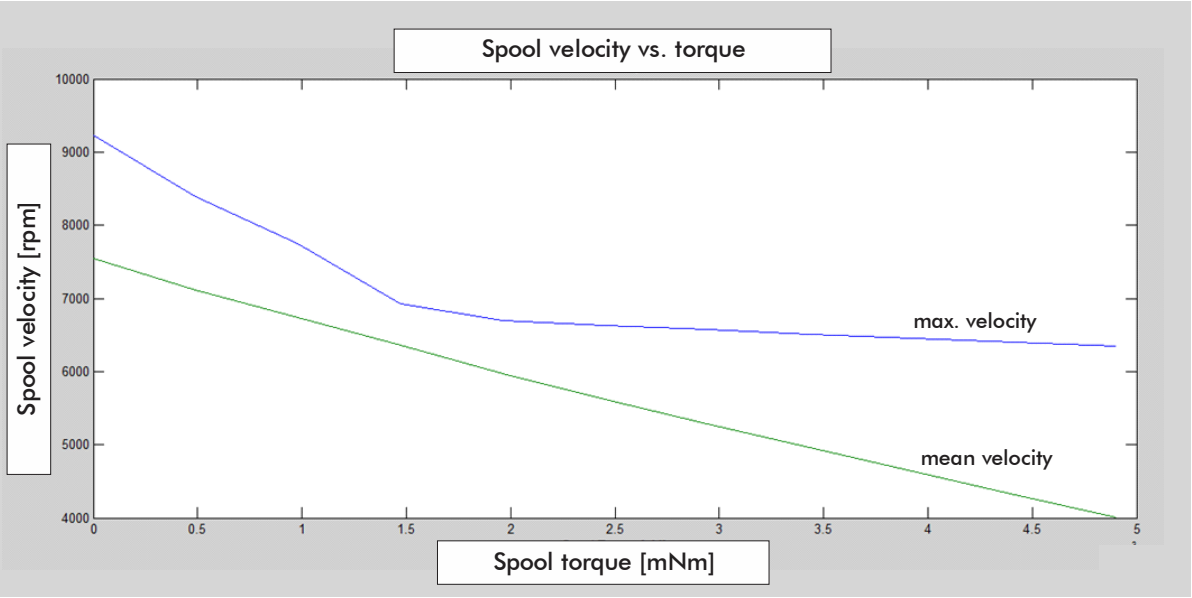

Figure 43: maximum and mean spool velocity for different values of torque. The spool velocity decreases with increasing force. The magnitudes indicate that the spool must turn at a very high speed, but that a small torque is sufficient to apply the line forces considered.

Controllability of the motor

The terminal voltage of the motor is the control output from the microcontroller, so it was also important to ensure that the force on the dragline would vary significantly with changes in this value. Examination of the equation used to model the motor shows that if the gear ratio of the motor is large, the magnitude of the force will be more dependent on the line speed, as its coefficient is proportional to the square of the gear ratio and will dominate:

$$F_m = \frac{KNr}{R_a} V_t - \frac{K^2 N^2}{R_a} \dot{L}$$

According to this model, the only ways to increase the influence of the voltage are to either make the radius of the spool very large, or keep the gear ratio small. As it is not feasible to have a sufficiently large spool on a mobile robot, this observation supports the previous conclusion that a gearless motor should be used.

Final motor selection

Having discounted the geared options, the sub-miniature coreless motor was selected over the toy motor as it is much smaller and lighter.

8.4.3 Perspex spool

The motor selected could not be directly coupled to the LEGO spool, so a custom spool was fabricated by gluing together Perspex rings. One side of the spool was then glued directly onto the shaft of the motor.

8.5 Software Design

To log the pitch angle data from the iNEMO module in Design 2 and Design 3, code needed to be written for both the iNEMO and the base station computer.

8.5.1 iNEMO Code

The code for the iNEMO was written in C using the Atollic TRUEstudio IDE. Callen Fisher wrote libraries of functions for performing basic activities on the iNEMO, and provided a base project which could be modified to perform the necessary tasks.

The role of the iNEMO code is to continuously take in data from the three gyroscopes, process it and output the pitch angle to the XBEE.

The gyroscope outputs the roll, pitch and yaw velocities, relative to the body frame, in degrees per second. These were then corrected by subtracting the sensor bias, and rotated into the inertial reference frame using equations derived from the DSM matrix. The position in terms of roll, pitch and yaw was then determined by integrating the velocities over the sampling period.

Although only the pitch angle would be output, the roll and yaw also had to be accounted for as previous position values are required to rotate the incoming velocities to the correct reference frame.

The pitch positions are output as floating point values, which must be sent over the UART as four separate characters. A sampling period of 20 milliseconds was used.

A description of how the sensor bias was calculated is provided in Appendix B.

8.5.2 Base Station Code

The code for receiving the pitch data on the computer was written using Python 2.7 VERSION with Pyserial, a library which enables sending and receiving serial data in Python.

This code was very simple, as its only tasks were to re-assemble the characters received into floating point numbers, and log them to a comma-separated variable (CSV) file. This format was selected as it is compatible with Microsoft Excel, where it can be plotted and analysed effectively.

To prevent the data corresponding to the relatively short aerial period from being lost amongst data from after the robot has landed, the code was set to stop logging once it had received a specified number of pitch readings.

9 Validation of LEAP Design

9.1 Testing Methodology

Due to the time constraints of the project, only the first design stage could be tested. Without the a means of regulating the tension in the dragline, a controller cannot be applied, so the variable of interest in this test is not whether the robot makes a safe landing, but whether the line is observed to bring about any pitch-modifying effects.

The launcher was set up at an angle of 15 degrees, and a height of 55 centimetres (to the feet of the robot.) The model was then launched three times with the dragline, and three times without it. Analysis of the footage showed that the initial velocity was around 2.4 metres per second.

The Gopro camera was used to record the jumps at 120 frames per second. These were then played back frame by frame to determine whether a pitch reversal took place.

9.2 Results

Screenshots from the clearest footage of the controlled and uncontrolled jump is shown in Figure 44. In both, the platform exhibited a slight initial rearward pitch, as was the case with the spider. It can be seen that, without the dragline, this rearward pitch continued throughout the jump, but when the dragline was applied, the pitch was reversed and the platform began to rotate forwards.

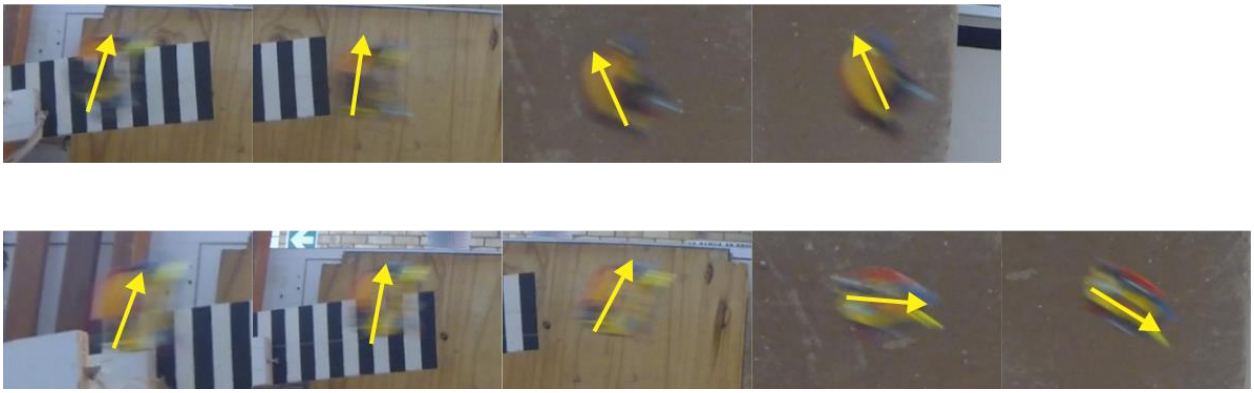

Figure 44: Footage of the stage 1 LEAP design launched with (bottom) and without (top) the dragline. The arrows indicate the direction of the body axis. The initial rotation was reversed when the dragline was applied.

9.3 Discussion

Despite the high frame rate of the camera used, there is still a large amount of motion blur in the stills obtained from the video. The stated initial velocity is therefore a rough approximation. Additionally, in some of the jumps, the platform tended to roll slightly. Combined with the blur, this made it impossible to precisely determine the pitch of the body, but it was still evident that the dragline was able to produce the expected reversal of the initial rotation.

Besides proving the concept that the dragline can be used to affect the pitch rotation of a mobile robot, this test illustrates some of the benefits of using this mechanism. Firstly, it is clear that the

dragline approach is not dependent on powerful actuators: in the previous chapter, the force applied to the line was found to be a small fraction of the body weight, yet it was still able to effectively bring about a change in the motion. The weight and space cost of the friction-based mechanism applied here is very small.

10 Conclusions

10.1 Review of the project objectives

The purpose of this project was to understand and evaluate the feasibility of using a dragline to implement pitch righting. To this end, a dynamic analysis of the system using simulated models was conducted, and a simple robotic testing platform designed. Although the full design could not be implemented and tested within the time constraints, the project is still felt to be a success, as it was able to provide some answers to all the research questions posed. To conclude this report, these questions will now be revisited:

What are the possible applications of a dragline-inspired mechanism in the field of mobile robotics?

The dragline could be used to solve the problem of aerial pitch righting and braking, which is necessary in robots designed to safely navigate rough terrain. Additionally, it could act as a safety line or allow the robot to descend from one surface to another.

How does the spider achieve pitch control utilizing the dragline?

During the jump, the spider uses an internal friction brake (likely the valve at the end of its silk duct [1] [11] [12]) to apply tension to the line. This force both slows the spider down and rotates it, allowing it to make a safe landing. The effects of small changes in body posture and aerodynamic forces can largely considered to be negligible compared to the action of the dragline [1] [10] [8] [10].

What are the effects of the initial velocity, launch angle, initial body rotation and magnitude of the silk force on jump performance?

These parameters were found to affect the range, final velocity and angular response of the jump. A summary of the effects is presented in Table 3.

How can the spider's observed pitch angle response be explained?

The significant features of the spider's angular response were that it does not settle at the target angle, and that it tends to reverse its pitch twice over the course of the jump. Due to the way the direction and magnitude of the moment caused by the dragline changes as the body rotates, the angle will always tend to oscillate sinusoidally. Rather than attempting to stabilize this inherently unstable response, the spider's control objective is to modify its frequency such that a favourable angle coincides with the time of landing.

The benefits of multiple pitch reversals were found to be tied to maximizing the range of the jump. It was hypothesized that some overestimation of the initial launch velocity is beneficial to the spider, but only up to a limit which would need further research to determine precisely.

What other methods of aerial righting are available, and how do they compare to the dragline solution?

Several biologically-inspired and artificial methods for achieving aerial righting were discussed. For application in a mobile robot, most approaches were either momentum-based, or relied on the manipulation of aerodynamic torques [6] [27] [23] [22] [26]. The dragline approach was specifically compared to flywheels and active tails. It was found to have advantages in terms of

size and multi-purpose usefulness, but potential complications associated with its use and implementation were raised as initially apparent drawbacks.

Is it possible to bring about pitch rotation in a mobile robot using only the dragline?

The tests performed on the first stage LEAP design showed that the initial pitch of the body was reversed when the dragline was applied. This shows that the dragline alone is sufficient to induce rotation or counteract an existing rotation in a mobile robot.

What are the advantages and disadvantages associated with the dragline as a method of aerial righting?

The dragline can be considered to be a low-cost method of aerial righting for robots where space and weight conservation is paramount, as unlike some other methods examined, its operation is not dependent on its size. The tests performed on the simple LEAP prototype confirm that it is possible to bring about rotation using a small mechanism producing a force which is a fraction of the weight of the body. Because the simulation indicated that the torque requirement is extremely small, the implementation of active spool control using a motor should not require a large, high-powered device.

Another benefit of the dragline is its multi-purpose applicability: it also provides braking during the jump to prevent rolling on landing, and could be used as a safety line to catch the robot after a fall or to allow it to move through its environment by descending from surface to surface.

Based on this initial investigation, the main drawback to the dragline is that it will most likely be very complicated to implement. From a control perspective, the way this mechanism affects the motion of the body is highly dependent on the time and current body position of the robot, so any effective controller will require accurate and comprehensive position and velocity data to regulate the angle. Additionally, the system has inherent marginal instability.

Other design complications are the requirements for a robust anchoring mechanism and the storage of sufficient disposable line, or alternatively, a line retrieval mechanism. The need for the line to be attached to the surface prior to the launch also limits the ability of this method to cope with unexpected ballistic motion.

10.2 Feasibility of the dragline as a pitch control mechanism

This thesis has shown that it is indeed possible to bring about pitch rotation in a mobile robot using tension in a dragline, and that this method has several distinct advantages over established aerial righting methods. Determining whether it is actually a practical method will, however require further research, particularly into possible methods of implementing a controller.

Although the results of this project cannot emphatically confirm the feasibility of the dragline as a method of aerial righting for mobile robots, they have shown that this method is at least worth investigating further.

11 Recommendations and Future Work

While this project did not leave any of the initial research questions entirely unanswered, it only began to scratch the surface of understanding the applications of the dragline. Throughout the course of this thesis, many further questions were raised and gaps in the existing literature discovered, making this topic ripe for further research across a variety of fields.

11.1 Control Theory

This report identified some of the control problems associated with the dragline system, but controller design was outside the scope of the project. The most obvious avenue for expanding on this research is therefore an investigation into the possible control methods which could be applied to regulate pitch angle using the dragline. As this paper only examined the motion of the body under the application of a constant line force, it would first be necessary to further the dynamic analysis to evaluate the effects of a time- or position-varying force.

11.2 Instrumentation

It was found that the angular response to the silk force is dependent on the time and body position at which that force is applied. An effective controller would therefore have to have access to the current positional data, as well as the silk angle. If the position at which the silk is anchored is known, it is possible to calculate the silk angle from the positional data, but if not, a sensor will be required to measure it. The design of a sensor which can do this accurately but without interfering with the motion of the dragline could be an interesting future project.

11.3 Biology

The best way to gain insights into the control of the dragline would most likely be to study a system where it has already been applied successfully: the jumping spider. Thus far, there has only been one study [1] examining how the dragline is used to regulate pitch in spiders, and this only considered a single type of jump. It is expected that the understanding of this motion could be immensely improved by repeating this experiment using jumps of varying lengths and angles.

From a biomechanics point-of-view, an expansion of the dynamic analysis in this paper could be beneficial. The body model used here was highly simplified, so there is room to repeat the tests incorporating changing body posture and a more accurate representation of the aerodynamic forces, so their role in pitch righting can be properly determined.

11.4 Improving the design of the LEAP

The second and third design phases of the LEAP were not able to be implemented completely within the time frame of this project. Producing a prototype based on the final LEAP design would be a good starting point for continuing this research, as its ability to actively control the tension in the dragline would facilitate physical experiments to validate the simulated results presented in this report. If the iNEMO code is expanded to obtain the x and y position of the robot in addition to the pitch, this platform could also be used to test controller designs.

From the tests conducted on the first stage prototype, the following changes could be made to improve the system:

- The launcher must be improved: tracks must be added to the launcher to prevent the robot from sliding into the sides as it travels down the chute, and it must be mounted on a sturdier base to prevent it from wobbling and shifting. The way the body left the launcher sometimes induced roll or yaw in the tests.

- A higher speed camera must be used: although the Gopro was able to show the general motion of the body, precise analysis of the motion would require a camera with a fast enough to prevent the motion blur observed.

- A more consistent open loop method of applying resistance to the spool must be found: because of the tendency of the LEGO components to shift slightly, it was difficult to maintain the same amount of drag on the spool.

11.5 Design of supporting components

Besides the mechanisms directly associated with the control of the tension in the dragline, practical solutions to the problems of line attachment, storage and retrieval would need to be developed for line-based righting to be implemented.

12 List of References

[1] Y.-K. Chen, C.-P. Liao, F.-Y. Tsai, and K.-J. Chi, "More than a safety line: jump-stabilizing silk of salticids," *Journal of the Royal Society Interface*, vol. 10, no. 87, Aug. 2013.

[2] M. Davis, C. Gouinaud, J. C. Fauroux, and P. Vaslin, "A review of self-righting techniques for terrestrial animals," in *International workshop on bio-inspired robots, Ecole des Mines and IRCCYN LAB*, Nantes, France, 2011.

[3] L. D. Paulson, "Biomimetic Robots," *Computer*, vol. 37, no. 9, pp. 48-53, 2004.

[4] L. Wang, U. Culha, and F. Iida, "A dragline-forming mobile robot inspired by spiders," *Bioinspiration & Biomimetics*, vol. 9, 2014.

[5] R. Siegwart and I. R. Nourbakhsh, *Introduction to Autonomous Mobile Robots*. Cambridge, Massachusetts: MIT Press, 2004.

[6] Y. Bar-Cohen, "Biomimetics - using nature to inspire human innovation," *Bioinspiration & Biomimetics*, vol. 1, pp. 1-12, 2006.

[7] F. Delcomyn, "Biologically Inspired Robots," in *Bioinspiration and Robotics: Walking and Climbing Robots*, M. K. Habib, Ed. Vienna, Austria: I-Tech Education and Publishing, 2007, ch. 17, pp. 279-300.

[8] R. F. Foelix, *Biology of Spiders*, 3rd ed. New York: Oxford University Press, 2011.

[9] D. Parry and R. Brown, "The jumping mechanism of salticid spiders," *Journal of Experimental Biology*, vol. 36, pp. 654-664, 1959.

[10] D. E. Hill, "Targeted jumps by salticid spiders (Araneae, Salticidae, Phidippus) ver. 9," 2006.

[11] T. Weihmann, M. Karner, R. J. Full, and R. Blickhan, "Jumping kinematics in the wandering spider Cupiennius salei," *Journal of Comparative Physiology A*, vol. 196, no. 6, pp. 421-438, Jun. 2010.

[12] R. S. Wilson, "Control of Drag-Line Spinning in Certain Spiders," *American Zoologist*, vol. 9, no. 1, pp. 103-111, Feb. 1969.

[13] C. S. Ortlepp and J. M. Gosline, "Consequences of Forced Silking," *Biomacromolecules*, vol. 5, pp. 727-731, 2004.

[14] R. W. Work, "Mechanism for the Deceleration and Support of Spiders on Draglines," *Transactions of the American Microscopical Society*, vol. 97, no. 2, pp. 180-191, Apr. 1978.

[15] T. A. Blackledge, "Spider silk: a brief review and prospectus on research linking biomechanics and ecology in draglines and orb webs," *Journal of Arachnology*, vol. 20, no. 1, pp. 1-12, 2012.

[16] C. Boutry, M. Rezac, and T. A. Blackledge, "Plasticity in Major Ampullate Silk Production in Relation to Spider Phylogeny and Ecology," *PLoS ONE*, vol. 6, no. 7, 2011, doi:10.1371/journal.pone.0022467.

[17] D. Saravanan, "Spider Silk - Structure, Properties and Spinning," *Journal of Textile and Apparel, Technology and Management*, vol. 5, no. 1, 2006.

[18] R. S. Wilson, "Control of dragline spinning in the garden spider," *Quarterly Journal of Microscopical Science*, vol. 104, pp. 557-571, 1962.

[19] R. S. Wilson, "The structure of the dragline control valves in the garden spider," *Quarterly Journal of Microscopical Science*, vol. 103, pp. 549-555, Dec. 1962.

[20] F. Vollrath and D. P. Knight, "Structure and function of the silk production pathway in the spider Nephila edulis," *International Journal of Biological Macromolecules*, vol. 24, pp. 243-249, 1999.

[21] J. M. Gosline, P. A. Guerette, C. S. Ortlepp, and K. N. Savage, "The mechanical design of spider silks: from fibroin sequence to mechanical function," *The Journal of Experimental Biology*, vol. 202, pp. 3295-3303, 1999.

[22] O. Emile, A. Le Floch, and F. Vollrath, "Shape Memory in Spider Draglines," *Nature*, vol. 440, pp. 621-621, 2006.

[23] A. Jusufi, Y. Zeng, R. J. Full, and R. Dudley, "Aerial Righting Reflexes in Flightless Animals," *Integrative and Comparative Biology*, vol. 51, no. 6, pp. 937-943, 2011.

[24] A. Jusufi, D. T. Kawano, T. Libby, and R. J. Full, "Righting and turning in mid-air using appendage inertia: reptile tails, analytical models and bio-inspired robots," *Bioinspiration & Biomimetics*, vol. 5, 2010.

[25] E. Chang-Siu, T. Libby, M. Tomizuka, and R. J. Full, "A Lizard-Inspired Active Tail Enables Rapid Maneuvers and Dynamic Stabilization in a Terrestrial Robot," in *IEEE/RSJ International Conference on Intelligent Robots and Systems*, San Francisco, USA, 2011.

[26] J. Zhao, et al., "Controlling Aerial Maneuvering of a Miniature Jumping Robot Using Its Tail," in *IEEE/RSJ International Conference on Intelligent Robots and Systems*, Tokyo, Japan, 2013.

[27] P. Tsiotras, H. Shen, and C. Hall, "Satellite Attitude Control and Tracking with Energy/Momentum Wheels," *Journal of Guidance, Control and Dynamics*, vol. 24, no. 1, pp. 23-34, 2001.

[28] M. Davis, P. Vaslin, J. C. Fauroux, C. Gouinaud, and L. Ju, "Experimental evaluation of the pitch angle righting capabilities of a high speed terrestrial vehicle in ballistic phase," *Applied Mechanics and Materials*, vol. 162, pp. 57-66, 2012.

[29] J. L. Meriam and L. G. Kraige, *Engineering Mechanics: Dynamics*, 6th ed. Wiley, 2009.

[30] G. Yassin. (2011) 1st year Classical Mechanics, III: Lagrangian Dynamics. [Online]. http://www.physics.ox.ac.uk/Users/Yassin/mechanics/notes/note5aplusb_2011_v0.pdf

[31] S. Widnell. (2009) 16.07 Dynamics, Fall 2009, Lecture L20 - Energy Methods: Lagrange's Equations (Massechusetts Institute of Technology: MIT OpenCourseWare). [Online]. http://ocw.mit.edu/courses/aeronautics-and-astronautics/16-07-dynamics-fall-2009/lecture-notes/MIT16_07F09_Lec20.pdf

[32] J. K. Vandiver. 2.003SC Engineering Dynamics, Fall 2011. Lecture 15: Introduction to Lagrange with Examples (Massechusetts Institute of Technology: MIT OpenCourseWare). [Online]. http://ocw.mit.edu/courses/mechanical-engineering/2-003sc-engineering-dynamics-fall-2011/lagrange-equations/#?w=535

[33] S. J. A. Malham. (2014, Mar.) An Introduction to Lagrangian and Hamiltonian mechanics. [Online]. http://www.macs.hw.ac.uk/~simonm/mechanics.pdf

[34] J. L. Coetser, "Low-cost Inertial Naviagtion Systme for use on moving platforms," University of Cape Town Undergraduate thesis, 2013.

[35] H. Alemi Ardakani and T. J. Bridges. (2010, Apr.) Review of the 3-2-1 Euler Angles: a yaw-pitch-roll sequence. [Online]. http://personal.maths.surrey.ac.uk/st/T.Bridges/SLOSH/3-2-1-Eulerangles.pdf

[36] N. Mohan, T. M. Undeland, and W. P. Robbins, *Power Electronics: Converters, Applications and Design*, 2nd ed. New York: John Wiley and Sons, Inc., 1995.

[37] J.-J. E. Slotine and W. Li, *Applied Nonlinear Control*. New Jersey, USA: Prentice Hall, 1991.

[38] Digi International. (2009, Sep.) XBEE(R)/XBEE Pro(R) RF Modules. [Online]. https://www.sparkfun.com/datasheets/Wireless/Zigbee/XBee-Datasheet.pdf

13 Appendix A: Supplementary Material

The following additional materials are included on the CD attached to this document:

13.1 Video of results

The file **ResultsVideo.mp4** in the root of the CD is a video showing animations of both simulation models and the Gopro footage of the stage 1 LEAP design compared to footage of the spider recorded by Chen, et al [1]. For each case, a jump without the effects of the dragline is shown first, followed by a jump where the dragline is applied.

13.2 MATLAB files

The **MATLAB folder** contains the MATLAB scripts and Simulink models used to implement the simulations:

- **lagrange_equations:** the script used to derive the equations of motion for Model 2 with the MATLAB symbolic toolbox
- **pendulum_spider_noVR:** Simulink model of Model 2, without the motor
- **pendulum_spider_complete_noVR:** Simulink model of Model 2, with the motor included
- **simple_spider_noVR:** Simulink model of Model 1
- **pendulum_spider_script:** the script used to set the initial parameter values for use in the simulation of Model 2
- **simple_spider_script:** the script used to set the initial parameter values for use in the simulation of Model 2

Because the 3D visualizations of the simulations require the installation of additional software to run, outside of the standard MATLAB package, the models are provided without the virtual reality components.

13.3 Papers

The **Papers Folder** contains the scientific papers cited in this thesis. They can also be found on Google Scholar from the information provided in the list of references.

13.4 iNEMO Code

The folder **scratchINEMO** is the Atollic TRUEstudio project used to code the iNEMO module. It was written by Callen Fisher, and modified to track the pitch angle.

14 Appendix B: Additional Information

This appendix provides additional information regarding the proposed LEAP design.

14.1 Calculation of sensor biases for iNEMO code

The gyroscopic sensor has an inherent bias in its output velocity values, which will cause the position values acquired by integrating the velocity to become increasingly inaccurate if they are not corrected for. To establish the bias in the sensor, the gyroscope was set to output the roll, pitch and yaw velocities for two minutes, while the module remained stationary. The average of these values was then taken to be the bias.

Plots of the readings taken are shown in Figure 45.

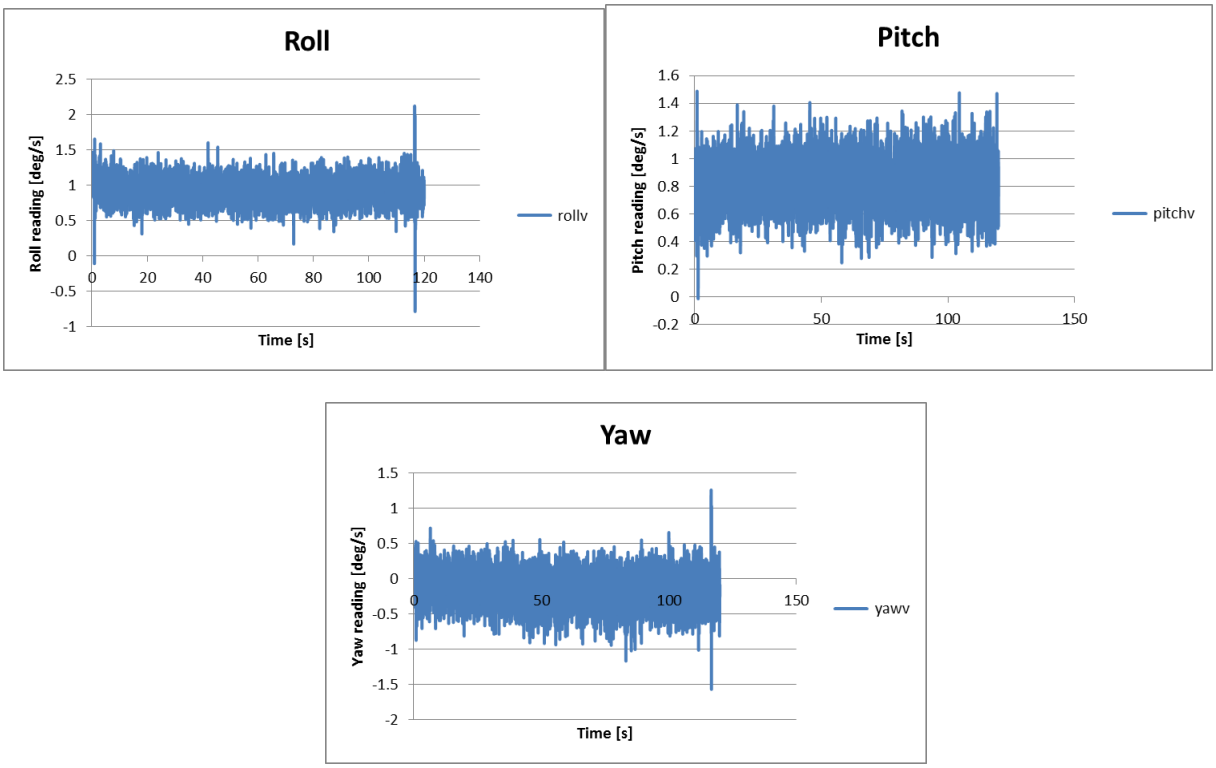

Figure 45: roll, pitch and yaw readings taken over two minutes

The bias of the gyroscope is temperature-dependent, and therefore will vary, but considering that the robot is in the air for a very short time and the bias values were all found to be less than one degree per second, it is assumed that this can be neglected without compromising the accuracy of the results.

14.2 LEGO parts list for chassis

Table 4: LEGO parts used in chassis

Part	Quantity	Part	Quantity
	4		4
	4	 (6)	2
	10	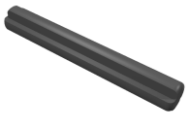 (3)	2
	2		2
	4	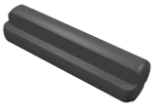 (2)	6
	1	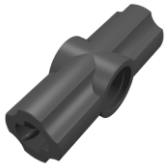	1
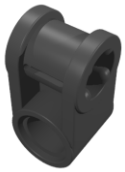	6		4
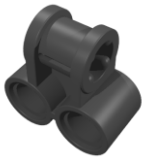	2		4
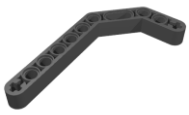	2		4